การสร้างอิเล็กโทรดแบบเลือกจำเพาะต่อไอออนซิลเวอร์และการประยุกต์ด้านไบโอเซ็นเซอร์

นางสาววันวิสา เจนรุ่งโรจน์สกุล

วิทยานิพนธ์นี้เป็นส่วนหนึ่งของการศึกษาตามหลักสูตรปริญญาวิทยาศาสตรดุษฎีบัณฑิต
สาขาวิชาเคมี ภาควิชาเคมี
คณะวิทยาศาสตร์ จุฬาลงกรณ์มหาวิทยาลัย
ปีการศึกษา 2554

FABRICATION OF SILVER ION SELECTIVE ELECTRODES AND THEIR APPLICATIONS IN BIOSENSORS

Miss Wanwisa Janrungroatsakul

A Dissertation Submitted in Partial Fulfillment of the Requirements
for the Degree of Doctor of Philosophy Program in Chemistry
Department of Chemistry
Faculty of Science
Chulalongkorn University
Academic Year 2011

Thesis Title	FABRICATION OF SILVER ION SELECTIVE ELECTRODES AND THEIR APPLICATIONS IN BIOSENSORS
By	Miss Wanwisa Janrungroatsakul
Field of Study	Chemistry
Thesis Advisor	Professor Thawatchai Tuntulani, Ph.D.

Accepted by the Faculty of Science, Chulalongkorn University in Partial Fulfillment of the Requirements for the Doctoral Degree

…….Dean of the Faculty of Science
(Professor Supot Hannongbua, Dr.rer.nat.)

THESIS COMMITTEE

…….. Chairman
(Assistant Professor Preecha Lertpratchya, Ph.D.)

…….……. Thesis Advisor
(Professor Thawatchai Tuntulani, Ph.D.)

…….. Examiner
(Assistant Professor Soamwadee Chaianansutcharit, Ph.D.)

…….. Examiner
(Assistant Professor Wanlapa Aeungmaitrepirom, Ph.D.)

…….. External Examiner
(Assistant Professor Wittaya Ngeontae, Ph.D.)

วันวิสา เจนรุ่งโรจน์สกุล : การสร้างอิเล็กโทรดแบบเลือกจำเพาะต่อไอออนซิลเวอร์และการประยุกต์ด้านไบโอเซ็นเซอร์. (FABRICATION OF SILVER ION SELECTIVE ELECTRODES AND THEIR APPLICATIONS IN BIOSENSORS) อ.ที่ปรึกษาวิทยานิพนธ์หลัก : ศ. ดร. ธวัชชัย ตันฑุลานิ, 108 หน้า.

ได้สังเคราะห์อนุพันธ์คาลิกซ์[4]เอรีน 6 ชนิด ที่มีอะตอมดอนเนอร์และโครงสร้างที่แตกต่างกัน (L1 – L6) และใช้เป็นไอโอโนฟอร์สำหรับสร้างอิเล็กโทรดแบบเลือกจำเพาะต่อไอออนซิลเวอร์ ในเมมเบรนพอลิเมอร์จะนำมาเปรียบเทียบลักษณะเพื่อเลือกไอโอโนฟอร์ที่ดีที่สุดในแง่ของการเลือกจับแบบโพเทนชิโอเมทริกและค่าคงที่ของการเกิดสารประกอบเชิงซ้อน โดยอิเล็กโทรดของ L2 ที่มีสองหมู่เบนโซไทอาโซลมีค่าการเลือกจำเพาะต่อไอออนซิลเวอร์สูงสุด ซึ่งเป็นผลมาจากอะตอมดอนเนอร์ของไนโตรเจนสองอะตอมและดอนเนอร์ของซัลเฟอร์ของหมู่เบนโซไทอาโซลสองอะตอมสามารถเกิดสารประกอบเชิงซ้อนกับไอออนซิลเวอร์ได้ดี ส่งผลให้ค่าคงที่ของการเกิดสารประกอบเชิงซ้อนสูง องค์ประกอบของ L2 ในเมมเบรนพอลิเมอร์นำมาปรับให้เหมาะสมเพื่อให้ได้ลักษณะที่ดีที่สุดของอิเล็กโทรดแบบเลือกจำเพาะต่อไอออนซิลเวอร์โดยใช้ L2 (10 มิลลิโมลต่อกิโลกรัม) และ KT*p*ClPB (50 เปอร์เซ็นต์โมลสัมพันธ์กับปริมาณไอโอโนฟอร์) ในเมมเบรนพีวีซีที่มี *o*-NPOE (พีวีซี: *o*-NPOE เป็น 1:2 เปอร์เซ็นต์โดยน้ำหนัก) ไอออนซีเล็กทีฟอิเล็กโทรดสำหรับตรวจวัดไอออนซิลเวอร์ที่ประดิษฐ์จาก L2 แสดงคุณสมบัติที่ดีโดยมีการตอบสนองแบบเนินสต์ (59.7 ± 0.8 มิลลิโวลต์ต่อดีเคด สำหรับแมกโครอิเล็กโทรด และ 59.8 ± 1.0 มิลลิโวลต์ต่อดีเคด สำหรับไมโครอิเล็กโทรด) ด้วยขีดจำกัดการตรวจวัดต่ำ (ประมาณ 5.0×10^{-7} โมลาร์) และช่วงการทำงานเชิงเส้นกว้าง (10^{-6} ถึง 10^{-2} โมลาร์) เซ็นเซอร์นี้สามารถนำมาใช้ในช่วงพีเอชที่กว้าง (พีเอช 2 – 8) ด้วยเวลาการตอบสนองน้อยกว่า 5 วินาที และนำมาใช้เป็นขั้วอิเล็กโทรดตัวบ่งชี้สำหรับการไตเตรทแบบอาเจนโตเมทริกของสารผสมระหว่างไอออนคลอไรด์และโบรไมด์ อิเล็กโทรดประดิษฐ์ได้นำมาใช้ในการวิเคราะห์รูปแบบของอนุภาคระดับนาโนเมตรของเงินเป็นครั้งแรกด้วยความแม่นและเที่ยงที่ดี

แมกโครอิเล็กโทรดที่ประดิษฐ์จาก L2 นำไปใช้เป็นไบโอเซ็นเซอร์ตรวจวัดน้ำตาลโดยใช้อนุภาคระดับนาโนเมตรของเงินเป็นตัวบ่งชี้ไอออนบวก โดยทั่วไปปฏิกิริยาของเอนไซม์-สารตั้งต้นระหว่างน้ำตาลกลูโคสและกลูโคสออกซิเดสให้ไฮโดรเจนเปอร์ออกไซด์เป็นผลิตภัณฑ์ ซึ่งสามารถออกซิไดส์อนุภาคระดับนาโนเมตรของเงินไปเป็นไอออนซิลเวอร์อิสระ ปริมาณของไอออนซิลเวอร์จะแปรผันตามความเข้มข้นของน้ำตาลกลูโคสซึ่งสามารถตรวจสอบได้โดยตรงโดยใช้ไอออนซีเล็กทีฟอิเล็กโทรดสำหรับตรวจวัดไอออนซิลเวอร์ พบว่าช่วงการทำงานเชิงเส้นคือ 0.1 – 3 มิลลิโมลาร์ ในบัฟเฟอร์ของแมกนีเซียมแอซีเตท 10 มิลลิโมลาร์ พีเอช 6.0 จากนั้นศึกษาปัจจัยที่มีผลกระทบต่ออัตราการเกิดปฏิกิริยา เช่น พีเอช และปริมาณของกลูโคสออกซิเดสและอนุภาคระดับนาโนเมตรของเงิน ด้วยขีดจำกัดการตรวจวัดคือ 1.0×10^{-5} โมลาร์ เซ็นเซอร์ที่นำเสนอทำงานแบบเลือกจำเพาะสองชั้น และสามารถนำมาใช้ตรวจสอบปริมาณน้ำตาลในเครื่องดื่มด้วยความแม่นและเที่ยง

ไมโครอิเล็กโทรดประดิษฐ์จาก L2 นำไปใช้ตรวจสอบไอออนซิลเวอร์ในตัวอย่าง 1000 ไมโครลิตร ด้วยขีดจำกัดการตรวจวัดประมาณ 1 ไมโครโมลาร์ โดยใช้ไมโครอิเล็กโทรดสำหรับตรวจวัดไอออนโซเดียมเป็นขั้วอ้างอิงเทียม นำการวัดแบบโพเทนชิโอเมทริกดังกล่าวไปประยุกต์ใช้เพื่อตรวจหาการไฮบริดของดีเอ็นเอบนพื้นผิวทองซึ่งตรึงด้วยกรดลิโปอิกดัดแปรด้วยไพร์โรลิดินิล พีเอ็นเอ ที่มี 2-อะมิโนไซโคลเพนเทนคาร์บอกซิลิกเป็นโพรบ โดยการออกซิไดส์อนุภาคระดับนาโนเมตรของเงินที่ห่อหุ้มด้วยประจุบวกด้วยไฮโดรเจนเปอร์ออกไซด์ ขีดจำกัดการตรวจวัดของดีเอ็นเอคือ 2 ไมโครโมลาร์ (20 พิโคโมล) ในตัวอย่าง 1000 ไมโครลิตร โพรบของพีเอ็นเอชนิดนี้สามารถเลือกจับดีเอ็นเอแบบเข้าคู่ แยกออกจากดีเอ็นเอแบบไม่เข้าคู่และดีเอ็นเอที่มีหนึ่งลำดับเบสไม่เข้าคู่โดยใช้วิธีโพเทนชิโอเมทริกแบบง่าย

ภาควิชา เคมี ลายมือชื่อนิสิต .....

สาขาวิชา เคมี ลายมือชื่อ อ.ที่ปรึกษาวิทยานิพนธ์หลัก .....

ปีการศึกษา 2554

507 38717 23: MAJOR CHEMISTRY

KEYWORDS: IONOPHORE / ION SELECTIVE ELECTRODE / BIOSENSOR

WANWISA JANRUNGROATSAKUL: FABRICATION OF SILVER ION SELECTIVE ELECTRODES AND THEIR APPLICATIONS IN BIOSENSORS. ADVISOR: PROF. THAWATCHAI TUNTULANI, Ph.D., 108 pp.

Six calix[4]arene derivatives containing various donor atoms and different topology (**L1** – **L6**) have been synthesized and used as neutral ionophores to fabricate silver ion selective electrodes (Ag-ISEs). The characteristics of six synthesized ionophores in polymeric membranes were compared in order to find the best one in terms of potentiometric selectivities and complex formation constants. The electrode based on **L2** containing two benzothiazole groups showed the highest selectivity coefficient towards Ag^+ which resulted from two nitrogen and two sulfur donor atoms of benzothiazole groups forming a stronger complex with Ag^+ yielding a high complex formation constant. **L2** was optimized in polymeric membrane to obtain the best characteristics of Ag-ISE using **L2** (10 mmol kg^{-1}) and KT*p*ClPB (50 mol% related to the ionophore) in the *o*-NPOE plasticized PVC membrane (1:2; PVC:*o*-NPOE by weight). The Ag-ISE fabricated from ionophore **L2** exhibited good properties with a Nernstian response (59.7 ± 0.8 mV $decade^{-1}$ for macroelectrode and 59.8 ± 1.0 mV $decade^{-1}$ for microelectrode) with a low detection limit (ca. 5.0×10^{-7} M) and a wide linear working range (10^{-6} to 10^{-2} M). The sensors could be used in a wide pH range (pH 2 – 8) with a response time less than 5 seconds. The electrodes were used as an indicator electrode for the argentometric titration of the mixture of Cl^- and Br^-. The fabricated electrodes were also used for the first time in speciation analysis of silver nanoparticles (AgNPs) with good accuracy and precision.

The macroelectrode fabricated from **L2** was then applied in glucose biosensor by using AgNPs as cation marker. Basically, the enzyme-substrate reaction between β-D-glucose and glucose oxidase (GOx) produced hydrogen peroxide (H_2O_2) as a product. The generated H_2O_2 was able to oxidize AgNPs to free Ag^+. The amount of Ag^+ corresponded to the concentration of glucose could be directly monitored using the Ag-ISE. The working linear range was 0.1 – 3 mM in 10 mM magnesium acetate buffer pH 6.0. Parameters affected the reaction rate such as pH and the amount of GOx and AgNPs were explored. The lower detection limit was 1.0×10^{-5} M. The proposed sensor provided a double selective function and could be used to determine glucose in beverages with good accuracy and precision.

The fabricated microelectrode from **L2** was used to determine Ag^+ in 1000 µL sample with the detection limit around 1 µM using sodium ion selective microelectrode as pseudo reference electrode. Such potentiometric measurement was then applied to detect the DNA hybridization on gold substrates immobilized with lipoic acid modified by pyrrolidinyl peptide nucleic acid carrying a 2-aminocyclopentanecarboxylic acid (Lip-acpcPNA) probe by dissolution of positively charged encapped AgNPs with H_2O_2. The detection limit of DNA was 2 µM (20 pmol) in 1000 µL sample. This Lip-acpcPNA probe could discriminate fully complementary DNA, non-complementary DNA and single base mismatched DNA using the simple potentiometric method.

Department: ……Chemistry…. Student's Signature .....

Field of Study: ….Chemistry..... Advisor's Signature .....

Academic Year: ……2011…… .....

ACKNOWLEDGEMENTS

I wish to express highest appreciation to my thesis advisor, Prof. Dr. Thawatchai Tuntulani, for the opportunity he has given me to work in his group and his valuable guidance, understanding and patience. His motivating spirit likes a shine when I feel confused and will always inspire me in my future career. My deepest thanks would be expressed to Asst. Prof. Dr. Wittaya Ngeontae for introducing me into the field of ion selective electrodes and his advices and encouragement throughout my thesis work. I am also grateful to Asst. Prof. Dr. Preecha Lertpratchya, Asst. Prof. Dr. Soamwadee Chaianansutcharit, Asst. Prof. Dr. Wanlapa Aeungmaitrepirom for their valuable suggestions and comments as committee members and thesis examiners.

This thesis cannot be complete without kindness and helps from many people. I would like to give my deep thanks to Assoc. Prof. Dr. Tirayut Vilaivan and Mrs Chotima Vilaivan for preparing PNA and the several interesting suggestions concerning PNA, Assoc. Prof. Dr. Sanong Ekgasit and Dr. Pattwat Maneewattanapinyo for providing silver nanoparticles, Asst. Prof. Dr. Chomchai Suksai and Mr. Sarayut Watchasit for preparing some ionophores for fabrication of Ag-ISEs and Asst. Prof. Dr. Wanlapa Aeungmaitrepirom for facilities and space in her lab. I wish to express my sincere thanks to members in the past and present of Supramolecular Chemistry Research Unit (SCRU) and Environmental Analysis Research Unit (EARU) for the friendship, help and support.

Recognition would be expressed to the Commission on Higher Education, the Thailand Research Fund (RTA5380003) and Center of Excellence on Petrochemical and Materials Technology for the financial support throughout my graduate study.

Finally, I would like to thank my family for their love, support and encouragement.

CONTENTS

PAGE

PAGE

PAGE

PAGE

LIST OF TABLES

LIST OF FIGURES

LIST OF ABBREVIATIONS

°C	Degree Celsius
^{13}C NMR	Carbon nuclear magnetic resonance
d	Doublet (^{1}H NMR spectrum)
DOS	Bis(2-ethylhexyl)sebacate
EMF	Electromotive force
g	Gram
GOx	Glucose oxidase
h	Hour
^{1}H NMR	Proton nuclear magnetic resonance
Hz	Hertz
ISE	Ion selective electrode
J	Coupling constant
KT*p*ClPB	Potassium tetrakis[4-chlorophenyl] borate
L	Ionophore
m	Multiplet (^{1}H NMR spectrum)
M	Molar
mL	Millilitre
mmol kg^{-1}	Millimole per kilogram
o-NPOE	*o*-Nitrophenyl octyl ether
PNA	Peptide nucleic acid
ppm	Part per million
PVC	Poly(vinyl chloride)
R^-	Cation exchanger
s	Singlet (^{1}H NMR spectrum)
SSM	Separate solution method
t	Triplet (^{1}H NMR spectrum)
THF	Tetrahydrofuran

v/v	Volume by volume
wt.%	Percent by weight
β_{ILn}	Stability constant for ion-ionophore complex
δ	Chemical shift
µL	Microliter

CHAPTER I

INTRODUCTION

It is well known that silver ions and silver-based compounds are important components in medical textile and clothes due to strong antimicrobial effects [1–2]. Silver nanoparticles (AgNPs) show better antimicrobial property compared to other silver-based compounds due to their small size with unique properties providing better contact with microorganism. However, antimicrobial mechanisms of silver ions and AgNPs are not well understood. Microbiologists have used a number of techniques to study the effects of AgNPs on microbial growth inhibition such as scanning electron microscope (SEM), transmission electron microscopy (TEM) [3] and electron spin resonance (ESR) [4]. Silver ion selective electrode (Ag-ISE) may be a valuable tool for measuring concentration of Ag^+ to find a suitable condition for synthesizing desired AgNPs and may be used to study antimicrobial properties of AgNPs.

Potentiometry based on ion selective electrodes (ISEs) has been widely used for determination the activity of metal ions for several decades [5] since ISEs offer several advantages, especially cheap and simple device. Recently, miniaturized- and micro-sized ISEs have been explored for detecting amounts of ions in microvolume samples [6] as potentiometry is less dependent on scaling laws. It, however, depends on components in a polymeric membrane electrode, especially ionophore or ion carrier acting directly on a selective analyte.

Ag-ISEs have been developed and successfully constructed from a diversity of ionophores [7–30] for monitoring and determination of Ag^+. Such ionophores for fabricated Ag-ISEs have coordination sites possessing π-electrons [22–23] or heteroatoms [7–21] for binding Ag^+, but interactions between ionophores possessing π-coordination and Ag^+ were very weak resulting in less discrimination from alkali, alkaline earth and transition metals. In addition, Szigeti and co-workers showed that selectivity coefficients of membranes containing π-coordinating calix[4]arene

ionophores were worse than those containing calix[4]arene incorporating sulfur donors [31].

Calixarene is a very popularly employed molecular platform for ionophores since calixarene derivatives possessing different functional groups with various donor atoms can offer different selectivity of ionophores toward Ag^+ [24–30]. Calix[4]arene derivatives modified with one or two phenolic groups still displayed good characteristics of Ag^+ ionophores [29, 32–33].

In this research, six synthesized ionophores based on calix[4]arene containing various donor atoms were used to construct Ag-ISEs in order to find the best electrode which is most selective to Ag^+ and give excellent selectivity with low interference of other cations, especially Hg^{2+} compared to the electrodes proposed in the previous reports. For a new generation of Ag-ISEs, we focused on fabrication of Ag-ISEs from ionophore-based calix[4]arene with different functional groups. The fabricated Ag-ISE can then possibly be applied in biosensing of glucose and DNA.

1.1 Research Objective

This research aims to fabricate new Ag-ISEs using calix[4]arene-based ionophores and the fabricated Ag-ISEs which will then apply in biosensors.

1.2 Scope of the Research

Six calix[4]arene derivatives were synthesized by modification of one or two opposite phenolic groups with a 2-aminothiophenol, dipicolylamine and hydrazone (**L1 – L6**) as shown in Figure 1.1. These synthesized ionophores were then incorporated into a plasticized poly(vinyl chloride) (PVC) matrix with a lipophilic cation exchanger for preparation of a membrane electrode. The fabricated Ag-ISEs were compared in order to find the best ones in term of selectivity, stability constant and lower detection limit. Membrane compositions were optimized to obtain the best Ag-ISE, which was examined the electrode characteristics such as selectivity, lower detection limit, response time, pH, reversibility and long-term stability. In addition, the fabricated Ag-ISE was used in glucose and DNA biosensors.

1.3 Benefits of the Research

We have expected to obtain novel Ag-ISE that could be used for the first time in speciation analysis of AgNPs. Furthermore, the fabricated Ag-ISE could be applied in biosensors such as glucose and DNA biosensors by using AgNPs as cation marker.

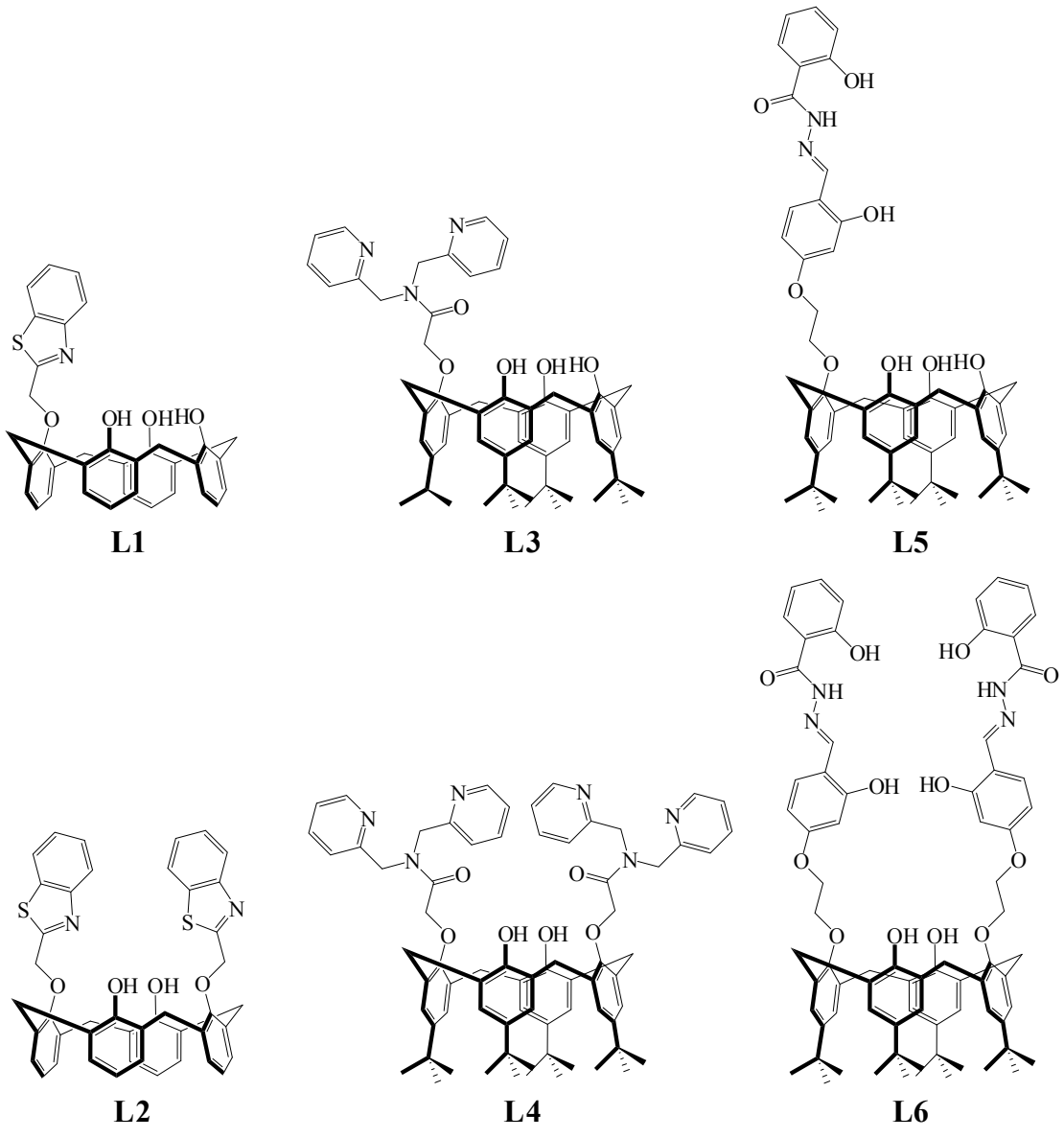

Figure 1.1 Structures of six synthesized ionophores (**L1** – **L6**).

CHAPTER II

THEORY AND LITERATURE REVIEWS

2.1 Ion Selective Electrodes (ISEs)

Ion selective electrodes (ISEs) are classified as potentiometric chemical sensors since some selective chemistry takes place at the surface of the electrode producing an interfacial potential [34]. The output of membrane electrical potential is proportional to the activity (or concentration) of the analyte whose the logarithmic value. Thus, the membrane must contain a component that will react chemically and reversibly with the analyte. This component is a receptor unit or carrier-based ISE, which has different structure and type of coordinate atoms to provide a variety of electrodes selective towards particular analyte ion. The binding between carrier-based ISE and analyte ion uses the basic of host-guest interaction or coordination chemistry.

The ISEs membranes are divided in four categories of membranes such as glass membranes, sparingly soluble inorganic salts membranes, polymer-immobilized ionophore membranes and gel-immobilized and chemically bonded enzyme membranes.

ISEs offer several advantages, especially cheap and simple device that can be compatible with miniaturization so they are one of the excellent tools in biomedical, industrial and environmental application fields. The polymeric membranes have been developed for determination of glucose concentration by using fluoride selective electrode as a detector for glucose in FIA system [35], a double enzymatic reaction with fluoride selective optical sensing coated in microtiter plate well [36], glucose oxidase entrapped in plasticized PVC of iodide ion selective electrode [37]. Recently, there has been increasing interest in the use of miniaturized ISEs for monitoring NADH [38], protein immonoassays [39] or DNA hybridization [40–42] in connection to Ag, CdS-nanocrystal labels, enzyme tags or liposomes.

2.1.1 Components of the polymeric ion selective electrodes

The ion-sensitive solvent polymeric membrane is physically a water immiscible liquid of high viscosity consisting of the components as listed below.

Polymer matrix

The polymeric membranes in ISEs are commonly prepared with PVC providing mechanical stability and elasticity to the membrane. In ideal cases it is inert and has no chemical interaction with the sensed ions.

Membrane solvent or plasticizer

The membrane solvent must be compatible with all membrane components to provide a homogenous organic phase. It should have high lipophilicity, high molecular weight, low tendency for exudation from polymeric membrane, low vapor pressure and high capacity to dissolve membrane components present in the polymeric membrane [43]. Although the plasticizers have different dielectric constants, structures and lipophilicity characteristics, they are usually used in polymeric liquid membranes, namely bis(2-ethylhexyl)sebacate (DOS, apolar) or ortho-nitrophenyl octyl ether (*o*-NPOE, polar) [44].

Ionic site additives

Lipophilic salts are cation or anion exchanger in ISE membranes to maintain membrane permselectivity (or Donnan exclusion) [45] that is ability of the membrane to allow only ions of the same charge as primary ion to pass resulting in the theoretical Nernstian response. Ionic sites also reduce membrane resistance and interference from counterions. Cation-selective membranes commonly used lipophilic tetraphenylborate salts while anion-selective systems employed tetraammonium derivatives.

Ionophore

Ionophore or ion carrier has the main important in the selectivity of ISE membrane. The ionophore can form complex with analyte ion and reversible complex to free ionophore with very fast reaction. The structure of ionophore must contain lipophilic groups to prevent the ionophore leaching from membrane to the sample phase.

2.1.2 Response mechanism

The potentiometric measurements consist of an ISE, a reference electrode and a potential-measuring device as shown in Figure 2.1. A reference electrode is an electrochemical half-cell which maintains virtually constant potential with respect to a solution.

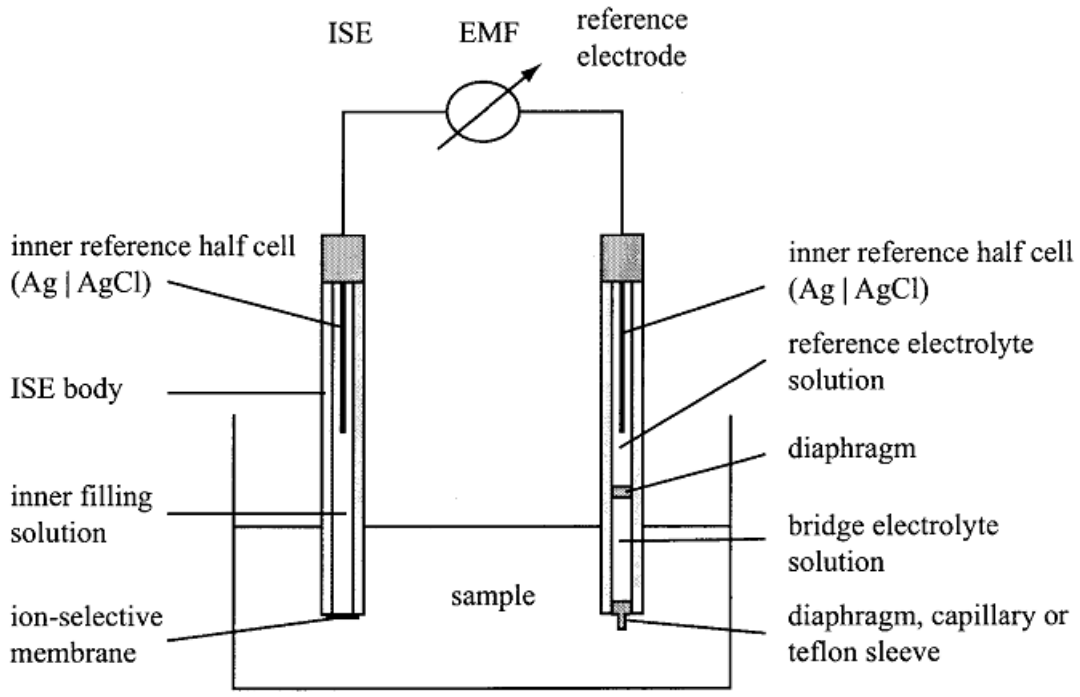

Figure 2.1 Schematic diagram of a potentiometric cell with an ISE [46].

The electromotive force (EMF) across the entire potentiometric cell is the sum of the individual potential contributions.

$$\text{EMF} = E_{\text{const}} + E_{\text{J}} + E_{\text{M}} \tag{2.1}$$

where E_{M} is the membrane potential, E_{J} is the liquid junction potential at the sample/bridge electrolyte interface which can be kept small and constant by using high concentration of bridge electrolyte (e.g., 1 M KCl, NH_4OH or LiOAc) according to the Henderson formalism [47–48] and E_{const} is the a constant contribution. The membrane potential (E_{M}) contains three separate potential contributions, i.e., the phase boundary potential at the membrane/sample solution interface ($E_{\text{PB}'}$), the phase boundary potential at the membrane/inner filling solution interface ($E_{\text{PB}''}$) and the diffusion potential within the membrane (E_{diff}).

$$E_{\text{M}} = E_{\text{PB}'} + E_{\text{PB}''} + E_{\text{diff}} \tag{2.2}$$

The potential at the membrane/inner filling solution interface is usually independent the sample. The diffusion potential within the membrane is negligible due to membranes showing a Nernstian response in most experiments.

$$E_{\text{M}} = E_{\text{const,1}} + E_{\text{PB}'} \tag{2.3}$$

Thus, the potential depends only on the phase boundary potential at the membrane/sample solution interface ($E_{\text{PB}'}$) arising from an unequal equilibrium distribution of ions between the aqueous sample and organic membrane phases. For aqueous solution containing ion I in equilibrium with the membrane, electrochemical potential, $\tilde{\mu}$, of the ion I aqueous phase is:

$$\tilde{\mu}(\text{aq}) = \mu(\text{aq}) + zF\phi(\text{aq}) = \mu^0(\text{aq}) + RT \ln a_{\text{I}}(\text{aq}) + zF\phi(\text{aq}) \tag{2.4}$$

and for the contacting organic phase:

$$\tilde{\mu}(\text{org}) = \mu(\text{org}) + zF\phi(\text{org}) = \mu^0(\text{org}) + RT \ln a_{\text{I}}(\text{org}) + zF\phi(\text{org}) \tag{2.5}$$

where μ is the chemical potential, μ^0 is chemical potential under standard conditions, z is the charge of the ion I, a_{I} is the activity of ion I, ϕ is the electrical potential, and R, T and F are the universal gas constant, the absolute temperature and the Faraday constant, respectively. It is now assumed that the interfacial ion transfer and

complexation processes are relatively fast so that the equilibrium holds at the interface, the electrochemical potentials for both phases are equal [45]. This leads to a simple expression for the phase boundary potential [49]:

$$-\frac{\mu^0(\quad g) - \mu^0(\quad)}{\quad} \quad \_\_ \quad \frac{\quad}{g}$$

where $\varnothing = \varnothing(\text{org}) - \varnothing(\text{aq})$. If $a_I(\text{org})$ is constant, it could be combined with other sample-independent terms into $E_{\text{const},2}$ and equation (2.6) reduce to the form of the Nernst equation.

__

Substitution of $E_{PB'}$ into equation (2.3) and (2.1) gives an equation describing the response of the ion selective electrode towards ion I in aqueous solution:

$$^0 \quad \_\_$$

where is a new constant including all sample-independent potential in a cell. The Nernstian slope of the response function is 2.303 RT/z_IF = 59.2 mV/z_I for z = 1 at 298 K.

In order to obtain exact Nernstian response of the electrode for uncharged carriers, the ion-exchange mechanism between the organic and aqueous phases is controlled by lipophilic anionic additive to ensure permselectivity. This process is shown schematically in Figure 2.2 for neutral ionophores based on ISE.

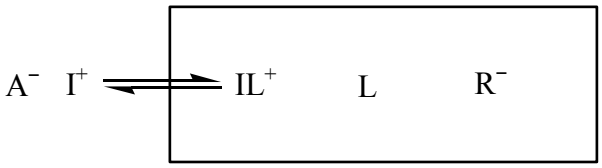

Figure 2.2 Neutral-carrier-based ion selective electrode with neutral (L, neutral carrier; R^-, negatively charged ionic sites). Square indicates species in the organic phase.

2.1.3 Electrode characteristics

2.1.3.1 Selectivity

Selectivity is one of the most important characteristic f SE d i defi e d as the degree of discrimination of an electrode to ions in solution other than the primary ion [50–52]. According to the Nicolskii-Eisenman formalism [53–54], the activity term in the Nernst equation is replaced by a sum of selectivity-weighted activities:

0 —

where a_I(IJ) and a_J(IJ) are the activities of primary ion I and interfering ion J in the mixed m e The Ni ki i e ffi ie , is the potentiometric selectivity e ffi ie for I over J. f he e ffi ie v ue i m i e d he g d selectivity of the electrode. When is very small and a_I(IJ) approaches the primary-ion activity a_I(I) in a solution without interfering ions according to the following equation:

( ) (2.10)

it means that there is no interference. If interference is observed, a lower activity a_I(IJ) of the mixed sample will give the same response as the activity a_I(I) of a solution containing no interfering ions.

For carrier-based ISEs, the selectivity is determined by the composition of the membrane. The relationship between the ion selectivity and the membrane composition of cation selective electrodes is explained in equation (2.11) considered from charge balance and mass balance [55].

$$\frac{(\quad)}{} \quad \frac{\bar{\quad}_T}{[\ _T - \ (\bar{\ }_T\ )]} \quad \left(\frac{[\ _T - \ (\bar{\ }_T\ )]}{_T}\right)$$

where K_{IJ} is the equilibrium constant for the ion exchange between the uncomplexed primary and interfering ions between the sample and the membrane phase, L_T and R_T are the total concentrations of ionophore and anionic site, z_I and z_J the charge of the primary ion and interfering ion, respectively, while is the complex formation constant of the ion–ionophore complex and n the complex stoichiometry.

Separate solution method (SSM)

Separate solution method is always used to determine the selectivity of an ISE as illustrated in Figure 2.3. The SSM concerns the measurement of two separate solutions, each containing the primary ion and interfering ion. The selectivity is calculated from the following equation:

$$g \qquad \frac{\{\ (\ )-\quad\}}{} \quad g\left(\frac{\quad}{\quad}\right)$$

where E(J) and E(I) are the recorded potentials in separate solutions for primary ion I and interfering ion J and a_I(I) and a_J(J) the activities of I and J in separate solutions. The b i e d e e ivi y e ffi ie values are e u he he m dy mi y defi e d ones as long as the response slopes of all of the ions are Nernstian.

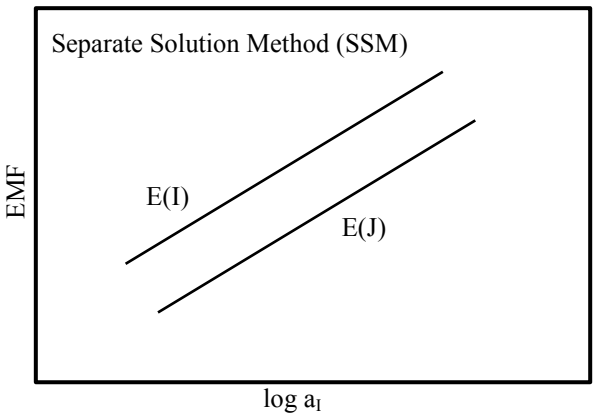

Figure 2.3 Schematic representation of ion selective electrode selectivity as determined by the separation solution method [56].

Fixed interference method (FIM) or Mixed interference method

In this method, an entire calibration curve for the primary ion is measured in the presence of an interfering ion which is fixed activity as the background (Figure 2.4). a_J(BG) is the activity of the constant interfering ion in the background. a_I(DL) is the low detection limit (LDL) of the Nernstian response curve of the electrode as a function of the primary ion activity. The selectivity of FIM is calculated from

g g ( )

The SSM and FIM require Nernstian response of both interfering ion and primary ion [45, 51–52].

Matched potential method (MPM)

In the MPM, a known amount of primary ions is added to a reference solution and the potential is measured. Another experiment, interfering ions are gradually added to an identical reference solution until the membrane potential matches with the other one obtained from the primary ion. The selectivity is calculated from the following equation:

g —

The advantage of this approach is that it can be used when the response of the electrode is not Nernstian or even linear. However, the drawback is that the selectivity e ffi ie m y h g e u de diffe e ex e ime di i i u y he concentrations at which the measurements were made. In most situations, the selectivity obtained from matched potential method cannot be directly compared to the values obtained from other methods.

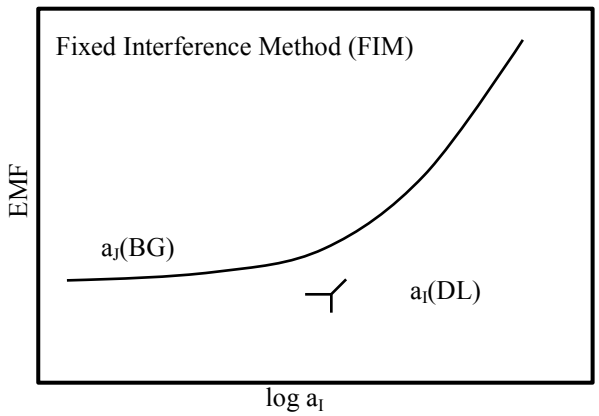

Figure 2.4 Schematic representation of ion selective electrode selectivity as determined by he fixed i e fe e e me h d [56].

2.1.3.2 Detection limits

Deviations of the electrode function from the linear response are normally observed at high and low activities of the measuring ion. According to the IUPAC recommendation [50], the detection limits are defined by the cross-section of the two extrapolated linear calibration curves as illustrated in Figure 2.5.

The upper detection limit is caused by the coextraction process of primary ion and interfering counterion from the sample into the membrane resulting in a loss of membrane permselectivity (so-called Donnan failure). Activity of membrane phase increases with increasing the activity of sample but the EMF difference is smaller than expected by the Nernst equation.

The lower detection limit can be dictated by two processes:

(a) the interference of a competing ion present in the sample. In this case the detection limit a_I(DL) is related to the Nikolsky equation (2.9) and is given by:

( ) (2.15)

(b) the leaching of primary ions from the membrane phase into the sample.

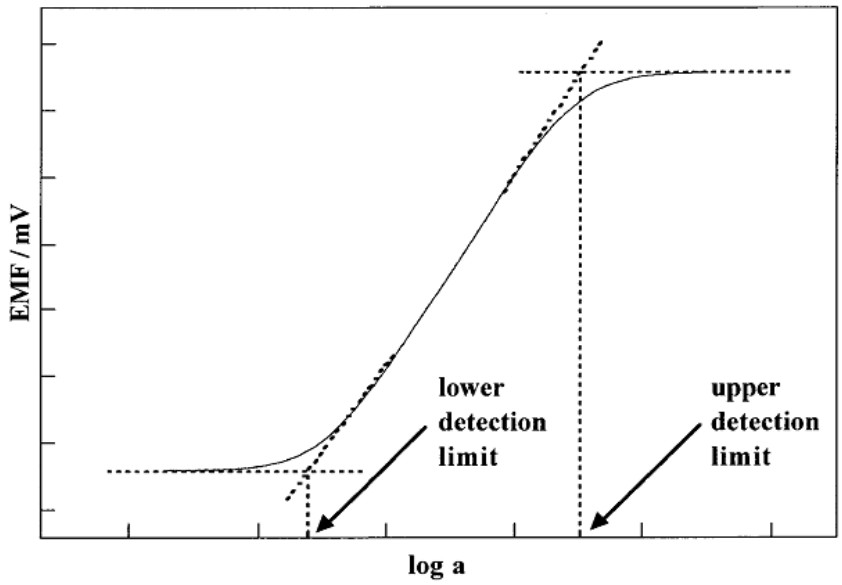

Figure 2.5 The detection limits of an ion selective electrode are defined according to the IUPAC recommendations [50] by the cross-section of the two extrapolated linear segments of the calibration curve.

2.1.3.3 Response time

The repose time is another important characteristic of the ISE. According to IUPAC [57], response time (E/ t) is the length of time which elapses between the instant when an ISE and the reference electrode are brought into contact with a sample solution (or at which the activity of the ion of interest in a solution is changed) and the first instant at which the EMF/time slope (E/ t) becomes equal to its steady-state value within 1 mV. The stirring rate and the composition of solution should be controlled in all experiments.

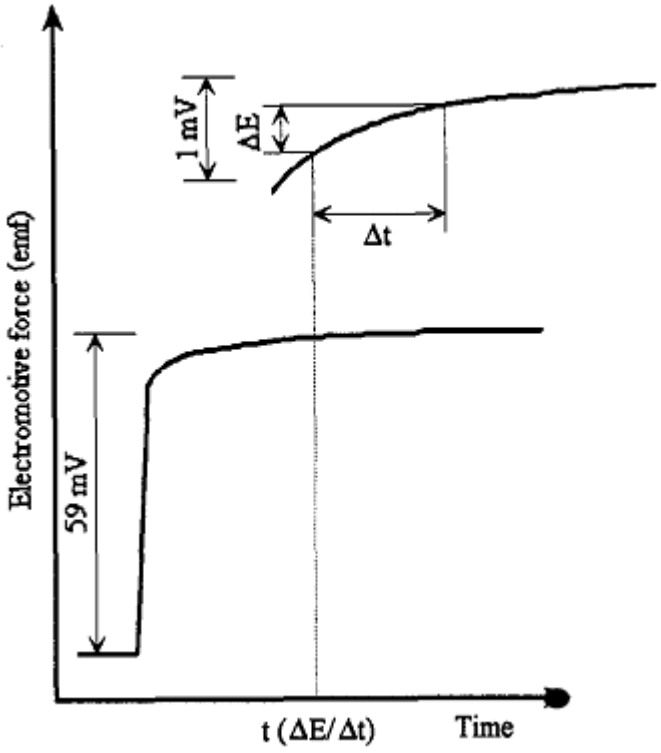

Figure 2.6 Definition and determination of response time t(E/ t) [57].

2.2 Ionophore for Silver(I) Ion Selective Electrodes

A variety of ionophores with different functional groups have been used to construct PVC-based membrane electrodes for Ag^+ for monitoring and determination of Ag^+ [7–30]. Structures of these ionophores containing π-electrons [22–23] or heteroatoms [7–21, 24–30] as a recognition unit for binding Ag^+ are shown in Figure 2.7 – 2.9. The response characteristics of some ionophores are summarized in Table 2.1.

Table 2.1 The response characteristics of some ionophores of reported Ag-ISE.

Ionophore	Linear working range (M)	Slope (mV decade^{-1})	Response Time (s)	Working pH range	Lifetime	Application	Ref.
A1	$5.0 \times 10^{-6} - 1.0 \times 10^{-2}$	56	< 10	3.0 – 8.5	1 month	Potentiometric titration of NaCl	[7]
A2	$1.0 \times 10^{-6} - 1.0 \times 10^{-3}$	60.2	< 20	2.0 – 8.0	1 month	Potentiometric titration of $AgNO_3$ with Cl^- in vitamin B_1 tablets and determination of Ag^+ in water samples	[8]
A3	$2.0 \times 10^{-8} - 1.0 \times 10^{-2}$	59.1 ± 0.7	10	2.5 – 8.7	2 months	Potentiometric titration of Ag^+ with Cl^- and determination of silver in suphadiazine cream and in fruit juice matrixes	[9]
A4	$5.5 \times 10^{-6} - 1.0 \times 10^{-1}$	59	14	2.0 – 9.5	–	Potentiometric titrations of Ag(I) ions	[10]
A5	$1.0 \times 10^{-5} - 1.0 \times 10^{-2}$	58.5 ± 1.0	< 2	–	> 1 month	–	[11]
A6	$1.0 \times 10^{-7} - 1.5 \times 10^{-2}$	59.5 ± 0.8	< 10	3.7 – 9.0		Potentiometric titration of vitamin B_1 with $AgNO_3$ solution	[12]

Table 2.1 The response characteristics of some ionophores of reported Ag-ISE (cont.).

Ionophore	Linear working range (M)	Slope (mV decade^{-1})	Response Time (s)	Working pH range	Lifetime	Application	Ref.
A7	$1.9 \times 10^{-6} - 2.7 \times 10^{-2}$	56.2 ± 0.7	5	2.5 – 7.0	6 weeks	Potentiometric titration of Ag^+ with KI and determination of silver in spiked wastewater and radiology film	[13]
A8	$1.0 \times 10^{-6} - 1.0 \times 10^{-1}$	59.3	< 5	4.0 – 10.0	1 month	Potentiometric titration of halides with Ag^+ and the determination of silver in radiology films	[14]
A9	$1.0 \times 10^{-6} - 1.0 \times 10^{-3}$	59.1 ± 0.5	20	3.0 – 7.0	2 months	Potentiometric titration of silver with iodide ion and determination of Ag^+ in waste water, photographic emulsion and radiographic and photographic fi m	[15]

Table 2.1 The response characteristics of some ionophores of reported Ag-ISE (cont.).

Ionophore	Linear working range (M)	Slope (mV decade^{-1})	Response Time (s)	Working pH range	Lifetime	Application	Ref.
A10	$1.0 \times 10^{-9} – 1.0 \times 10^{-5}$	54.5	–	–	25 days	Potentiometric titration of the mixture of chloride, bromide and iodide ions with $AgNO_3$ and determination of Ag^+ in spiked tap water	[16]
A11	$1.26 \times 10^{-6} – 1.00 \times 10^{-1}$	58.4 ± 0.1	10	2.2 – 8.5	3 months	Potentiometric titration of Ag^+ and determination of Ag^+ in waste from photographic films	[17]
A12	$5.0 \times 10^{-5} – 5.0 \times 10^{-1}$	55.4 ± 2	< 30	–	3 months	–	[18]
A13	$5.6 \times 10^{-8} – 1.0 \times 10^{-1}$	59.3	12	3.0 – 8.0	4 months	Determination of silver in blood samples of occupationally exposed persons	[19]
A14	$6.0 \times 10^{-3} – 3.2 \times 10^{-3}$	59 ± 1	< 10	2.0 – 7.5	–	Potentiometric titration of Ag^+	[20]

Table 2.1 The response characteristics of some ionophores of reported Ag-ISE (cont.).

Ionophore	Linear working range (M)	Slope (mV decade^{-1})	Response Time (s)	Working pH range	Lifetime	Application	Ref.
A15	$1.0 \times 10^{-6} – 1.0 \times 10^{-2}$	> 50	8	–	< 2 weeks	–	[21]
A16	$1.0 \times 10^{-5} – 1.0 \times 10^{-1}$	56	–	–	–	–	[22]
A17	$1.0 \times 10^{-4} – 1.0 \times 10^{-1}$	58.3 ± 0.7	fast	–	–	As Ag^+ assay in model samples for waste fixing solutions for photography	[23]
A18	$5.0 \times 10^{-6} – 1.0 \times 10^{-2}$	57	< 10	2.5 – 7.0	1 month	Potentiometric titration of Br^- and Cl^- with Ag^+	[24]
A19	$1.0 \times 10^{-5} – 1.0 \times 10^{-1}$	59.0	20	1.0 – 6.5	> 6 months	Potentiometric titration of $AgNO_3$ with NaCl and analysis of water samples spiked with silver(I)	[25]
A20	$5.0 \times 10^{-6} – 5.0 \times 10^{-2}$	53.2	< 10	2.5 – 7.0	1 month	Potentiometric titration of Ag^+ with Cl^- ions	[26]
A21	$5.0 \times 10^{-8} – 1.0 \times 10^{-1}$	61.4	5 – 10	3.0 – 7.0	At least 1 month	Potentiometric titration of Ag^+ solution with NaCl	[27]

Table 2.3 The response characteristics of some ionophores of reported Ag-ISE (cont.).

Ionophore	Linear working range (M)	Slope (mV decade^{-1})	Response Time (s)	Working pH range	Lifetime	Application	Ref.
A22	$1.0 \times 10^{-6} – 1.0 \times 10^{-2}$	53.8 ± 1.6	5 – 10	2.0 – 6.0	At least 2 months	Potentiometric titration of a mixture of KI, KBr, KCl with $AgNO_3$	[28]
A23	$<10^{-3}$	58.6	<10	2.5 – 7.0	–	–	[29]
A24	$1.26 \times 10^{-7} – 6.31 \times 10^{-3}$	50.5	<12	–	–	–	[30]

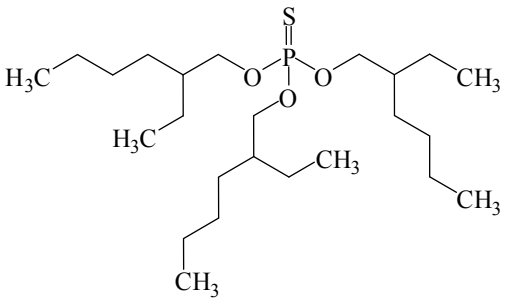

A1

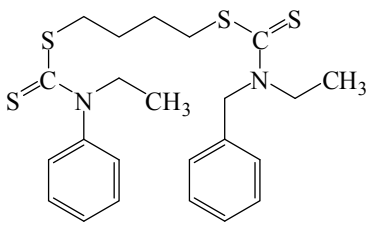

A2

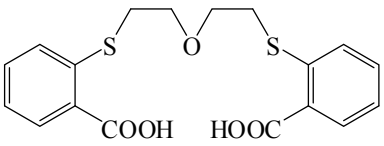

A3

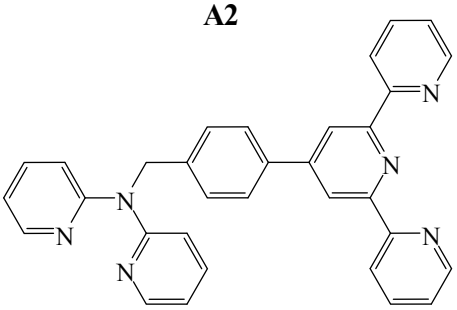

A4

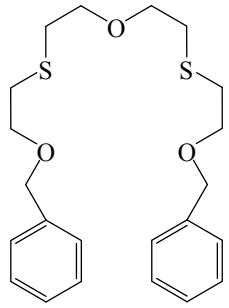

A5

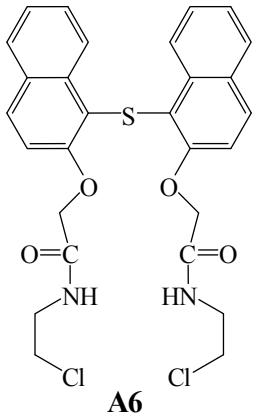

A6

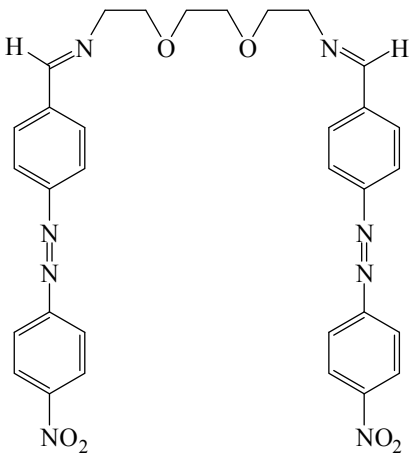

A7

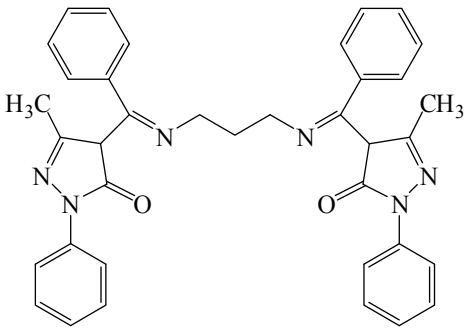

A8

Figure 2.7 Some ionophores based on non-macrocyclic for Ag-ISEs.

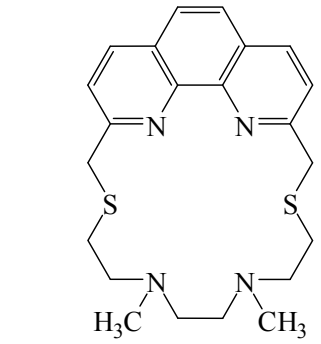

A9

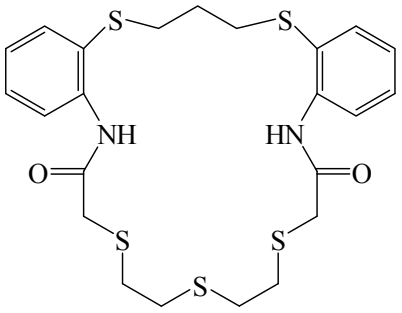

A10

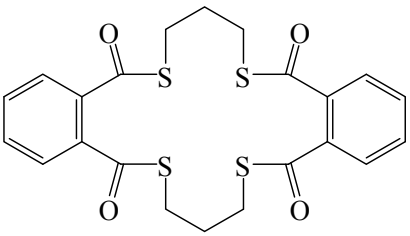

A11

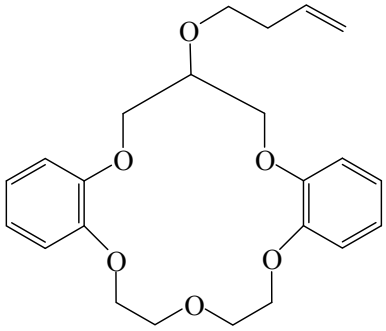

A12

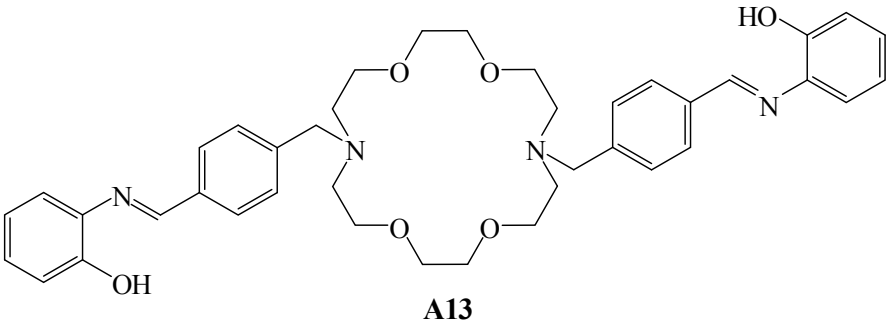

A13

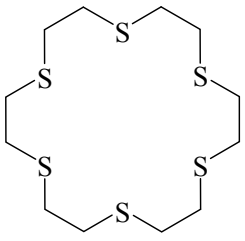

A14

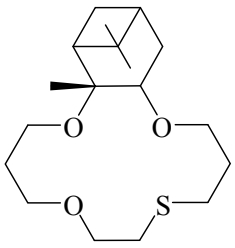

A15

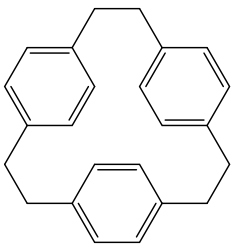

A16

Figure 2.8 Some ionophores based on macrocyclic for Ag-ISEs.

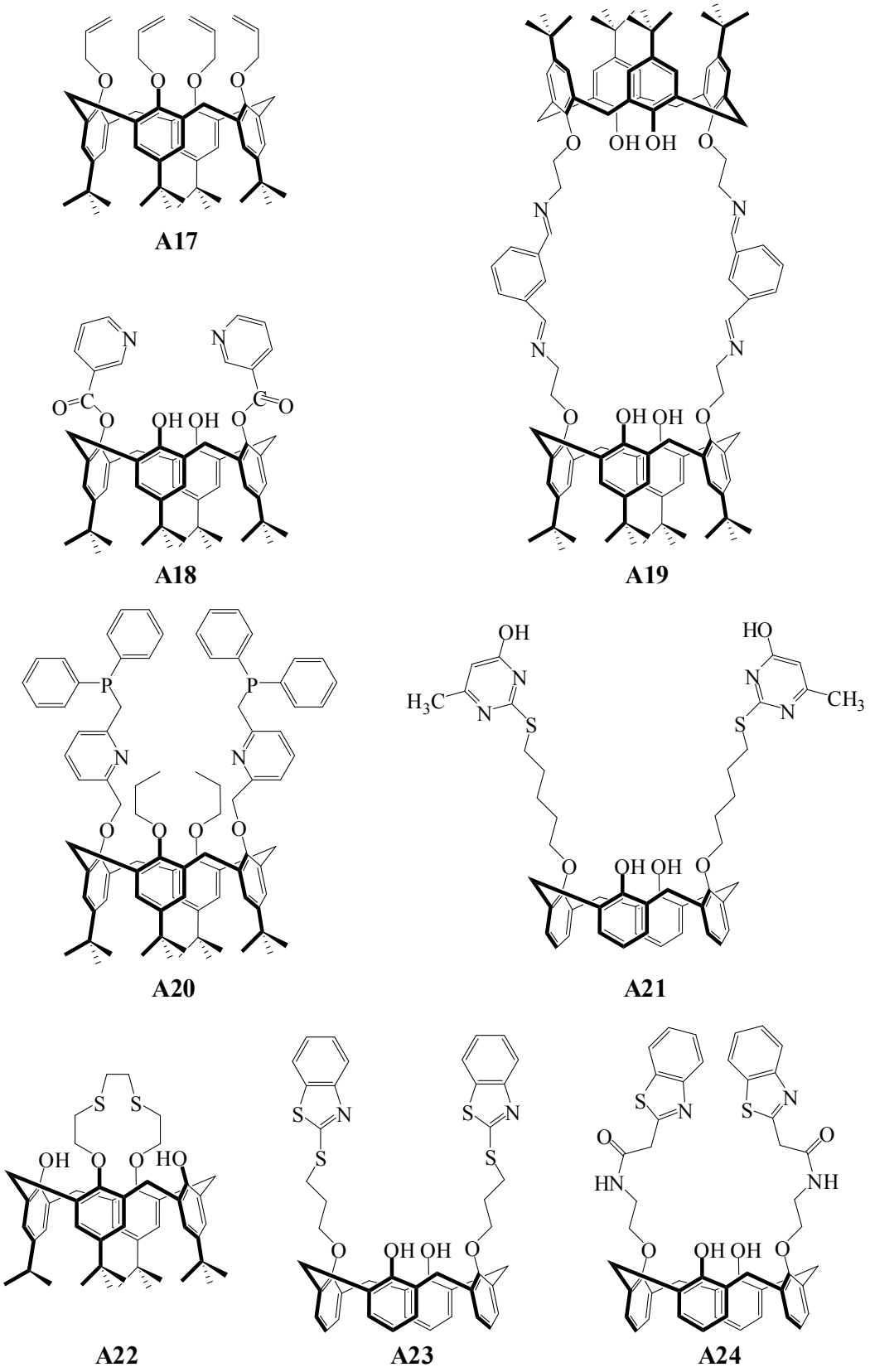

Figure 2.9 Some ionophores based on calixarene for Ag-ISEs.

2.3 Application based on Polymeric Membrane

The polymeric membranes have been used successfully for the direct determination the activity of ion in solution and/or applied as indicator electrode in potentiometric titration. Polymeric membranes can be used in advance applications for biological and clinical detections, for example, the use of polymeric membranes to detect glucose concentration. Polymeric membrane fluoride-selective electrodes based on zirconium(IV) 5,10,15,20-tetraphenylporphyrin were developed as a detector in a flow-injection analysis (FIA) system for glucose determination [35]. This FIA system was used with a flow-through reactor containing immobilized enzymes (glucose oxidase (GOD) and horseradish peroxidase (HRP)) which produced fluoride anions and could be detected with the ISE. Fluoride anions were generated from fluoroorganic compound reacting with H_2O_2 as shown in equation 2.16 – 2.17. The ionophore-based electrode as a detector in enzymatic FIA system could be applied to determine glucose concentration in synthetic samples.

$$\text{glucose} + O_2 \xrightarrow[\text{oxidase}]{\text{glucose}} \text{gluconic acid} + H_2O_2 \qquad (2.16)$$

$$H_2O_2 + \text{fluoroorganic compound} \xrightarrow{\text{peroxidase}} F^- + \text{derivative of fluorooganic compound} \qquad (2.17)$$

Abd-Rabboh and Meyerhoff [36] developed highly selective fluoride sensing optical film containing aluminium(III) octaethylporphyrin (Al[OEP]) ionophore and the chromoionophore ETH7075 within a thin polymeric film coated at the bottom wells of a 96-well polypropylene microtiter plate for determination glucose in beverages (Figure 2.10). A double enzymatic reaction of GOD and HRP was used to catalyze the oxidation of 4-fluorophenol which then released fluoride ions corresponded to the concentration of glucose with a linear range of 0.9 – 40 mmol L^{-1}. Besides, H_2O_2 producing from glucose and GOD can also be detected by this method in the

range of 0.1 – 50 mmol L^{-1} involving H_2O_2 oxidation of 4-flu he yzed by HRP.

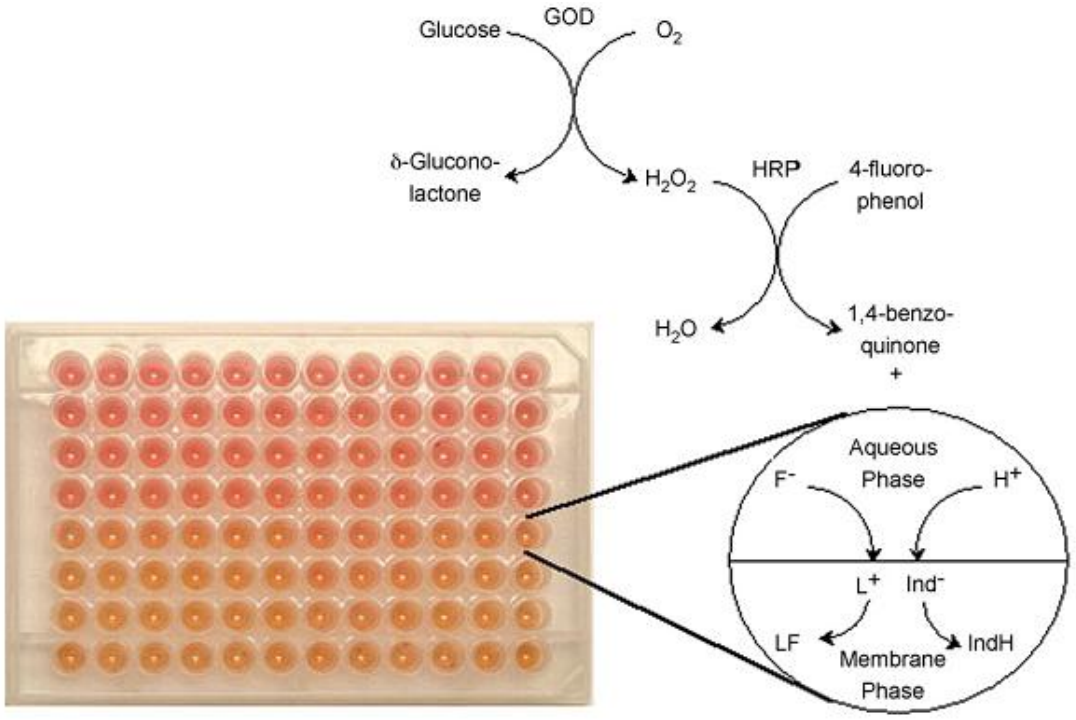

Figure 2.10 ie z ym i hw y flu ide i -membrane response mechanism, and a picture of the U-shaped 96-well microtiter plate with the optical membranes [36].

A new potentiometric glucose sensor based on GOD immobilized on an iodide i e e ive e e d e w i du ed by K y ı d -workers [37]. Glucose concentration in the system was determined by the decrease of iodide concentration which reacted with H_2O_2 generating from the reaction of glucose (equation 2.16 and 2.18).

$$H_2O_2 + 2I^- \xrightarrow{\text{Mo(VI)}} I_2 + H_2O \qquad (2.18)$$

The iodide electrode showed linear response in the 4×10^{-4} to 4×10^{-3} M glucose concentration (75 – 650 mg/100 mL blood) range with a slope of about 79 mV decade^{-1} in blood serum with high accuracy and precision.

The conventional ISEs have been demonstrated using in glucose sensors by many researchers [35–37]. The miniaturized- and micro-sized ISEs have been developed to reduce the size of conventional ISEs and use in small volume applications to detect small amounts of compounds. Then, the simple miniaturization of ISEs was applied in DNA biosensors [40–42]. Numnuam and co-workers [40] illustrated for the first time the use of potentiometric microsensors for detecting DNA hybridization. The use of Cd^{2+}-selective microelectrodes was monitored DNA hybridization for capturing a secondary oligonucleotide bearing CdS-nanocrystal tags, which was dissolved in H_2O_2 as shown in Figure 2.11. The miniaturized solid contact Cd-ISE exhibited lower detection limit of 10^{-9} M Cd^{2+} in samples of 200 μL microwells, using a calcium ion selective electrode as a pseudo reference electrode. The method can discriminate signals between complementary DNA, 2-base mismatch DNA and noncomplementary DNA. The target DNA showed a dynamic range of 0.01 – 300 nM in 200 μL sample with a lower detection limit of 10 pM.

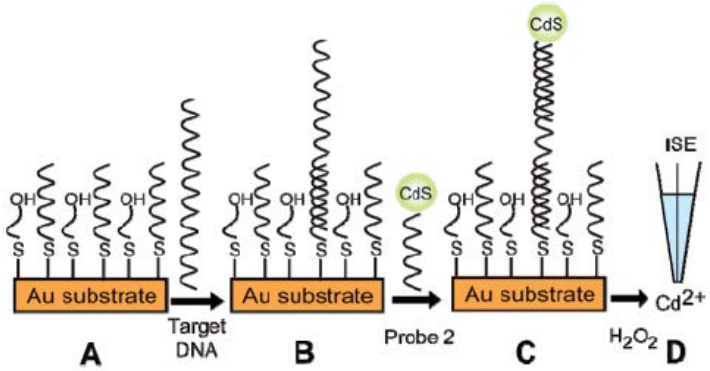

Figure 2.11 Schematic steps involved in the nanoparticle-based potentiometric detection of DNA hybridization [40].

Wu and co-workers [41] reported on a highly sensitive potentiometric DNA hybridization for detecting the decrement of Ag^+ that were induced by the alkaline-phosphatase enzyme tag in the presence of AuNPs as shown in Figure 2.12.

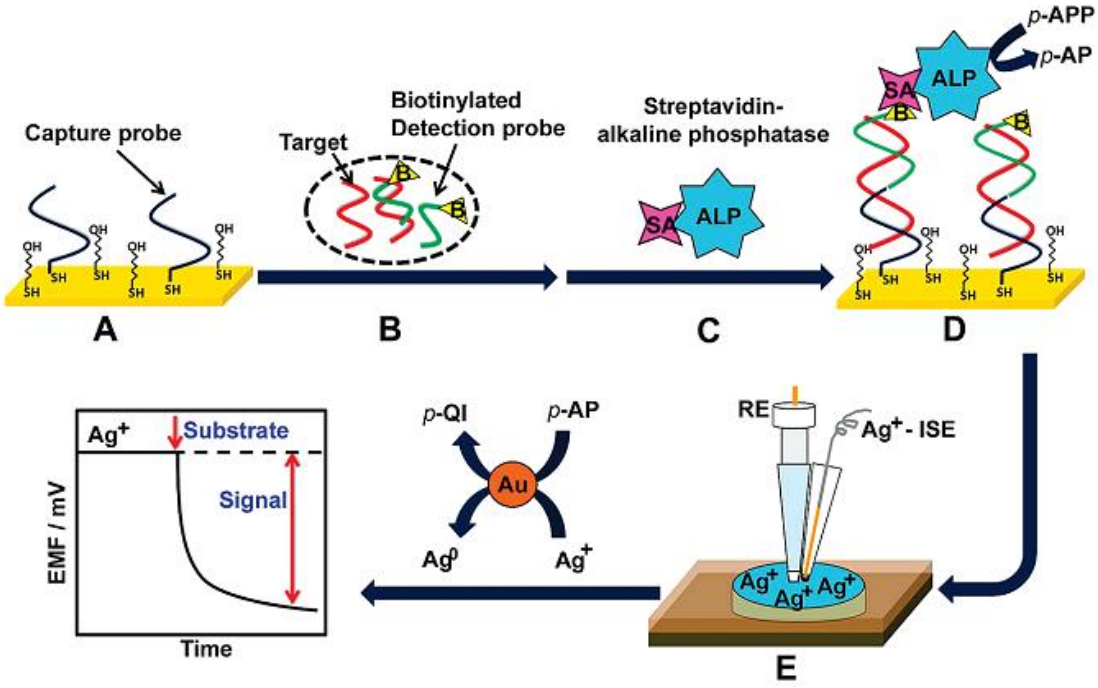

Figure 2.12 Representation of the potentiometric detection of DNA hybridization [41].

Figure 2.12 shows step (A) formation of the mixed thiol monolayer (thiolated DNA capture probe and MCH) on the gold substrate; (B) hybridization of the target DNA/biotinylated detection-probe mixture with the surface capture probe; (C) binding of the SA-ALP enzyme; (D) addition of the ALP substrate to initiate the enzymatic reaction, and (E) potentiometric detection of changes in the level of the Ag^+ upon adding an aliquot of the enzymatic reaction mixture to the Ag-ISE cell. Such potentiometric DNA assay was applied successfully to monitor the 16S rRNA of *E. coli* pathogenic bacteria in micro-volume down to 4 µL sample with a low detection limit 10 CFU.

The u e i m e ‘ ie ’ f m ified e i m e i bi detection of DNA hybridization was reported [42]. As illustrated in Figure 2.13, a sandwich hybridization on gold surface was followed by the capture of calcium-loaded liposomes and added a surfactant for releasing calcium signaling ions measured using a Ca^{2+}-ISE. The ion-loaded liposome resulted in DNA detection limits down to sub-femtomole. The new potentiometric bioassay can also be applied for the detection of low levels of *E. coli* bacteria. This system offers further advantages as calcium ig i g i w ‘g ee ’ m ed wi h he x i Ag d CdS i e g used previously in potentiometric bioassays [40–41].

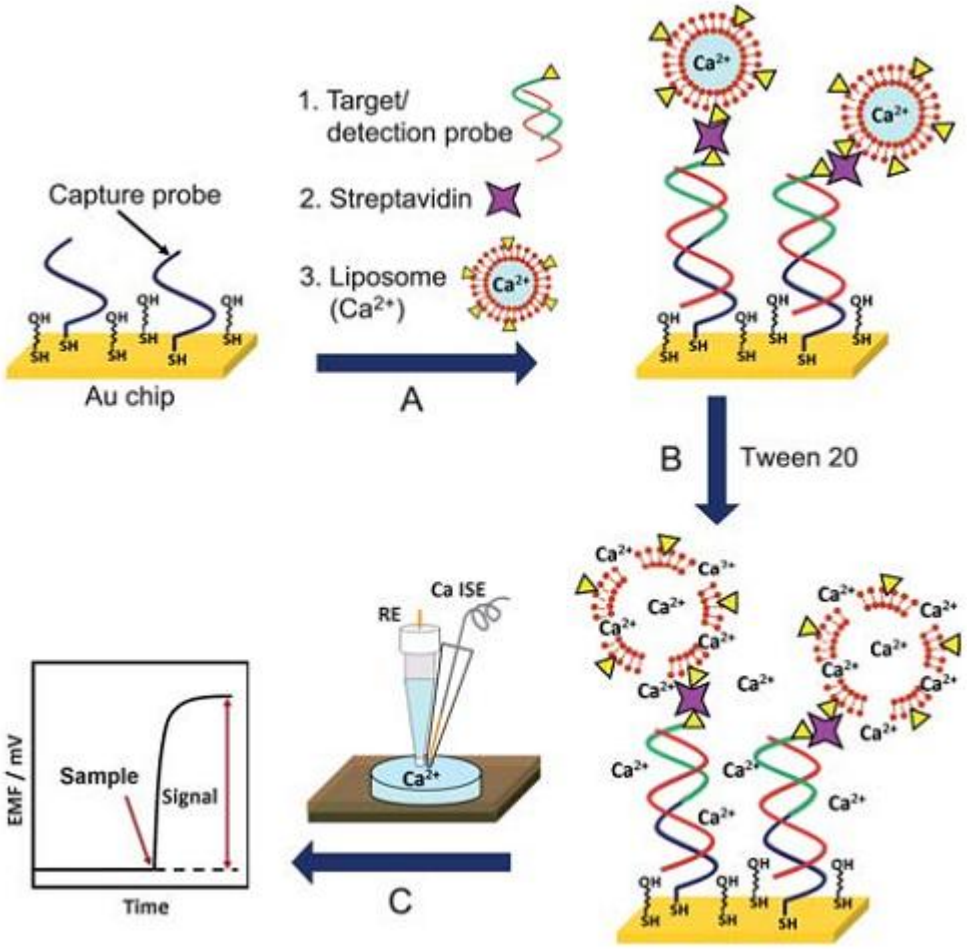

Figure 2.13 Representation of the potentiometric detection of DNA hybridization based on ion-loaded liposomes and Ca^{2+}-ISE [42].

CHAPTER III

EXPERIMENTAL

3.1 General Procedures

3.1.1 Apparatus

Nuclear magnetic resonance (NMR) spectra were recorded on a varian Mercury Plus 400 MHz nuclear magnetic resonance spectrometer. MALDI-TOF mass spectra were recorded on a Micromass Platform II. Absorption spectra were obtained from a Varian Cary 50 Probe UV-Vis spectrophotometer. A 16-channel electrode monitor (Lawson Labs Inc., Malvern, PA 19355, USA) was used to record EMF measurements. A reference electrode Ag/AgCl (Metrohm 6.0726.100) was used with 1 M LiOAc as salt bridge electrolyte. pH values were determined with an Orion 2-Star Benchtop pH meter (Thermo Fisher Scientific).

3.1.2 Materials

All materials and reagents were standard analytical grade, and used without further purification. Commercial grade solvents such as methanol, dichloromethane, hexane and ethyl acetate were purified by distillation. Acetonitrile, dichloromethane and toluene were dried over CaH_2 and freshly distilled under nitrogen for set up the reaction. Column chromatography was carried on silica gel (Kieselgel 60, 0.063-0200 mm). Thin layer chromatography (TLC) was performed on silica gel plates (Kieselgel 60, F_{254}, 1 mm). Compounds on TLC plates were monitored by the UV-light.

Chemicals used for membrane preparation (KT*p*ClPB, DOS, *o*-NPOE, PVC, THF) were purchased in selectophore® grade form Fluka. All solutions used in ISE experiments were prepared with Milli-Q (Bedford, MA, USA) water using Nanopure Millipore water purification system.

Glucose oxidase from *Aspergillus niger* (GOx, EC 1.1.3.4, 208.17 U mg^{-1}), β-D-Glucose from Sigma-Aldrich, magnesium acetate tetrahydrate ($Mg(OAc)_2 \cdot 4H_2O$), fructose and sucrose from Fluka and urea and glycine from Merck were used for glucose biosensor.

Materials used for DNA biosensor, all oligonucleotides were purchased from Biogenomed Co., Ltd. The sequences of complementary DNA target, single base mismatched DNA target and non-complementary DNA target were 5′-GTCATAGCATCA-3′, 5′-GTCATCGCATCA-3′ and 5′-AAGGCCTATGTC-3′, respectively. Cetyltrimethylammonium bromide (CTAB) and sodium borohydride ($NaBH_4$) were obtained from Merck. Hydrogen peroxide (H_2O_2) was purchased from Fisher Scientific. Gold substrates were obtained from Sigma-Aldrich.

3.2 Synthesis of the Ionophores

p-tert-Butylcalix[4]arene (**1**) and calix[4]arene (**2**) were prepared according to the previously described procedures [58–59]. The reactions are outlined below.

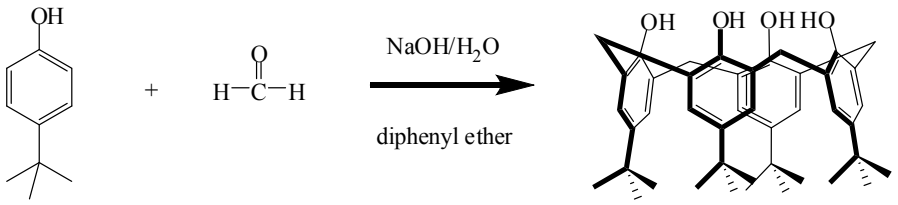

1 (46%)

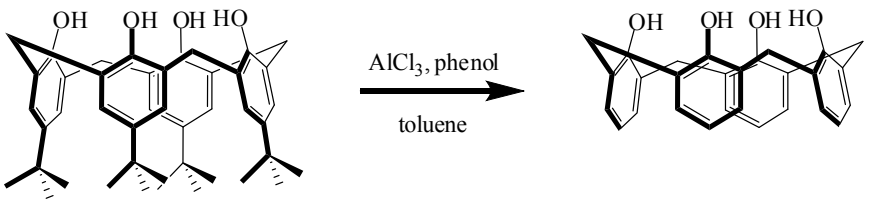

1 **2** (77%)

3.2.1 Synthesis of compound 3

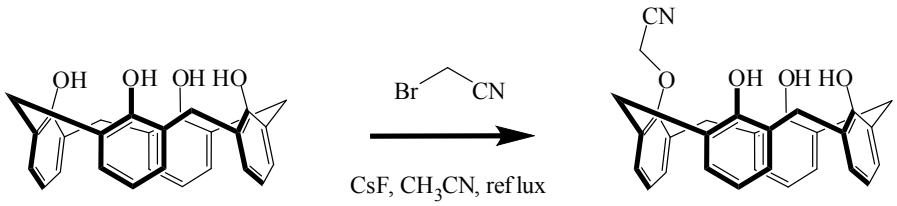

2 **3** (22%)

Compound **2** (5.06 g, 11.92 mmol) and cesium fluoride (2.34 g, 15.41 mmol) were added in 120 mL acetonitrile, and the mixture was stirred under nitrogen at room temperature for 1 h. Bromoacetonitrile (2.25 g, 18.84 mmol) was slowly added and the mixture was heated at reflux for 7 h. The mixture was cooled to room temperature and then filtered. The filtrate was evaporated to reduce the volume of the solution. Methanol was then added to precipitate a crude product which was purified by silica gel chromatography using 100% dichloromethane as an eluent to obtain compound **3** (1.21 g, 22%).

Characterization data for **3**:

^{1}H NMR spectrum (400 MHz, $CDCl_3$, ppm): δ 9.25 (s, 1H, ArO*H*), 8.41 (s, 2H, ArO*H*), 7.10–7.04 (m, 6H, Ar*H*), 6.98 (d, 2H, *J* = 7.2 Hz, Ar*H*), 6.94 (t, 1H, *J* = 7.6 Hz, Ar*H*), 6.72–6.66 (m, 3H, Ar*H*), 5.02 (s, 2H, CH_2CN), 4.33 (d, 2H, *J* = 13.2 Hz, ArCH_2Ar), 4.22 (d, 2H, *J* = 14.0 Hz, ArCH_2Ar), 3.57 (d, 2H, *J* = 13.6 Hz, ArCH_2Ar), 3.48 (d, 2H, *J* = 13.6 Hz, ArCH_2Ar).

^{13}C NMR spectrum (100 MHz, $CDCl_3$, ppm): δ 150.76, 150.23, 148.74, 133.47, 130.10, 129.18, 128.88, 128.44, 128.37, 128.12, 127.57, 122.16, 121.09, 114.54, 60.49, 31.75, 31.58.

MALDI-TOF (*m/z*): $[M]^+$ Calcd for $[C_{30}H_{25}NO_4]^+$, 463.178; Found, 463.852.

3.2.2 Synthesis of compound L1

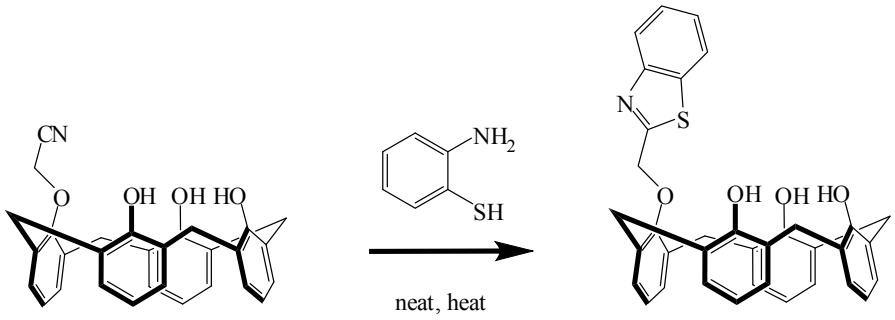

3 **L1** (71%)

Compound **3** (0.62 g, 1.08 mmol) was mixed with excess of 2-aminothiophenol. The reaction mixture was stirred and refluxed for 3 h under nitrogen. The reaction mixture was then cooled to room temperature. Dichloromethane (50 mL) was added into the mixture, and methanol was subsequently added to precipitate the crude product. Then, the solid was recrystallized with methanol for several times to give **L1** as a gray solid (0.44 g, 71%).

Characterization data for **L1**:

^{1}H NMR spectrum (400 MHz, $CDCl_3$, ppm): δ 9.59 (s, 1H, ArO*H*), 9.11 (s, 2H, ArO*H*), 8.16 (d, 1H, *J* = 7.6 Hz, Ar*H*), 8.07 (d, 1H, *J* = 7.6 Hz, Ar*H*), 7.59 (t, 1H, *J* = 8.2 Hz, Ar*H*), 7.49 (t, 1H, *J* = 8.2 Hz, Ar*H*), 7.15–7.02 (m, 8H, Ar*H*), 6.95 (t, 1H, *J* = 7.6 Hz, Ar*H*), 6.72 (t, 3H, *J* = 7.6 Hz, Ar*H*), 5.62 (s, 2H, ArOCH_2), 4.49 (d, 2H, *J* = 13.2 Hz, ArCH_2Ar), 4.31 (d, 2H, *J* = 13.6 Hz, ArCH_2Ar), 3.52 (t, 4H, *J* = 14.2 Hz, ArCH_2Ar).

^{13}C NMR spectrum (100 MHz, $CDCl_3$, ppm): δ 165.79, 152.72, 151.20, 150.94, 149.10, 135.48, 133.94, 129.74, 128.95, 128.89, 128.67, 128.44, 128.18, 128.01, 126.79, 126.53, 125.79, 123.46, 122.20, 122.03, 120.91, 75.23, 31.89, 31.48.

HRMS-ESI (positive mode, *m/z*): $[M + H]^+$ Calcd for $[C_{36}H_{29}NO_4S + Na]^+$, 594.1710; Found, 594.1681.

3.2.3 Synthesis of compound **4** [60]

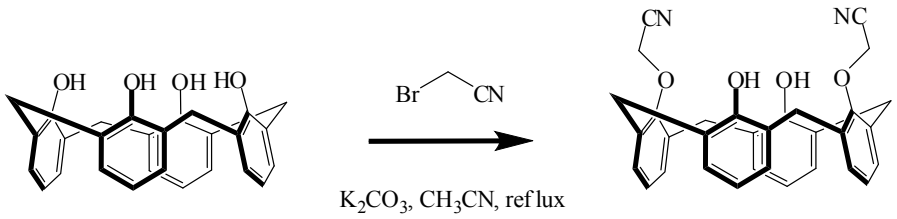

2 **4** (60%)

In a 250 mL two-necked round bottom flask equipped with a magnetic bar, compound **2** (5.00 g, 11.80 mmol), potassium carbonate (4.60 g, 33.20 mmol) and acetonitrile (120 mL) were stirred under nitrogen at room temperature for 1 h. Bromoacetonitrile (6.20 g, 51.60 mmol) was then added and the mixture was heated at reflux for 7 h. The mixture was cooled to room temperature and filtered. The filtrate was evaporated to reduce the volume of the solution. Methanol was then added to precipitate compound **4** as a white solid (3.60 g, 60%).

Characterization data for **4**:

^{1}H NMR spectrum (400 MHz, $CDCl_3$, ppm): δ 7.13 (d, 4H, *J* = 7.2 Hz, Ar*H*) 6.83 (d, 4H, *J* = 7.6 Hz, Ar*H*) 6.79–6.73 (m, 4H, Ar*H*) 6.02 (s, 2H, ArO*H*) 4.85 (s, 4H, CH_2CN) 4.26 (d, 4H, *J* = 13.6 Hz, ArCH_2Ar) 3.52 (d, 4H, *J* = 13.6 Hz, ArCH_2Ar).

^{13}C NMR spectrum (100 MHz, $CDCl_3$, ppm): δ 152.56, 150.87, 132.54, 129.59, 128.88, 127.95, 126.65, 119.86, 114.75, 60.41, 31.41.

MALDI-TOF (*m/z*): $[M]^+$ Calcd for $[C_{32}H_{26}N_2O_4 + Na]^+$, 525.179; Found, 524.965.

3.2.4 Synthesis of compound L2 [60]

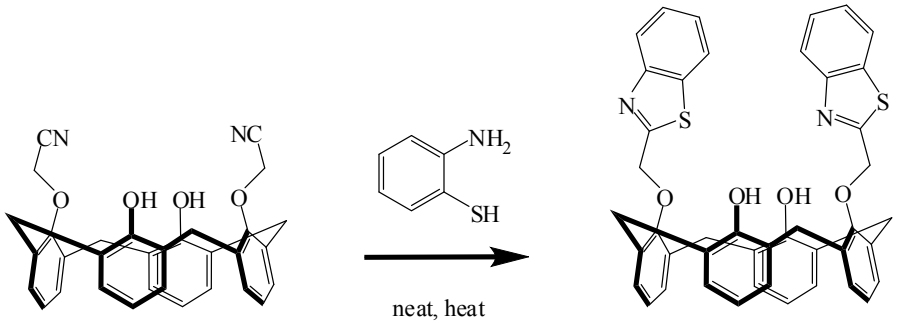

4 **L2** (81%)

Compound **4** (0.50 g, 1.00 mmol) was mixed with excess of 2-aminothiophenol. The reaction mixture was heated at reflux and stirred for 3 h under nitrogen. The reaction mixture was then cooled to room temperature. Dichloromethane (50 mL) was added into the mixture, and methanol was subsequently added to precipitate **L2** as a white solid (0.58 g, 81%).

Characterization data for **L2**:

^{1}H NMR spectrum (400 MHz, $CDCl_3$, ppm): δ 8.05 (d, 2H, *J* = 8.4 Hz, Ar*H*), 7.51 (t, 2H, *J* = 7.6 Hz, Ar*H*), 7.43 (d, 2H, *J* = 8.4 Hz, Ar*H*), 7.29 (t, 2H, *J* = 7.6 Hz, Ar*H*), 7.25 (s, 2H, ArO*H*), 7.11 (d, 4H, *J* = 7.6 Hz, Ar*H*), 6.89 (d, 4H, *J* = 7.6 Hz, Ar*H*), 6.78 (t, 2H, *J* = 7.2 Hz, Ar*H*), 6.72 (t, 2H, *J* = 7.4 Hz, Ar*H*), 5.45 (s, 4H, ArOCH_2), 4.42 (d, 4H, *J* = 13.6 Hz, ArCH_2Ar), 3.47 (d, 4H, *J* = 13.6 Hz, ArCH_2Ar).

^{13}C NMR spectrum (100 MHz, $CDCl_3$, ppm): δ 167.54, 153.28, 152.89, 151.54, 135.23, 132.70, 129.35, 128.72, 127.76, 126.16, 126.00, 125.22, 123.08, 122.00, 119.23, 75.45, 31.29.

MALDI-TOF (*m/z*): $[M]^+$ Calcd for $[C_{44}H_{34}N_2O_4S_2]^+$, 718.196; Found, 718.698.

3.2.5 Synthesis of compound 5

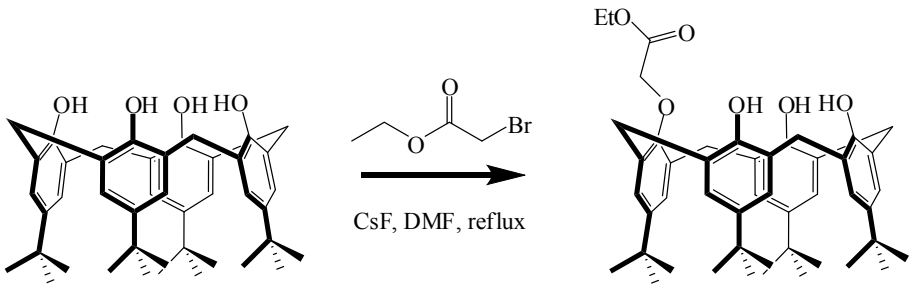

1 **5** (43%)

To a solution of compound **1** (5.00 g, 7.70 mmol) in dried dimethylformamide (200 mL) were added cesium fluoride (2.34 g, 15.40 mmol) and ethyl bromoacetate (2.55 mL, 20.10 mmol). The reaction mixture was heated at 60 °C under nitrogen for 70 h. Then, the reaction was quenched with 2 M hydrochloric acid (150 mL) and stirred for 30 min at room temperature and extracted with ethyl acetate (3 × 200 mL). The combined organic layers were washed with water (5 × 200 mL) and dried with anhydrous $MgSO_4$. After solvent removal, the remaining crude product was purified by column chromatography (SiO_2) using 50% hexane in dichloromethane as eluent followed by crystallization in methanol afforded compound **5** as a white solid (2.26 g, 43%).

Characterization data for **5**:

^{1}H NMR (400 MHz, $CDCl_3$, ppm): δ 10.27 (s, 1H, ArO*H*), 9.30 (s, 2H, ArO*H*), 7.13 (s, 2H, Ar*H*), 7.09 (s, 4H, Ar*H*), 7.01 (s, 2H, Ar*H*), 4.92 (s, 2H, OCH_2CO), 4.52 (d, 2H, *J* = 12.8 Hz, ArCH_2Ar), 4.44 (q, 2H, *J* = 7.2 Hz, CH_2CH$_3$), 4.34 (d, 2H, *J* = 13.6 Hz, ArCH_2Ar), 3.47 (d, 4H, *J* = 12.0 Hz, ArCH_2Ar), 1.43 (t, 3H, *J* = 7.2 Hz, CH$_2$CH_3), 1.25 (s, 36H, C(CH_3)$_3$).

^{13}C NMR (100 MHz, $CDCl_3$, ppm): δ 169.52, 150.00, 148.36, 148.23, 148.13, 143.41, 143.13, 133.31, 128.03, 127.74, 126.64, 125.79, 125.61, 72.03, 61.88, 32.52, 32.30, 31.48, 31.23, 14.19.

MALDI-TOF (*m/z*): $[M]^+$ Calcd for $[C_{47}H_{62}O_6 + Na]^+$, 757.444; Found, 757.104.

3.2.6 Synthesis of compound 6

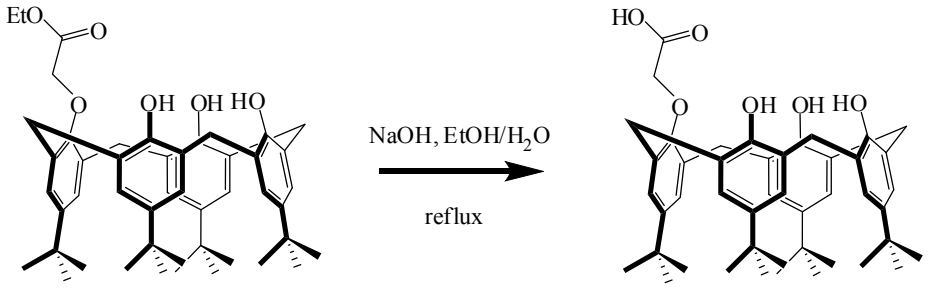

5 **6** (70%)

A mixture of the monoester **5** (2.26 g, 3.00 mmol) and 15% aq. NaOH (5 mL) in ethanol (100 mL) was stirred and refluxed under nitrogen for 24 h. The reaction mixture was concentrated under reduced pressure to yield a white residue. The residue was diluted with cold water (500 mL), and 3 M hydrochloric acid was added with vigorous stirring until pH 1 was reached. The solid was filtered, dried, and further dissolved in dichloromethane. The colorless crystal of monoacid product **6** was obtained after recrystallization the white solid in aqueous acetone (1.50 g, 70 %).

Characterization data for **6**:

^{1}H NMR (400 MHz, $CDCl_3$, ppm): δ 9.05 (br, 1H, COO*H*), 8.55 (s, 3H, ArO*H*), 7.10–7.00 (m, 8H, Ar*H*), 4.80–4.70 (m, 6H, ArCH_2Ar and OCH_2CO), 4.26 (dd, 4H, *J* = 17.6 Hz and 14.0 Hz, ArCH_2Ar), 1.24 (m, 36H, C(CH_3)$_3$).

^{13}C NMR (100 MHz, $CDCl_3$, ppm): δ 170.02, 147.69, 143.92, 132.94, 132.91, 128.02, 127.53, 127.39, 126.96, 126.15, 125.97, 125.89,125.83, 72.95, 33.99, 32.92, 32.52, 31.70, 31.49, 31.16, 30.99.

MALDI-TOF (*m/z*): $[M]^+$ Calcd for $[C_{46}H_{58}O_6 + Na]^+$, 729.413; Found, 728.979.

3.2.7 Synthesis of compound L3

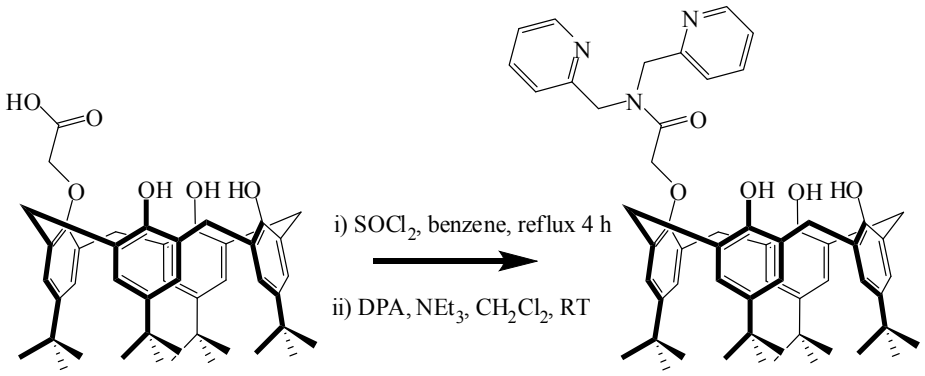

6 **L3** (35%)

To a 100 mL round-bottomed flask, dried benzene (50 mL), *p-tert*-butylcalix[4]arene monoacid **6** (1.50 g, 2.08 mmol) and thionyl chloride (6 mL) were added and refluxed under nitrogen for 4 h. The solvent and residual thionyl chloride were removed under reduced pressure to yield monoacid chloride as white solid. The solid was dissolved in dried dichloromethane (15 mL) and a mixture of dipicolylamine, DPA (0.50 g, 4.16 mmol) and triethylamine (0.86 mL, 6.24 mmol) in dichloromethane (5 mL) was added dropwise. The reaction mixture was stirred for 12 h at room temperature under nitrogen, and the solvent was removed under reduced pressure. The residue was dissolved in dichloromethane (50 mL) and washed with water (3 × 50 mL). The separated organic layer was dried over anhydrous $MgSO_4$. After the evaporation of solvent, the crude product was purified by column chromatography (SiO_2) using 20% ethyl acetate in dichloromethane as eluent to give **L3** as a white powder (0.64 g, 35%).

Characterization data for **L3**:

^{1}H NMR spectrum (400 MHz, $CDCl_3$, ppm): δ 9.72 (br, 3H, ArO*H*), 8.53 (m, 2H, Py*H*), 7.66 (m, 2H, Py*H*), 7.49 (d, 2H, *J* = 7.2 Hz, Ar*H*), 7.22–7.12 (m, 8H, Ar*H*), 6.99 (s, 2H, Ar*H*), 4.59 (s, 4H, NCH_2), 4.55 (t, 2H, *J* = 14.4 Hz, OCH_2CO), 3.73 (d, 4H, *J* = 13.2 Hz, ArCH_2Ar), 3.43 (dd, 4H, *J* = 17.0 Hz and 14.2 Hz, ArCH_2Ar), 1.24 (m, 36H, C(CH_3)$_3$).

^{13}C NMR (100 MHz, $CDCl_3$, ppm): δ 169.21, 156.65, 155.50, 150.92, 150.07, 148.96, 148.48, 147.70, 143.40, 142.87, 141.58, 137.16, 137.06, 134.82, 133.87, 132.87, 128.50, 126.77, 126.37, 126.32, 125.81, 125.72, 125.61, 125.36, 125.30, 125.25, 124.74, 124.54, 123.32, 122.87, 122.64, 121.68, 73.04, 51.93, 51.30, 34.37, 34.14, 34.03, 33.85, 33.12, 32.97, 32.64, 31.66, 31.58.

3.2.8 Synthesis of compound **7** [61]

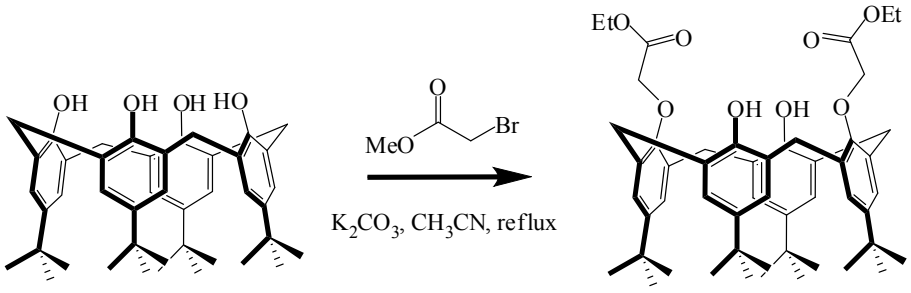

1 **7** (50%)

Compound **1** (5.00 g, 7.70 mmol), potassium carbonate (2.13 g, 15.40 mmol), and ethyl bromoacetate (5.04 mL, 30.80 mmol) were mixed in dried acetone (700 mL), stirred and refluxed for 15 h under nitrogen. The reaction mixture was cooled to room temperature and filtered through a bed of celite, washed with dichloromethane and concentrated to dryness. Recrystallization of the residue from ethanol yielded the white solid of diester **7** (3.25 g, 50%).

Characterization data for **7**:

^{1}H NMR spectrum (400 MHz, $CDCl_3$, ppm): δ 7.06 (s, 2H, ArO*H*)**,** 7.02 (s, 4H, Ar*H*), 6.82 (s, 4H, Ar*H*), 4.73 (s, 4H, OCH_2CO)**,** 4.45 (d, 4H, *J* = 13.2 Hz, ArCH_2Ar), 4.30 (q, 4H, CH_2CH$_3$), 3.32 (d, 4H, *J* = 13.4 Hz, ArCH_2Ar), 1.34 (t, 6H, *J* = 7.02 Hz, CH$_2$CH_3), 1.26 (s, 18H, C(CH_3)$_3$), 0.98 (s, 18H, C(CH_3)$_3$).

3.2.9 Synthesis of compound **8** [61]

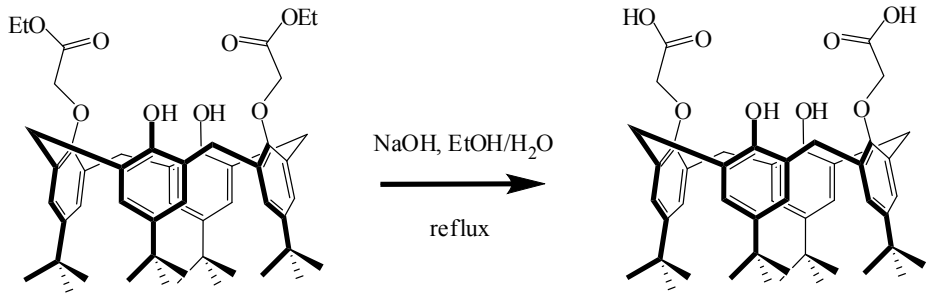

7 **8** (47%)

A mixture of the diester **7** (5.00 g, 6.10 mmol) and 15% aq. NaOH (16 mL) in ethanol (250 mL) was stirred and refluxed for 24 h under nitrogen. The reaction mixture was evaporated under reduced pressure to yield a white residue. The residue was diluted with cold water (500 mL). Hydrochloric acid (3 M) was added with vigorous stirring until pH 1 was reached. The white solid was filtered off and dried. The colorless crystal of diacid product **8** was obtained after recrystallization of the white solid in aqueous acetone (1.55 g, 47%).

Characterization data for **8**:

^{1}H NMR spectrum (400 MHz, $CDCl_3$, ppm): δ 9.00 (s, 2H, COO*H*), 8.25 (s, 2H, ArO*H*), 7.07 (s, 4H, Ar*H*), 6.99 (s, 4H, Ar*H*), 4.70 (s, 4H, OCH_2CO), 4.13 (d, 4H, J = 13.44 Hz, ArCH_2Ar), 3.46 (d, 4H, J = 13.74 Hz, ArCH_2Ar), 1.30 (s, 18H, C(CH_3)$_3$), 1.10 (s, 18H, C(CH_3)$_3$).

3.2.10 Synthesis of compound **L4** [61]

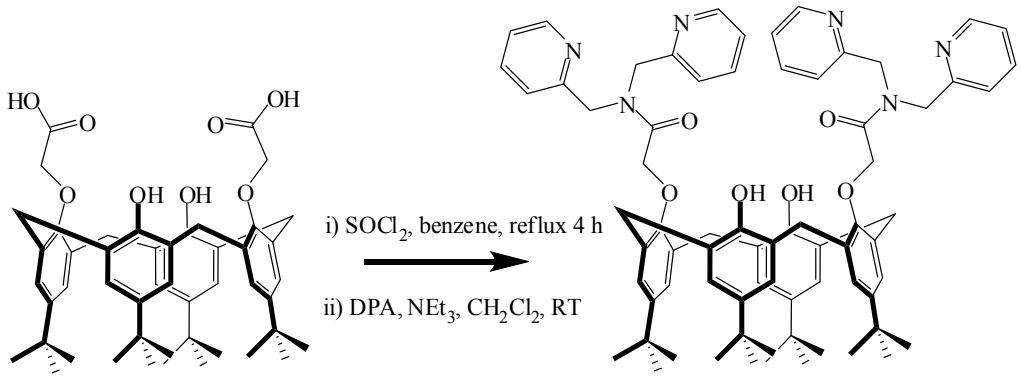

8 **L4** (22%)

To dried benzene (100 mL) in a 250 mL round-bottomed flask, diacid **8** (1.00 g, 1.28 mmol) and thionyl chloride (6 mL) were added and refluxed under nitrogen for 4 h. The solvent and residual thionyl chloride were removed under reduced pressure to yield diacid chloride as a white solid. The solid was dissolved in dried dichloromethane (15 mL) and a solution of dipicolylamine (0.46 g, 3.86 mmol) and triethylamine (1.50 mL, 11.58 mmol) in dichloromethane (10 mL) was added dropwise. The reaction mixture was stirred for 24 h at room temperature under nitrogen and the solvent was removed *in vacuo*. The residue was dissolved in dichloromethane (50 mL) and washed with water (3 × 50 mL). The separated organic layer was dried over anhydrous $MgSO_4$. After removing solvent, the crude product was purified by column chromatography (SiO_2) using 70% ethyl acetate in dichloromethane as eluent to obtain **L4** as a white powder (0.38 g, 22%).

^{1}H NMR and ^{13}C NMR spectra of **L4** were the same as the spectra in previous report [61].

Characterization data for **L4**:

^{1}H NMR spectrum (400 MHz, $CDCl_3$, ppm): δ 8.47 (s, 2H, ArO*H*), 8.36 (s, 2H, Py*H*), 7.48 (m, 6H, Py*H*), 7.34 (d, 2H, J = 7.6 Hz, Py*H*), 7.19 (m, 2H, Py*H*), 7.08–7.06 (m, 2H, Py*H*), 6.96 (s, 4H, Ar*H*), 6.70 (s, 4H, Ar*H*), 4.91 (s, 4H, NCH_2), 4.88 (s, 4H,

NCH_2), 4.66 (s, 4H, OCH_2CO), 4.29 (d, 4H, J = 13.2 Hz, ArCH_2Ar), 3.21 (d, 4H, J = 12.8 Hz ArCH_2Ar), 1.22 (s, 18H, C(CH_3)$_3$), 0.87 (s, 18H, C(CH_3)$_3$).

^{13}C NMR (100 MHz, $CDCl_3$, ppm): δ 169.15, 157.15, 156.30, 150.60, 149.80, 148.88, 147.04, 141.27, 136.86, 136.68, 132.60, 127.81, 125.58, 124.98, 122.56, 122.49, 122.12, 74.35, 52.12, 51.34, 33.89, 33.80, 31.79, 31.70, 30.98.

3.2.11 Synthesis of compound 9

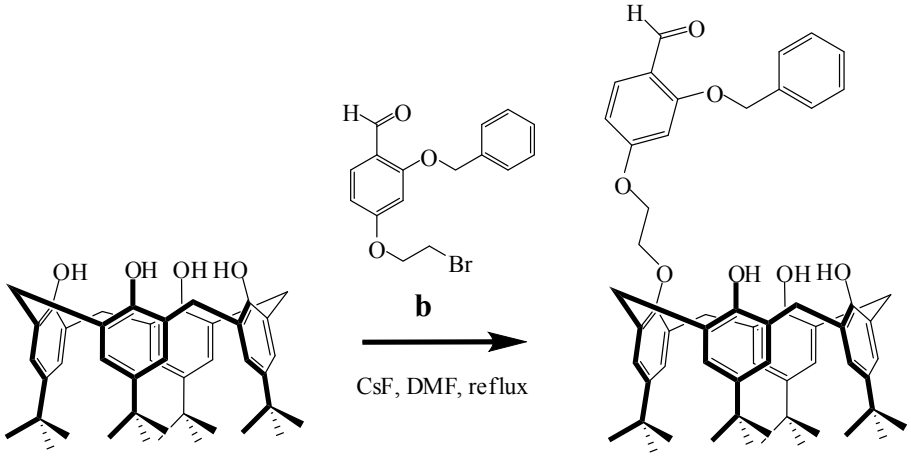

1 **9** (14%)

To a solution of compound **1** (7.99 g, 12.40 mmol) in dimethylformamide (200 mL) were added cesium fluoride (2.18 g, 14.40 mmol) and 2-(benzyloxy)-4-(2-bromoethoxy) benzaldehyde (5.57 g, 24.30 mmol). The reaction mixture was refluxed at 60 ^{o}C for 70 h. Then, the reaction was quenched with 2 M hydrochloric acid (150 mL) and stirred for 30 min. The reaction mixture was extracted with ethyl acetate (3 × 200 mL). The combined organic layers were washed with water (5 × 200 mL) and dried with anhydrous $MgSO_4$. After evaporation of the solvent, the remaining crude product was purified by column chromatography (SiO_2) using 50% hexane in dichloromethane as eluent, followed by crystallization in methanol to obtain **9** as a white solid (1.58 g, 14%).

Characterization data for **9**:

^{1}H NMR (400 MHz, $CDCl_3$, ppm): δ 10.47 (s, 1H, C*H*O), 10.04 (s, 1H, ArO*H*), 9.37 (s, 2H, ArO*H*), 7.95 (d, 2H, *J* = 8.8 Hz, Ar*H*), 7.46–7.37 (m, 6H, Ar*H*), 7.12 (d, 2H, *J* = 2.4 Hz, Ar*H*), 7.04 (d, 2H, *J* = 2.4 Hz, Ar*H*), 7.08 (s, 2H, Ar*H*), 6.82–6.77 (m, 2H, Ar*H*), 5.20 (s, 2H, OCH_2Ar), 4.72–4.70 (m, 2H, OCH_2CH_2O), 4.59–4.57 (m, 2H, OCH_2CH_2O), 4.48 (d, 2H, *J* = 13.2 Hz, ArCH_2Ar), 4.24 (d, 2H, *J* = 13.6 Hz, ArCH_2Ar), 3.48 (t, 4H, *J* = 12.8 Hz, ArCH_2Ar), 1.26 (s, 36H, $C(CH_3)_3$).

3.2.11.1 Synthesis of 4-(2-bromoethoxy)-2-hydroxybenzaldehyde (a) [62]

4-(2-Bromoethoxy)-2-hydroxybenzaldehyde (**a**) was synthesized following the previous method.

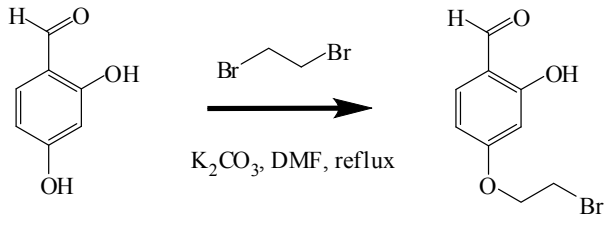

a (45%)

To a suspension of anhydrous potassium carbonate (6.00 g, 43.51 mmol) in dimethylformamide (100 mL) was added sequentially 2,4-dihydroxybenzaldehyde (6.00 g, 43.47 mmol) and 1,4-dibromoethane (6.50 mL, 75.08 mmol). The mixture was heated at 60 ^oC for 3 h under nitrogen. The reaction mixture was quenched with 2 M NaOH (100 mL) and the mixture was extracted with ethyl acetate (3 × 250 mL). The organic phase was combined, washed with water (5 × 250 mL) and dried over anhydrous Na_2SO_4. After removing solvent, the crude product was then purified by column chromatography (SiO_2) using 50% hexane in dichloromethane as eluent to obtain compound **a** (6.61 g, 45%).

Characterization data for **a**:

^{1}H NMR (400 MHz, $CDCl_3$, ppm): δ 11.47 (s, 1H, ArO*H*), 9.75 (s, 1H, C*H*O), 7.47 (d, 1H, *J* = 8.0 Hz, Ar*H*), 6.59 (d, 1H, *J* = 12.0 Hz, Ar*H*), 6.44 (s, 1H, Ar*H*), 4.35 (t, 2H, *J* = 6.0 Hz, OCH_2), 3.67 (t, 2H, *J* = 6.4 Hz, CH_2Br).

^{13}C NMR (100 MHz, $CDCl_3$, ppm): δ 194.49, 165.12, 164.41, 135.44, 108.54, 101.39, 68.00, 28.26.

3.2.11.2 Synthesis of 2-(benzyloxy)-4-(2-bromoethoxy)benzaldehyde (b) [62]

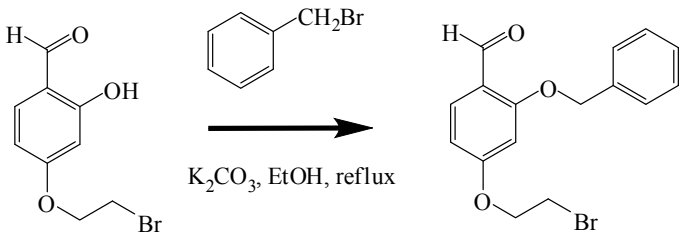

a **b** (85%)

A mixture of compound **a** (2.06 g, 14.93 mmol) and potassium carbonate (3.20 g, 23.20 mmol) in dried ethanol (50 mL) was stirred and refluxed under nitrogen for 30 minutes. Benzyl bromide (1.50 mL, 12.61 mmol) was added and the mixture was refluxed for 2 h. The reaction mixture was allowed to cool to room temperature and the solvent was removed *in vacuo*. The residue was portioned between dichloromethane (50 mL) and deionized water (50 mL). The aqueous layer was extracted with dichloromethane (3 × 50 mL). The combined organic layer was dried over anhydrous Na_2SO_4 and concentrated *in vacuo*. Recrystallization of the crude product in hexane afforded a white solid of compound **b** (2.40 g, 85%).

Characterization data for **b**:

^{1}H NMR (400 MHz, $CDCl_3$, ppm): δ 10.42(s, 1H, C*H*O), 7.87 (d, 1H, *J* = 9.2 Hz, Ar*H*), 7.48–7.37 (m, 5H, Ar*H*), 6.58–6.56 (m, 2H, Ar*H*), 5.19 (s, 2H, OCH_2Ar), 4.36 (t, 2H, *J* = 6.4 Hz, OCH_2), 3.66 (t, 2H, *J* = 6.0 Hz, CH_2Br).

^{13}C NMR (100 MHz, $CDCl_3$, ppm) δ 188.22, 164.41, 162.75, 135.85, 130.62, 128.78, 128.37, 127.31, 119.88, 106.45, 100.06, 70.55, 67.99, 28.45.

3.2.12 Synthesis of compound 10

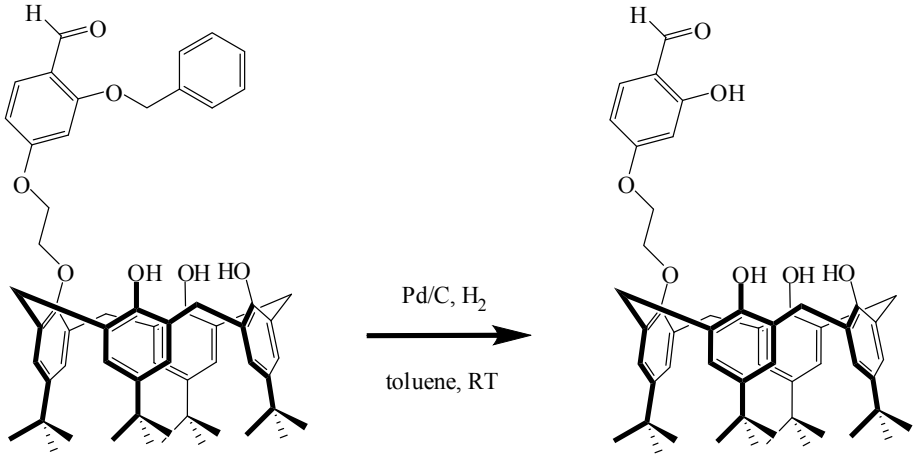

9 **10** (60%)

To a solution of compound **9** (2.04 g, 2.26 mmol) in toluene (100 mL), Pd/C (0.10 g) was added, and the mixture was stirred vigorously under hydrogen for 12 h. The catalyst was removed by filtration through a celite pad, and the filtrate was concentrated *in vacuo*. Crystallization of the crude product in methanol afforded **10** as a white solid (1.10 g, 60%).

Characterization data for **10**:

^{1}H NMR (400 MHz, $CDCl_3$, ppm): δ 11.58 (s, 1H, C*H*O), 10.10 (s, 1H, ArO*H*), 9.80 (s, 1H, ArO*H*), 9.36 (s, 2H, ArO*H*), 7.54 (d, 1H, *J* = 8.0 Hz, Ar*H*), 7.16–7.02 (m, 8H, Ar*H*), 6.80 (d, 1H, *J* = 8.0 Hz, Ar*H*), 6.66 (s, 1H, Ar*H*), 4.69 (d, 2H, *J* = 3.6 Hz, OCH_2CH_2O), 4.60 (d, 2H, *J* = 4.0 Hz, OCH_2CH_2O), 4.47 (d, 2H, *J* = 13.2 Hz, $ArCH_2Ar$), 4.25 (d, 2H, *J* = 13.6 Hz, $ArCH_2Ar$), 3.47 (t, 4H, *J* = 15.6 Hz, $ArCH_2Ar$), 1.25 (s, 36H, $C(CH_3)_3$).

^{13}C NMR spectrum (100 MHz, $CDCl_3$, ppm): δ 194.57, 194.57, 165.55, 164.52, 149.04, 148.57, 148.34, 148.32, 147.86, 143.60, 143.24, 135.59, 135.55, 133.58,

128.11, 128.01, 127.76, 126.63, 125.85, 125.78, 125.70, 115.71, 108.82, 101.65, 101.60, 73.70, 67.04, 34.32, 34.02, 33.98, 33.01, 32.19, 31.53, 31.29.

MALDI-TOF (*m/z*): $[M]^+$ Calcd for $[C_{53}H_{64}O_7 + K]^+$, 851.428; Found, 851.032.

3.2.13 Synthesis of compound L5

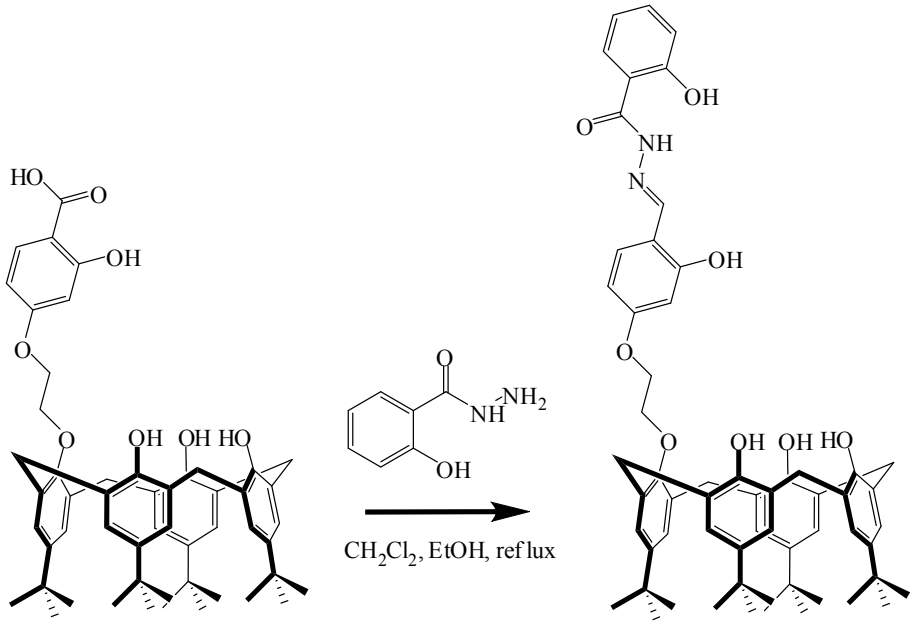

10 **L5** (80%)

A solution of 2-hydroxybenzohydrazide (0.20 g, 1.35 mmol) in ethanol (30 mL) was added to a solution of compound **10** (0.40 g, 1.35 mmol) in dried dichloromethane (50 mL). The reaction mixture was refluxed for 4 h under nitrogen. After the mixture cooled to room temperature, the white solid was filtered and washed with ethanol to yield **L5** (0.85 g, 80%).

Characterization data for **L5**:

^{1}H NMR (400 MHz, $CDCl_3$, ppm): δ 11.70 (s, 1H, ArO*H*), 11.28 (br, 1H, ArO*H*), 10.22 (s, 1H, ArO*H*), 9.57 (br, 1H, N*H*), 9.42 (s, 2H, ArO*H*), 8.31 (s, 1H, Ar*H*), 7.60 (d, 1H, *J* = 7.6 Hz, Ar*H*), 7.48–7.44 (m, 1H, Ar*H*), 7.18–7.01 (m, 10H, Ar*H* and C*H*N), 6.91 (t, 1H, *J* = 7.6 Hz, Ar*H*), 6.70–6.66 (m, 2H, Ar*H*), 4.57–4.53 (m, 4H,

OCH_2CH_2O), 4.47 (d, 2H, *J* = 12.8 Hz, ArCH_2Ar), 4.24 (d, 2H, *J* = 13.6 Hz, ArCH_2Ar), 3.45 (t, 4H, *J* = 10.4 Hz, ArCH_2Ar), 1.26 (s, 36H, C(CH_3)$_3$).

^{13}C NMR (100 MHz, $CDCl_3$, ppm): δ 161.85, 161.48, 160.62, 149.09, 148.44, 148.21, 147.81, 143.60, 143.27, 134.86, 133.55, 132.48, 128.12, 128.10, 127.74, 126.56, 125.78, 125.70, 119.16, 118.76, 113.25, 111.32, 107.58, 102.44, 74.00, 66.62, 34.27, 33.99, 33.94, 33.04, 32.13, 31.48, 31.25.

HRMS-ESI (positive mode, *m/z*): $[M + H]^+$ Calcd for $[C_{60}H_{70}N_2O_8 + K]^+$, 985.4764; Found, 985.4422.

3.2.14 Synthesis of compound 11

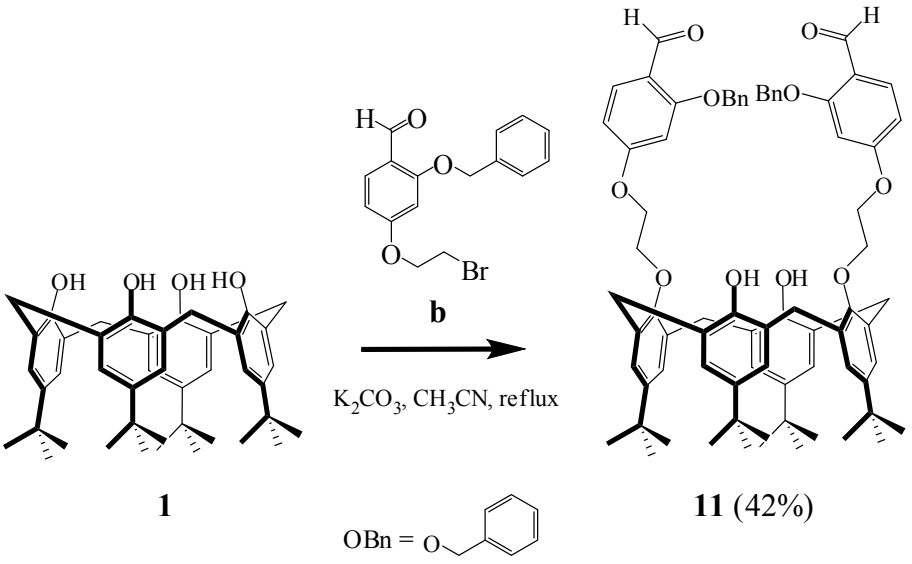

A mixture of compound **1** (5.00 g, 7.75 mmol), potassium carbonate (4.25 g, 31.00 mmol), and 2-(benzyloxy)-4-(2-bromoethoxy)benzaldehyde (6.89 g, 19.41 mmol) in 100 mL of acetronitrile was refluxed under nitrogen for 48 h. The reaction mixture was allowed to cool to room temperature and filtered through celite and washed with dichloromethane. The filtrate was evaporated to give a brown solid which was purified by column chromatography (SiO_2) using 70% hexane in dichloromethane as eluent to obtain compound **11** as a white solid (1.58 g, 42%).

Characterization data for **11**:

^{1}H NMR (400 MHz, $CDCl_3$, ppm): δ 10.43 (s, 2H, C*H*O), 7.87 (d, 2H, *J* = 8.0 Hz, Ar*H*), 7.42 (s, 2H, ArO*H*), 7.40–7.37 (m, 10H, Ar*H*), 7.15 (s, 4H, Ar*H*), 6.92 (s, 4H, Ar*H*), 6.61 (s, 4H, Ar*H*), 5.03 (s, 4H, OCH_2Ar), 4.45 (d, 4H, *J* = 12.0 Hz, ArCH_2Ar), 4.38–4.31 (m, 8H, OCH_2CH_2O), 3.38 (d, 4H, *J* = 13.2 Hz, ArCH_2Ar), 1.36 (s, 18H, C(CH_3)$_3$), 1.07 (s, 18H, C(CH_3)$_3$).

^{13}C NMR (100 MHz, $CDCl_3$, ppm): δ 188.28, 165.07, 162.70, 150.56, 149.60, 147.32, 141.73, 135.98, 132.65, 130.51, 128.76, 128.70, 128.28, 128.23, 127.81, 127.34, 127.29, 125.81, 125.35, 119.56, 106.95, 100.38, 73.63, 70.36, 67.15, 31.77, 31.68, 31.29, 31.11.

MALDI-TOF (*m/z*): $[M]^+$ Calcd for $[C_{76}H_{84}O_{10} + K]^+$, 1195.570; Found, 1196.560.

3.2.15 Synthesis of compound 12

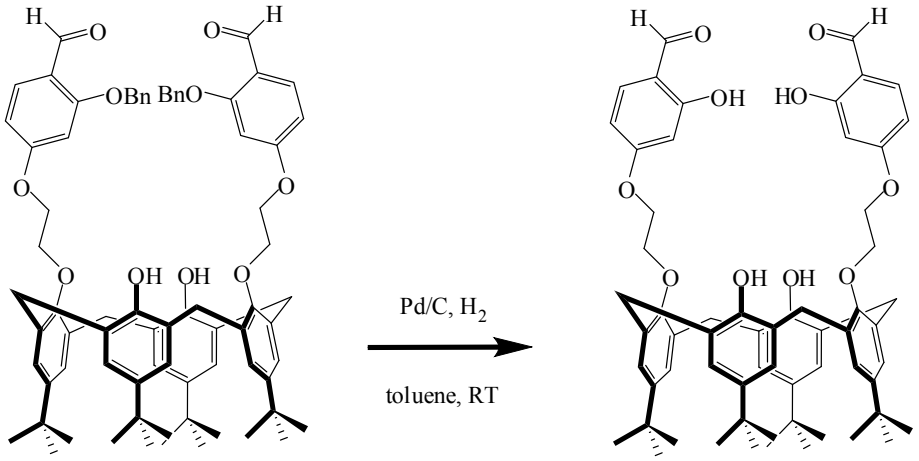

11 **12** (60%)

To the solution of compound **11** (1.20 g, 0.10 mmol) in toluene (100 mL), Pd/C (0.10 g) was added, and the mixture was stirred vigorously under hydrogen for 12 h. The catalyst was removed by filtration through a celite pad, and the filtrate was concentrated *in vacuo*. Crystallization of the crude product in methanol yielded compound **12** (1.10 g, 60%).

Characterization data for **12**:

^{1}H NMR (400 MHz, $CDCl_3$, ppm): δ 11.48 (s, 2H, C*H*O), 9.74 (s, 2H, ArO*H*), 7.45 (d, 2H, *J* = 8.0 Hz, Ar*H*), 7.33 (s, 2H, ArO*H*), 7.08 (s, 4H, Ar*H*), 6.89 (s, 4H, Ar*H*), 6.62 (d, 2H, *J* = 8.8 Hz, Ar*H*), 6.47 (s, 2H, Ar*H*), 4.40–4.36 (m, 12H, ArCH_2Ar and OCH_2CH_2O), 3.35 (d, 4H, *J* = 12.0 Hz, ArCH_2Ar), 1.31 (s, 18H, C(CH_3)$_3$), 1.04 (s, 18H, C(CH_3)$_3$).

^{13}C NMR (100 MHz, $CDCl_3$, ppm): δ 194.47, 165.71, 164.37, 150.50, 149.60, 147.24, 141.62, 135.39, 132.68, 127.83, 125.74, 125.19, 115.14, 108.85, 101.47, 73.40, 67.02, 31.64, 31.06.

MALDI-TOF (*m/z*): $[M]^+$ Calcd for $[C_{62}H_{72}O_{10}]^+$, 976.513; Found, 976.843.

3.2.16 Synthesis of compound L6

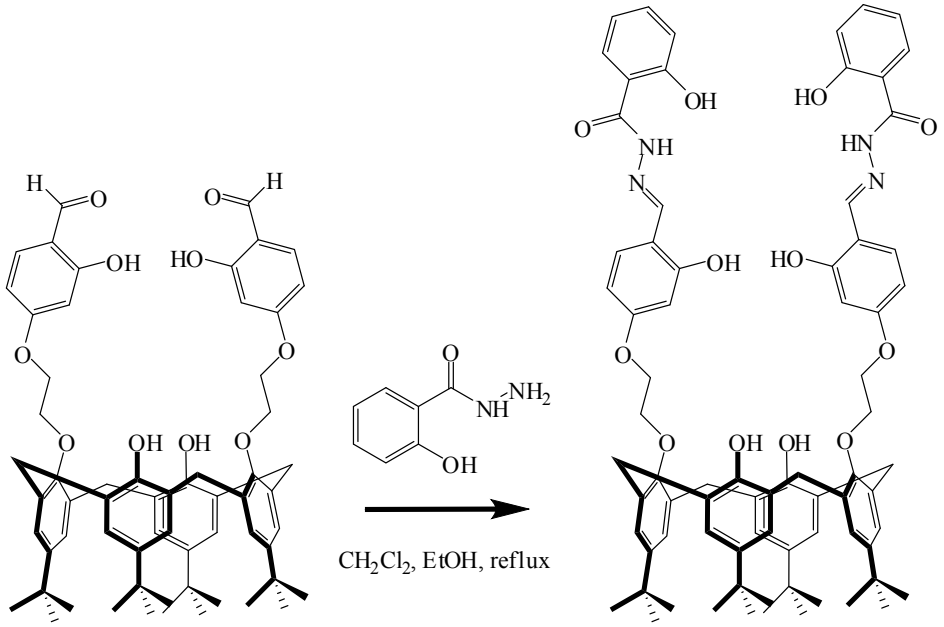

12 **L6** (42%)

A solution of 2-hydroxybenzohydrazide (0.30 g, 2.00 mmol) in ethanol (30 mL) was added to a solution of compound **12** (0.97 g, 1.00 mmol) in dried dichloromethane (50 mL). The reaction mixture was refluxed for 12 h under nitrogen.

After the mixture cooled to room temperature, the white solid was filtered and washed with ethanol to obtain compound **L6** (0.85 g, 42%).

Characterization data for **L6**:

^{1}H NMR (400 MHz, DMSO-d_6, ppm): δ 11.98 (br, 2H, N*H*), 11.60 (s, 2H, ArO*H*), 8.58 (s, 2H, C*H*N), 8.36 (s, 2H, ArO*H*), 8.26 (s, 2H, ArO*H*), 7.87 (d, 2H, *J* = 4.0 Hz, Ar*H*), 7.50–7.41 (m, 4H, Ar*H*), 7.13 (s, 4H, Ar*H*), 7.10 (s, 4H, Ar*H*), 6.98–6.93 (m, 4H, Ar*H*), 6.57–6.56 (m, 4H, Ar*H*), 4.29–4.24 (m, 12H, ArCH_2Ar and OCH_2CH_2O), 3.39 (d, 4H, *J* = 12.0 Hz, ArCH_2Ar), 1.16 (s, 18H, C(CH_3)$_3$), 1.12 (s, 18H, C(CH_3)$_3$).

^{13}C NMR (100 MHz, DMSO-d_6, ppm): δ 164.77, 161.66, 159.86, 159.41, 150.46, 150.21, 150.02, 147.53, 141.75, 134.41, 133.84, 131.86, 128.93, 128.03, 126.10, 125.64, 119.53, 117.73, 115.91, 112.54, 107.13, 102.62, 74.10, 67.18, 34.40, 34.00, 31.78, 31.35.

HRMS-ESI (positive mode, *m/z*): $[M + H]^+$ Calcd for $[C_{76}H_{84}N_4O_{12} + Na]^+$, 1267.5978; Found, 1267.5651.

3.3 Ion Selective Electrode Studies

3.3.1 Preparation of the electrode

The membrane cocktail (220 mg total mass) consisted of ionophore (10 mmol kg^{-1}), KT*p*ClPB, 33 wt.% PVC and 66 wt.% plasticizer (*o*-NPOE or DOS). All components were dissolved in 2.5 mL of THF or MeOH/$CHCl_3$/THF (1:2:10 v/v) and poured into a glass ring (30 mm i.d.) fixed on a glass plate. Then, the solvent was allowed to evaporate at room temperature overnight. A transparent membrane of about 200 μm in thickness was obtained. The membrane was punched into small size (7.5 mm i.d.) and glued with a PVC/THF slurry on the top of PVC tube and connected to micropipette tip as an electrode body.

For microelectrodes, the tip of 1 mL micropipette (0.5 mm i.d.) was dipped into membrane cocktail for 3 seconds. It was left to stand in vertical position to allow the solvent to evaporate. The membrane thickness was around 0.5 mm.

An internal filling solution containing 0.01 M $AgNO_3$ was put into this PVC tube which connected to micropipette tip and a AgCl-coated silver wire was placed into it. The prepared membrane electrode was conditioned in 0.01 M $AgNO_3$ solution overnight prior to use.

3.3.2 The EMF measurements

All potentiometric measurements were carried out at ambient temperature by using a 16-channel electrode monitor (Lawson Labs Inc., Malvern, PA 19355, USA). The external reference electrode was a double junction type Ag/AgCl glass electrode (type 6.0726.100, Metrohm AG, CH-9010 Herisau, Switzerland) with 1 M LiOAc as a salt bridge electrolyte. The electrochemical cell for the EMF measurements was Ag, AgCl/3 M KCl//1 M LiOAc//sample solution/ISE membrane/IFS/AgCl, Ag. EMF values for the ISEs versus reference electrode were measured in stirred solution in the concentration range from 10^{-8} M to 10^{-2} M. The activities of metal ions in sample solutions were calculated according to the Debye-Hückel approximation [63]. The detection limit was determined according to IUPAC recommendations.

3.3.3 Selectivity measurements

The potentiometric selectivity coefficients were determined by the separate solution method (SSM) [45]. The membranes were conditioned in the solution of interfering metal ions (nitrate salt) overnight. The response of the electrode was first measured against the interfering metal ions (10^{-7} to 10^{-2} M) by using 0.01 M the same interfering cations (chloride salt) as inner filling solution. The electrode was then used to measure the response of silver nitrate solutions. Selectivity coefficients of each metal were performed in triplicate (using new membrane for one replicate). The interfering ions in this study were Na^+, K^+, Ca^{2+}, Mg^{2+}, Ni^{2+}, Cu^{2+}, Zn^{2+}, Cd^{2+}, Pb^{2+} and Hg^{2+}. For determination of the selectivity coefficients of Hg^{2+} and Pb^{2+}, the pH of

solution was adjusted to 2 and 4, respectively with HNO_3 to avoid precipitation. The selectivity coefficients were calculated from mean value of triplicate experiments with standard deviation.

3.3.4 Preparation of sandwich membranes

In order to determine ion-ionophore complex formation constants in the solvent polymeric membrane, it requires membrane potential measurements on two-layer sandwich membranes [64–66], where only one side contains the ionophore.

The conventional standard size membranes, with and without ionophore, were conditioned in 0.005 M $AgNO_3$ for overnight. Then, the membranes were dried with tissue paper without washing with water. The sandwich membrane was prepared by attaching two individual membranes together and visibly checked for air bubbles before placing in the electrode body. The membrane containing ionophore was contacted with sample solution (0.005 M $AgNO_3$) that is the same solution as the conditioning and inner filling solutions. All potentiometric measurements were carried out at ambient temperature in unstirred salt solution versus a Ag/AgCl reference electrode with 1 M LiOAc as a salt bridge electrolyte. The range of time required from attaching the membrane until the membrane potential measurement was less than 1 min. The potential value was continuously recorded for several hours.

Membrane potential values, E_M, were determined by subtracting the cell potential for membrane without ionophore from that of the sandwich membrane. The formation constants were calculated using equation (4.1).

$$\log \beta_I \quad \left(\frac{I}{2.303}\right) - \log\left({}_T - \frac{T}{I}\right) \tag{4.1}$$

L_T is the total concentration of the ionophore. R_T is the concentration of lipophilic ion exchanger. R, T, F, n and z_I are the gas constant, the absolute temperature, the Faraday constant, the complex stoichiometry and the charge of the tested ion, respectively.

3.3.5 Effects of the solution pH

The reference electrode and pH electrode were immersed in 0.1 M KNO_3 solution and the solution was adjusted to pH 8 with 1% KOH. Subsequently, 500 µL of 0.01 M $AgNO_3$ was added into the solution to obtain 10^{-4} M Ag^+ sample solution. The pH of the solution was varied from 8 to 1.6 by gradually adding 0.01 M HNO_3. Both pH and EMF values were read simultaneously. These measurements were carried out using the same electrode, but the concentrations of the sample solution were varied from 10^{-4} to 10^{-2} M.

3.3.6 Reversibility

The membrane reversibility was examined by measuring the EMF of Ag-ISE in a 10^{-4} M Ag^+ solution. Subsequently, the electrode was rinsed and dipped into a 10^{-3} M Ag^+ solution. The cycle was repeated three times.

3.3.7 Electrode lifetime

After conditioning a membrane overnight in 0.01 M $AgNO_3$, Ag-ISE's responses were recorded over the concentration range of 10^{-8} to 10^{-2} M Ag^+. This procedure was repeated several times. The slopes and response potentials during a period of 30 days were recorded. The electrodes were kept in the dark after use.

3.4 Applications of Fabricated Ag-ISE from L2

3.4.1 Application as the indicator electrodes for argentometric titration

The Ag-ISE was used as an indicator electrode in potentiometric titrations to determine the concentration of mixed Cl^- and Br^-. Sample solutions were prepared by adding 25 µL of 1 M KCl and 1 M KBr into 50 mL ultra pure water. The mixed solution was stirred and titrated with 0.01 M $AgNO_3$.

3.4.2 Application for determination of AgNPs

Water colloids of high concentration AgNPs (10,000 ppm) were synthesized via the chemical reduction process adapted from previous reports [67–69]. An aqueous solution of $AgNO_3$, 0.094 M was prepared with methyl cellulose as a stabilizer. An aqueous solution of 0.07 M $NaBH_4$ reducing agent with the methyl cellulose solution as a solvent was sequentially prepared. The silver solution was then added dropwise to the $NaBH_4$ solution under a vigorous stirring. A dark cloud appeared and turned to yellowish brown within a few seconds. When all reactants were completely added, the solution turned dark brown. The solution appeared golden yellow when diluted with distilled water under the concentration lower than 10 ppm.

The speciation analysis of AgNPs was started by determination of free Ag^+. The AgNPs (1 mL) was diluted to 10 mL by Mill-Q water. The Ag-ISE can be directly immersed to the dilute solution. The response signal was corresponding to the concentration of free Ag^+. Total amount of Ag^+ in AgNPs was then determined by adding 40 μL of AgNPs into 10 mL of water. Subsequently, 4% (v/v) H_2O_2 (5 μL) was added into the solution and the EMF of the solution was measured. The procedure was repeated several times. The calibration curve was always evaluated before and after each experiment.

3.5 Glucose Biosensor based on Polymeric Membrane Ag-ISE from L2

3.5.1 Preparation of Ag-ISE and EMF measurements

The Ag-ISE was prepared from the ionophore **L2** (10 mmol kg^{-1}), KT*p*ClPB (5 mmol kg^{-1}), 33 wt.% PVC and 66 wt.% *o*-NPOE dissolved in 2.5 mL of THF. The cocktail solution was then poured into a glass ring (30 mm i.d.) fixed on a glass plate. The solvent was allowed to evaporate overnight at room temperature to give a transparent membrane (thickness ~0.2 mm). The membrane was punched into small sizes (7.5 mm i.d.) and glued with a PVC/THF slurry on the top of PVC tube and connected to a micropipette tip as an electrode body. The polymeric membrane electrodes were conditioned overnight in 0.01 M $AgNO_3$ identical to the filling

solution. Potentiometric measurements were carried out with a 16-channel electrode monitor (Lawson Labs Inc., Malvern, PA 19355, USA). A Ag/AgCl was used as reference electrode with 1 M LiOAc as salt bridge electrolyte. Membrane potentials were measured in a stirring solution at ambient temperature in a galvanic cell: Ag, AgCl/3 M KCl//1 M LiOAc//sample solution/membrane/0.01 M $AgNO_3$/AgCl, Ag.

3.5.2 Determination of the releasing Ag^+ from oxidized AgNPs using H_2O_2

AgNPs (1000 ppm, 100 µL) were added into 10 mL of a buffer solution. Then, 0, 10, 30 and 100 µL of 0.092 M H_2O_2 was added separately in each solution. After stirring for 30 minutes, solutions were directly measured by the Ag-ISE to determine the activity of free Ag^+. The experiment was repeated by increasing H_2O_2 concentration from 0.092 to 9.2 M and 10,000 ppm AgNPs was employed.

3.5.3 The EMF measurements for glucose biosensor

A buffer solution (10 mL) of 10 mM magnesium acetate was used as enzyme assay solution. The solution was adjusted to an appropriate pH by dilute acetic acid. Glucose was first diluted in a buffered solution, and the E F was then measured. Subsequently, AgNPs was added into the solution of glucose. After the EMF was stable, GOx (308 U mL^{-1}) was added and the EMF increased consecutively. The experiments were repeated three times for each point. The initial slope method described by Hassan et al. [70–73] was used in all measurements. The EMF was continuously monitored every 3 seconds (defined as an interval time). Plots of reaction rate were obtained from the differentiation of the change of EMF per interval time under assumption that the rate of potential change (dEMF/dt) is directly related to the change in [H_2O_2]. The maximum rate of potential change (dEMF/dt) was graphically determined by using the rate portion of the curve.

3.5.4 Studies of interferences

The Ag-ISE was immersed in the buffer solution (25 mL) containing GOX, and the base line EMF was then recorded. Subsequently, 50 µL of AgNPs (1000 ppm) was added. The EMF immediately jumped to higher base line because of the residual

Ag^+ in AgNPs. After the EMF was stable, urea (8.5 mM), glycine (0.5 mM), fructose (10 mM) and sucrose (10 mM) were added after one another. The EMF was recorded after each addition.

3.5.5 Real sample measurements

A carbonated beverage was diluted by 10 mM magnesium acetate buffer, and pH was adjusted to pH 6. AgNPs (1000 ppm, 20 µL) and GOx (308 U mL^{-1}) were added into the sample solution. The EMF was then recorded. For a glucose-spiked sample, a known amount of glucose was added into the carbonated beverage. AgNPs and GOx were then added in the same manner as described previously. The experiment was carried out in triplicate. The amount of glucose in the sample and the glucose-spiked sample were determined from the maximum rate of the enzyme-substrate reaction.

3.6 DNA Biosensor based on Polymeric Membrane Silver Ion Selective Microelectrode (Ag-ISµE) from L2

3.6.1 Preparation of Ag-ISµE and EMF measurements

The cocktail membrane contained **L2** (10.31 mmol kg^{-1}), KT*p*ClPB (5.03 mmol kg^{-1}), PVC (32.99 wt.%) and *o*-NOPE (66.02 wt.%) in an appropriate volume of THF after stirring 1 h. The Ag^+-microelectrode was fabricated from the tip of 1000 µL micropipette (0.5 mm i.d.) dipped into membrane cocktail for 3 seconds. It was left to stand in vertical position to allow the solvent to evaporate. The membrane thickness is around 0.5 mm. The resulting microelectrodes were conditioned in 10 mM $AgNO_3$ solution for overnight prior to use. An internal filling solution containing 10 mM $AgNO_3$ was put into micropipette tip and a AgCl-coated silver wire was placed into it.

Na^+-microelectrode (Na-ISµE) was used as reference electrode containing Na(X) (10.00 mmol kg^{-1}), KT*p*ClPB (5.03 mmol kg^{-1}), PVC (32.85 wt.%) and DOS (65.91 wt.%). The components were dissolved in THF. The fabricated Na-ISµE was

the same as Ag-ISμE as described above. The inner filling solution was 10 mM NaCl and conditioning solution was 10 mM $NaNO_3$.

Potentiometric measurements were performed in 1000 μL samples with a Na-ISμE as pseudo reference electrode in unstirred solutions with a 16-channel electrode monitor (Lawson Labs Inc., Malvern, PA 19355, USA) at room temperature (25 °C).

3.6.2 Synthesis of lipoic acid modified acpcPNA probe (Lip-acpcPNA)

The acpcPNA probe with a sequence of TGATGCTATGAC-Lys(Mtt) was synthesized from the respective *N*-Fmoc-protected monomers on a solid support (Tentagel, Rink amide linker) according to a previously published protocol [74–75]. After *N*-Fmoc and nucleobase side-chain deprotections, it was further modified at the *N*-terminus with an aminoethoxyethoxyacetyl (O) linker followed by DL-lipoic acid (HATU/DIEA activation). The PNA was then cleaved from the solid support using TFA and purified by reverse phase HPLC. The sequence was confirmed by MALDI-TOF mass spectrometry (Lip-O-TGATGCTATGAC-LysNH_2, Calcd.: m/z = 4540.0, Found: m/z = 4539.7) and by hybridization with its complementary DNA (d 5′-GTCATAGCATCA-3′) (T_m = 76.7 °C at 1.0 μM PNA, 1.0 μM DNA in 10 mM sodium phosphate buffer pH 7.0 containing 100 mM NaCl).

3.6.3 Preparation of Positively Charged CTAB-coated AgNPs

The preparation of CTAB-coated AgNPs was carried out using the previous published procedure [76–77]. The solution of CTAB (2 mL, 1 mM) in ethanol was added in aqueous solution of $AgNO_3$ (25 mL, 5 mM) and stirred for 10 minutes. Then, 1% freshly $NaBH_4$ was added under rigorous stirring. The mixture immediately turned yellow-green and left stirring for 1 h.

3.6.4 Preparation of immobilized Lip-acpcPNA on gold substrate

Gold substrates were cut by shearing machine to identically small pieces (10 × 5 × 0.25 mm) of uniform thickness. The Gold substrates were cleaned with piranha solution (3:1 H_2SO_4: 30% (v/v H_2O_2)) and thoroughly rinsed with Milli-Q water.

They were then washed in absolute ethanol and dried with pure nitrogen gas. Lip-acpcPNA solution was dropped on the gold substrate with 100 µL of 10 µM Lip-acpcPNA in 10 mM $NaNO_3$. The gold substrate was incubated at 4 °C for 40 h, followed by washing with Milli-Q water.

3.6.5 DNA hybridization and EMF measurements for DNA biosensor

The immobilized Lip-acpcPNA on gold substrate was treated with target DNA, solution in 10 mM $NaNO_3$ (0, 2, 5, 10, 15, 20, 40 and 80 µM, 100 µL) at room temperature for 3 h. The washing procedure was done in three times to remove unbound DNA. Then, a solution of CTAB-coated AgNPs (250 ppm, 50 µL) was deposited onto gold substrate at room temperature for 2 h. The gold substrate was washed in three times with Milli-Q water.

Hydrogen peroxide was used for dissolution of CTAB-coated AgNPs to Ag^+. 100 µL 0.2 M of H_2O_2 was added on the gold substrate and left for 45 minutes. The solution on gold substrate was transferred to eppendorf tube and adjusted volume to 1000 µL with 10 mM $NaNO_3$. The solution was stirred to destroy the remainder H_2O_2. The detection of Ag^+ in sample was performed in 1000 µL eppendorf tube by using a Na-ISµE as reference electrode.

CHAPTER IV

RESULTS AND DISCUSSION

4.1 Design and Synthesis of Ionophores

Calix[4]arene derivatives were designed and synthesized by attaching different functional groups to obtain different topology with various donor atoms for binding Ag^+. Each compound was modified by one or two opposite phenolic groups of calix[4]arene by a benzothiazole, a dipicolylamine and a hydrazone derivatives yielding calix[4]arene derivatives, **L1** – **L6**. **L1** and **L2** containing soft nitrogen and sulfur atoms and **L3** – **L6** containing soft nitrogen and hard oxygen atoms were used as donors which came from different functional groups. In preliminary studies, all synthesized ionophores incorporated in polymeric membranes responded to Ag^+. Ionophore **L4** was synthesized by Joseph and co-workers [61] and was found to be highly selective towards Ag^+ using fluorescence, absorption, and ^1H NMR spectroscopy. Generally, Hg^{2+} was a major interference for Ag-ISEs because soft metal ions, Ag^+, Hg^{2+} and Pb^{2+}, preferred to coordinate with soft donor atoms such as sulfur and nitrogen according to Pearson [78].

4.1.1 Synthesis of ionophores L1 – L6

Synthesis of ionophores **L1** – **L6** was outlined in Figure 4.1. These ionophores were synthesized using calix[4]arene as a building block. In the first step of **L1**, calix[4]arene was reacted with bromoacetonitrile in the presence of cesium fluoride to give compound **3**. Then, a condensation of cyano compound with 2-aminothiophenol was carried out by heating the two reactants together to give compound **L1** in 71% yield. Compound **L2** was synthesized in 81% yield from the condensation reaction between disubstituted compound **4** and 2-aminothiophenol [60].

For the synthesis of **L3**, *p-tert*-butylcalix[4]arene was reacted with ethyl bromoacetate in the presence of cesium fluoride to give compound **5**. Subsequently,

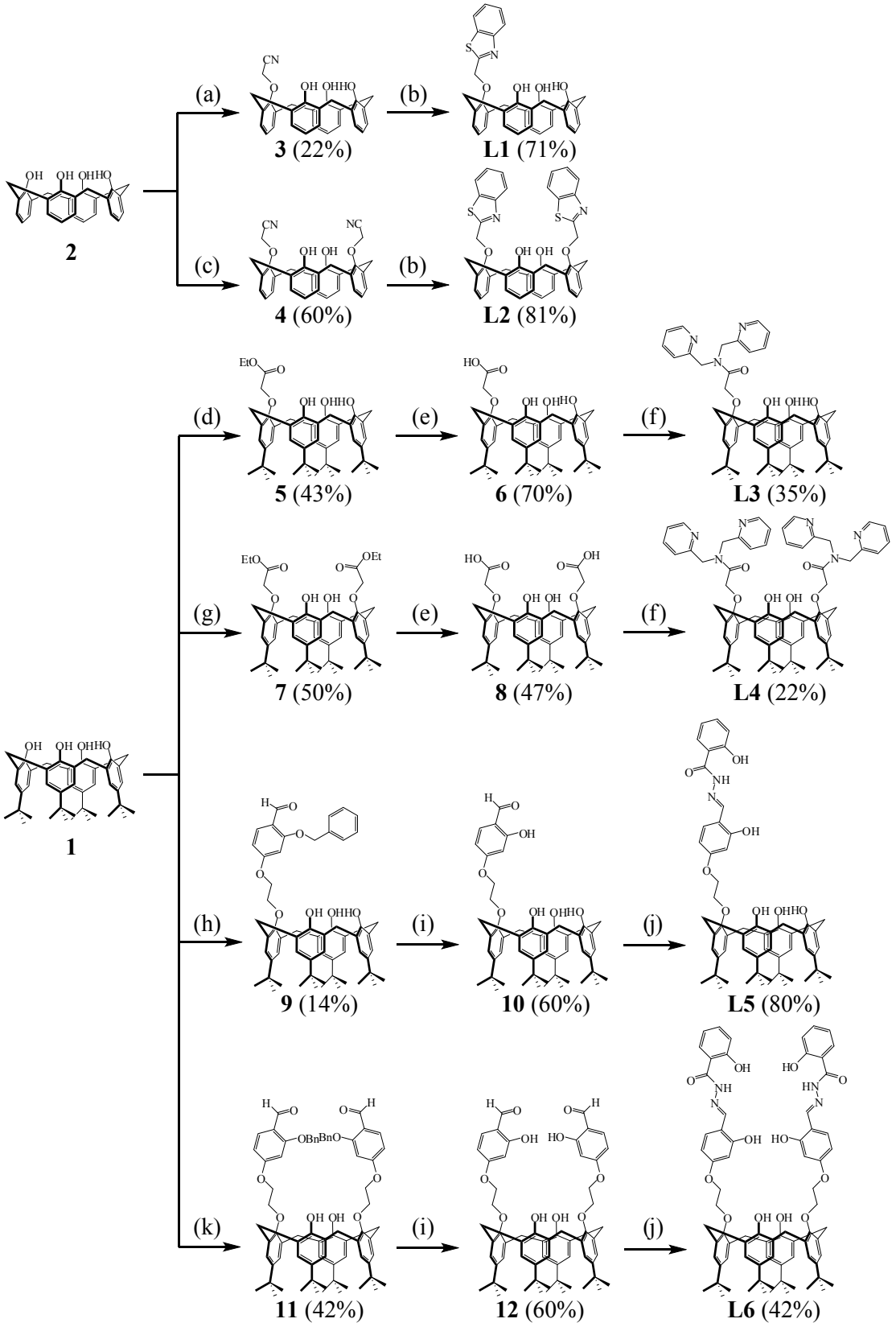

Figure 4.1 Synthetic rotes of **L1** – **L6**.

Reagents and conditions: (a) bromoacetonitile, CsF, CH_3CN, reflux for 7 h; (b) 2-aminothiophenol, neat, heat; (c) bromoacetonitile, K_2CO_3, CH_3CN, reflux for 7 h; (d) ethyl bromoacetate, CsF, DMF, reflux for 70 h; (e) NaOH, EtOH/water, reflux for 24 h; (f) $SOCl_2$, DPA, NEt_3, CH_2Cl_2, RT; (g) ethyl bromoacetate, K_2CO_3, CH_3CN, reflux for 15 h; (h) 2-(benzyloxy)-4-(2-bromoethoxy)benzaldehyde, CsF, DMF, reflux for 70 h; (i) Pd/C, H_2, toluene, RT; (j) 2-hydroxybenzohydrazide, CH_2Cl_2, EtOH, reflux for 4 h (**L5**) or 12 h (**L6**); (k) 2-(benzyloxy)-4-(2-bromoethoxy)benzaldehyde, K_2CO_3, CH_3CN, reflux for 48 h.

the hydrolysis reaction of ester compound with sodium hydroxide in ethanol produced the acid derivative. The acid derivative was then changed to a more reactive chloro carbonyl group. Nucleophilic addition of dipicolylamine produced **L3** as a final product in 35% yield. Compound **L4** was synthesized in 22% yield by a modified published procedure [61].

For synthesis of **L5**, the nucleophilic substitution reaction of *p-tert*-butylcalix[4]arene with 2-(benzyloxy)-4-(2-bromoethoxy)benzaldehyde which was prepared from 4-(2-bromoethoxy)-2-hydroxybenzaldehyde in two steps gave compound **9**. Benzyl group was deprotected by Pd/C in toluene under hydrogen. Condensation between compound **10** and 2-hydroxybenzohydrazide gave **L5** in 80% yields. Compound **L6** was synthesized in 42% yield from the condensation reaction between disubstituted compound **12** and 2-hydroxybenzohydrazide.

Ionophore **L2**, **L4** and **L6** containing two functionalized of opposite phenolic groups of calix[4]arene could be synthesized in the similar pathway as **L1**, **L3** and **L5**, respectively. Synthesis of two substitution of calix[4]arene employed potassium carbonate as base instead of cesium fluoride since potassium carbonate was a stronger base than cesium fluoride and gave a disubstituted calix[4]arene.

The characterization of intermediate compounds (**3 – 12)** and final products (**L1 – L6**) was carried out by ^{1}H NMR, ^{13}C NMR and mass spectroscopy. The results agree well with the proposed structures.

^{1}H NMR spectra of **L1** – **L6** showed the chemical shifts of bridging methylene proton around 4.5 – 3.5 ppm with coupling constants of 12 – 13 Hz. This confirmed the cone conformation of calix[4]arene in **L1** – **L6**. The ^{1}H NMR spectra of **L1** and **L2** gave the characteristic patterns which were different from the reactant chemical shifts due to the appearance of aromatic rings of benzothiazole groups at 8 – 6 ppm (d, d, t, t). In the case of **L3** and **L4** modified with dipicolylamine, the ^{1}H NMR spectra showed the chemical shifts of protons of pyridine and methylene groups around 8 – 7 and 5 – 4, respectively. The results indicated that the dipicolylamine was connected to the acid derivative of calix[4]arene. The ^{1}H NMR spectra of **L5** and **L6** showed the characteristic signals of –N*H*C(=O)– and –C*H*N– at 9.57 and 7.01 ppm for **L5** and at 11.98 and 8.58 ppm for **L6**, respectively suggesting that the Schiff base linkage was formed.

4.1.2 Effect of different functional groups of calix[4]arene on the selectivity

The ion selectivity features in Figure 4.2 of electrodes based on one substituted phenolic group of calix[4]arene with benzothiazole **L1**, dipicolylamine **L3** and hydrazone **L5** were investigated. These ionophores possessed soft nitrogen donors as a major component from different functional groups to form complex with Ag^+. **L3** containing three nitrogen and one oxygen donors from dipicolylamine and carbonyl, respectively exhibited most interference from Hg^{2+}. The introduction of heteroatoms of one sulfur and one nitrogen donors from benzothiazole **L1** and three oxygen and two nitrogen donors from hydrazone and hydroxyl **L5** displayed better selectivity towards Ag^+ than **L3** and decreased the interference from Hg^{2+}. However, **L1** exhibited better selectivity towards Ag^+ relative to other cations than that of **L5**. This difference was due to the presence of soft sulfur donor in **L1** preferring to bind soft Ag^+ but **L5** containing hard oxygen donor which may cause intramolecular hydrogen bonding between hydroxyl –*O*H and amide –C(=O)N*H*– of hydrazone group in **L5** resulting in decreasing in ion selectivity.

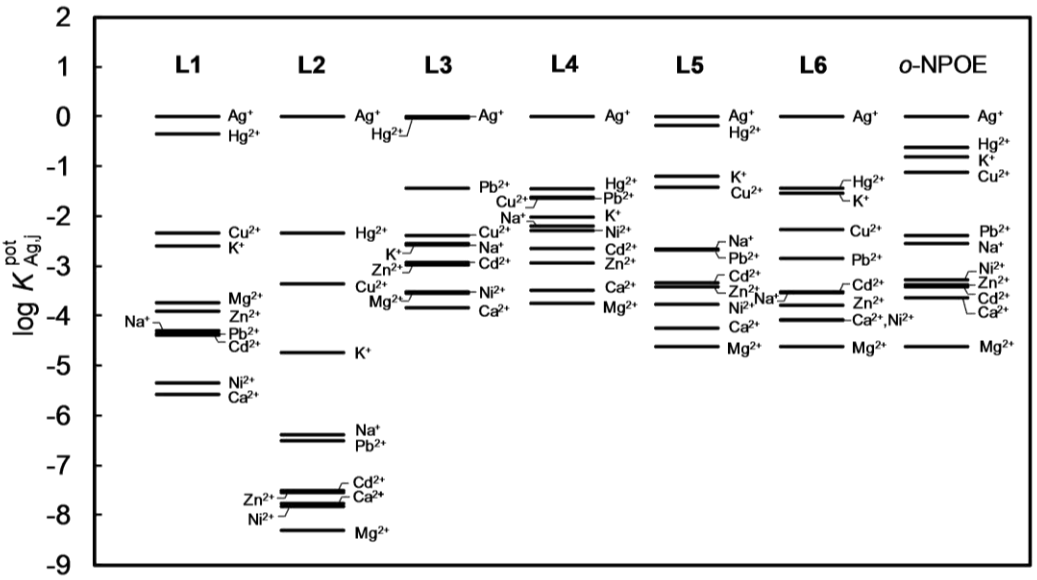

Figure 4.2 Comparison of selectivity coefficients (log $K^{pot}_{g,j}$) of electrodes base on **L1** – **L6** and *o*-NPOE (blank membrane). The membrane compositions are 10 mmol kg^{-1} ionophore and 7.5 mmol kg^{-1} KT*p*ClPB in *o*-NPOE membrane.

4.1.3 Effect of increasing the number of substituted phenolic group of calix[4]arene on the selectivity

Disubstituted derivatives of calix[4]arene with two benzothiazole **L2**, two dipicolylamine **L4** and two hydrazone **L6** were synthesized in order to investigate the effect of increasing the number of donors compared with the ion selectivity of one substituted phenolic group of calix[4]arene **L1**, **L3** and **L5**. The membranes having two substituted phenolic groups gave higher selectivity coefficients to Ag^+ than that of the others: **L2 > L1, L4 > L3 and L6 > L5. This suggested that more donor atoms of two substituted calix[4]arene could participate and coordinate with Ag^+ effectively. Furthermore, the increased lipophilicity of two substituted phenolic groups can prevent ionophore leaching from membrane electrodes.**

The ion selectivity features of electrodes based on L4 and L6 were similar to that of L3 and L5, respectively but interference from Hg^{2+} significantly decreased with increasing donor atoms in ionophores L4 and L6. L4 contained mixed nitrogen and oxygen donors in the same manner as L6, but N and O donors of L4 obtained

from dipicolylamine and carbonyl groups as N and O donors of **L6** obtained from hydrazone and hydroxyl groups. **L6** had more donors than **L4** and also contained π-electrons (from Schiff base in hydrazone) which interacted with Ag^+ resulting in discrimination from other cations than that of **L4**. Ionophore **L6** having more donors and π-electrons gave ion selectivity which was almost the same as that of the membrane electrode prepared with only the membrane solvent (*o*-NPOE) and the lipophilic anion additive (KT*p*ClPB). Since **L6** had more nitrogen and oxygen donors, more oxygen donors could undergo more intramolecular hydrogen bonding interactions leading to decreasing coordination force towards Ag^+ and the silver ion selectivity of **L6** possessing more donors and π-electrons [22–23] were interfered from other cations when comparing with **L2**. However, **L2** with two nitrogen and two sulfur donors from benzothiazole groups gave the best membrane selectivity towards Ag^+ compared to others and exhibited a good discrimination with 10000 times higher than all tested cations except Hg^{2+}. The results indicated that different types and numbers of functional groups affected the membrane selectivity towards Ag^+.

4.1.4 Complex formation constants of L1 – L6 with Ag^+

The complexation between ionophores and Ag^+ can be explained using the basic concept of host guest interactions or coordination chemistry. These ionophores (**L1** – **L6**) have donor atoms possessing lone pair electrons which interacted with Ag^+ using ion-dipole interactions. Although Ag^+ (d^{10}) can form 2 – 6 coordinated complexes [79], it prefers forming complexes with a linear shape due to its filled d-orbitals. The slopes of calibration curves for six synthesized ionophores were close to theoretical nernstian slope for monovalent cation (z = 1) as presented in Table 4.1 indicating 1:1 ion-ionophore complexes.

The complex formation constants between Ag^+ and ionophores **L1** – **L6** assuming a 1:1 ion-ionophore stioichiometry were determined with segmented sandwich membranes and the results were shown in Table 4.2. The results showed that ionophores having benzothiazole (**L1** and **L2**) and dipicolylamine groups (**L3** and **L4**) have higher complex formation constants than ionophores having hydrazone groups (**L5** and **L6**) for about 2 – 3 orders of magnitude. Ionophores **L2** and **L3**

Table 4.1 Membrane compositions and response properties based on ionophore **L1** – **L6**.

Ionophore	**Membrane composition (wt.%)**				**Slope**	**Linear range**	**Detection**
	Ionophore	**KT*p*ClPB**	**PVC**	**Plasticizer**	**(mV**	**(M)**	**limit (M)**
	(mmol kg^{-1})	**(mmol kg^{-1})**			**decade^{-1})**		
L1	0.59 (10.27)	0.37 (7.47)	32.91	*o*-NPOE, 66.13	43.1 ± 0.6[a]	10^{-5} to 10^{-2}	3.9×10^{-6}
L2	0.73 (10.10)	0.37 (7.49)	32.93	*o*-NPOE, 65.97	58.8 ± 0.6	10^{-6} to 10^{-2}	4.8×10^{-7}
L3	0.88 (9.96)	0.37 (7.40)	33.00	*o*-NPOE, 65.75	56.3 ± 0.8	10^{-6} to 10^{-2}	1.0×10^{-6}
L4	1.15 (10.24)	0.37 (7.40)	32.78	*o*-NPOE, 65.70	51.0 ± 0.9	10^{-6} to 10^{-2}	5.0×10^{-6}
L5	0.97 (10.25)	0.37 (7.50)	32.78	*o*-NPOE, 65.87	51.3 ± 0.7	10^{-6} to 10^{-2}	8.5×10^{-7}
L6	1.25 (10.01)	0.37 (7.49)	32.84	*o*-NPOE, 65.54	55.5 ± 0.9	10^{-6} to 10^{-2}	8.7×10^{-7}
o-NPOE	–	0.37 (7.46)	33.11	*o*-NPOE, 66.52	44.3 ± 1.5	10^{-5} to 10^{-2}	4.9×10^{-6}

[a] Standard deviations in triplicate experiments.

formed strong and stable complexes with Ag^+ in the same order with logarithmic complex formation constants, 5.25 ± 0.05 and 5.31 ± 0.08, respectively. However, the silver ion selectivity of **L3** was badly interfered from Hg^{2+} compared to that of **L2**. Moreover, the high complex formation value of **L2** corresponded to its best membrane selectivity and electrode characteristics towards Ag^+. This characteristic may be attributed to the two symmetrical benzothiazole groups on the calix[4]arene that could offer two nitrogen and two sulfur donors and rearrange in a suitable geometry to form complexes with Ag^+ rather than other interfering ions. Steric hindrance of the bulky *tert*-butyl groups of the calixarene framework also resulted in Nernstian slope of **L3** (56.3 ± 0.8 mV decade^{-1}) which is much lower than that of **L2** (58.8 ± 0.6 mV decade^{-1}) [29]. Therefore, **L2** was chosen as the ionophore to optimize the membrane composition for Ag-ISEs.

Table 4.2 Experimental membrane potentials and corresponding ionophore complex formation constants determined with segmented sandwich membranes for ionophores **L1** – **L6** in PVC membranes assuming a 1:1 stoichiometry of the ionophore and Ag^+.

Ionophore	Ionophore L_T (mmol kg^{-1})	Anionic sites R_T (mmol kg^{-1})	Membrane potential E_M (mV)	Formation constant log β_{ILn}
L1	10.45	7.52	126 ± 6[a]	4.66 ± 0.10[a]
L2	10.38	7.37	162 ± 3	5.25 ± 0.05
L3	10.00	7.30	162 ± 5	5.31 ± 0.08
L4	10.38	7.47	134 ± 9	4.80 ± 0.16
L5	10.02	7.05	20 ± 5	2.87 ± 0.09
L6	10.05	7.31	46 ± 4	3.34 ± 0.06

[a] Standard deviations in triplicate experiments.

4.2 Fabrication of Ag-ISEs from L2

4.2.1 Optimization of the membrane composition from L2

It is well known that for PVC membrane electrodes the type and percentage of each composition are critical parameters that affected the sensing characteristic of the fabricated electrode such as the working concentration range, lifetime, selectivity and sensitivity. However, the ratio between PVC and plasticizer are already optimized at

1:2 ratio by weigh which is provided the best component in many reports [80]. Two types of plasticizers, DOS and *o*-NPOE, were used, and the responses of their corresponding ISE's were compared as shown in Figure 4.3. Figure 4.3 (a) showed that the response characteristic of DOS membrane was highly dependent on the amount of the ion exchanger. In the presence of 25 mol% of KT*p*ClPB (relative to ionophore) the membrane did not give the expected EMF changed while the concentrations of Ag^+ were increased. However, when the ion exchanger was increased to 50 and 75 mol%, the membrane response gave a slope of 51.5 ± 0.5 and 56.2 ± 1.2 mV decade^{-1}, respectively. For the membrane plasticized with *o*-NPOE the response characteristic shown in Figure 4.3 (b) seemed to be independent from the amount of the ion exchanger added. Moreover, the slopes obtained from *o*-NPOE membranes were close to the theoretical Nernstian slope as summarized in Table 4.3. This behavior may stem from the better complexation of the ionophore **L2** towards Ag^+ in a more polar matrix.

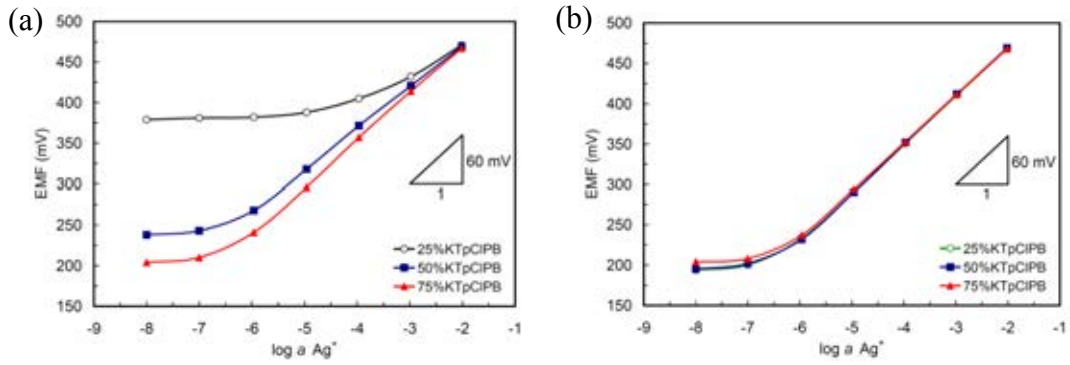

Figure 4.3 Effect of % ion exchanger (relative to the ionophore) to the membrane response in different plasticizer (a) DOS and (b) *o*-NPOE.

The lower detection limits were found to be relatively low. In the membrane plasticized with DOS the lower detection limits (IUP C definition) were found to be 7.9×10^{-5}, 3.9×10^{-7} and 3.9×10^{-7} M for the membrane containing 25%, 50% and 75% KT*p*ClPB, respectively. The lower detection limit in membrane plasticized with *o*-NPOE was found to be around 4.0×10^{-7} M or about 47 ppb which is comparable to the detection limit in FAAS method.

Table 4.3 Membrane compositions and electrode response properties of **L2**.

Electrode number	**Membrane composition (wt.%)**				**Slope (mV decade^{-1})**	**Linear range (M)**	**Detection limit (M)**
	Ionophore (mmol kg^{-1})	**KT*p*ClPB (mmol kg^{-1})**	**PVC**	**Plasticizer**			
I	0.72 (10.00)	0.11 (2.23)	32.42	DOS, 66.74	40.8 ± 1.0[a]	10^{-3} to 10^{-2}	7.9×10^{-5}
II	0.73 (10.17)	0.25 (5.03)	33.02	DOS, 66.00	51.5 ± 0.5	10^{-6} to 10^{-2}	3.9×10^{-7}
III	0.78 (10.94)	0.37 (7.47)	33.02	DOS, 65.82	56.2 ± 1.2	10^{-6} to 10^{-2}	3.9×10^{-7}
IV	0.69 (9.67)	0.11 (2.23)	32.22	*o*-NPOE, 66.97	59.4 ± 0.3	10^{-6} to 10^{-2}	4.0×10^{-7}
V-Macro	0.72 (10.05)	0.25 (5.04)	32.42	*o*-NPOE, 66.60	59.7 ± 0.8	10^{-6} to 10^{-2}	4.4×10^{-7}
V-Micro	0.73 (10.12)	0.25 (5.06)	32.87	*o*-NPOE, 66.14	59.8 ± 1.0	10^{-6} to 10^{-2}	5.0×10^{-7}
VI	0.76 (10.50)	0.36 (7.30)	32.72	*o*-NPOE, 66.16	58.5 ± 0.3	10^{-6} to 10^{-2}	4.2×10^{-7}

[a] Standard deviations in triplicate experiments.

According to phase-boundary model, the EMF of a polymeric membrane electrode is directly proportional to the logarithmic activity of analyte ions. This means the electrode area or electrode size does not affect the ISE response. From this principle we have fabricated a microelectrode from **L2** using *o*-NPOE as plasticizer. A smaller electrode has an advantage that very low concentration of an analyte can be measured or the electrode can be used in a limited space. The response characteristics of the microelectrode have also been evaluated in the same manner as macroelectrode (*o*-NPOE as plasticizer). The electrode behaviors were similar to the macroelectrode. Theoretical Nernstian slope (59.8 ± 1.0 mV decade^{-1}) was observed and the lower detection limit was 5.0×10^{-7} M (54 ppb). The performance characteristics of the micro-size electrode are thus comparable with the regular size electrode.

4.2.2 Potentiometric selectivity coefficient of the Ag-ISE from L2

Selectivity of an ionophore is the most crucial characteristic of an ISE. The ionophore should have good selectivity over interfering ions in order to avoid the bias response from such interfering ions. The selectivity of the ionophore results from the complex formation between the ionophore and an analyte ion. The selectivity of ISE's was explored based on the so-called "unbiased selectivity coefficient" proposed by Szigeti and co-workers [31]. The calibration curve of the interfering ion was performed by membranes that did not expose to the Ag^+ solution. Most studied ions showed near Nernstian slope in which such behavior was not seen when the membrane was conditioned in 0.01 M $AgNO_3$. Subsequently, the same membrane was used again to record a calibration curve for Ag^+. The super Nernstian slopes were always observed at concentration of Ag^+ below 10^{-4} M due to the effect of the strong inward ion flux to the inner solution of the membrane [81]. However, when the concentration of Ag^+ increased from 10^{-4} to 10^{-2} M, the expected Nernstian slopes were observed. The selectivity order of standard-size membrane plasticized with *o*-NPOE and DOS and microelectrode using *o*-NPOE as plasticizer are shown in Figure 4.4.

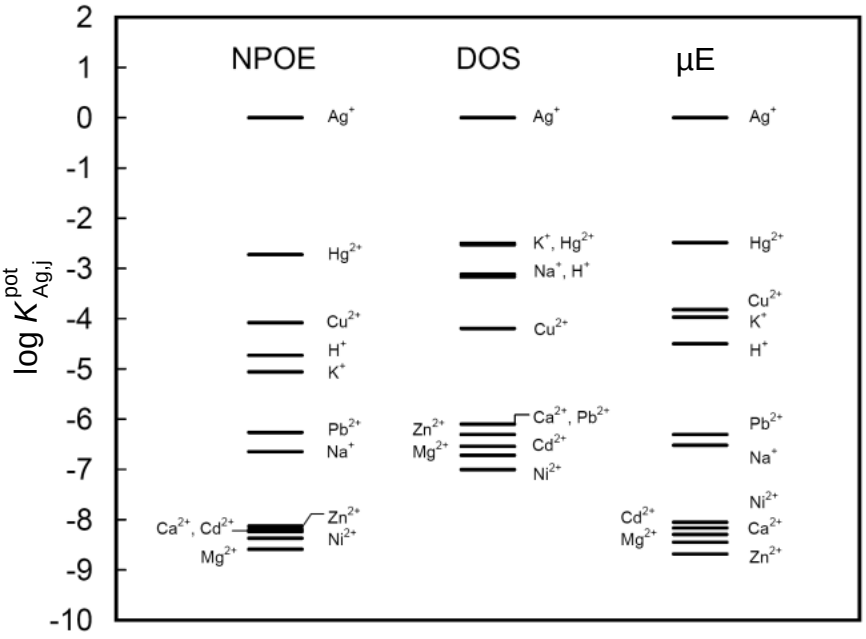

Figure 4.4 Comparison of selectivity coefficients (log $^{pot}_{g\,j}$) in membrane plasticized with *o*-NPOE and DOS (in macroelectrode) and *o*-NPOE (in microelectrode, μE). The membrane compositions are 10 mmol kg^{-1} ionophore and 5 mmol kg^{-1} KT*p*ClPB in *o*-NPOE membrane and 10 mmol kg^{-1} ionophore and 7.5 mmol kg^{-1} KT*p*ClPB in DOS membrane.

From Figure 4.4, it can be seen that the synthesized ionophore, **L2**, exhibited the selectivity over transition metals up to log $^{pot}_{g\,j} = -8$. The synthesized ionophore **L2**, can thus be used in the presence of several metal ions in high concentration levels. The most common interfering ion for Ag-ISE's is Hg^{2+} due to its mercaptophilic property [82]. The synthesized ionophore, **L2**, shows clearly that it can be used in the system contained Hg^{2+} with the logarithmic selectivity coefficient around −2.5. In order to evaluate the usable range of the electrode in the presence of Hg^{2+}, the electrode responses towards Ag^+ in different concentrations of Hg^{2+} have been measured. The results are shown in Figure 4.5. It can be seen that the linear working range decreases while the concentration of Hg^{2+} increases. Nevertheless, it can be deduced that the electrode can be used with Nernst's slope up to 5×10^{-6} M Hg^{2+} with working concentration ranging of 10^{-4} to 10^{-2} M. The selectivity pattern of the microelectrode-based *o*-NPOE is similar to the macroelectrode using *o*-NPOE. This

can be concluded that the size of the electrode does not affect the selectivity of the ionophore when the membrane composition was identical. The polar *o*-NPOE (ε = 24) increased the mobility of ionophore to coordinate and form a strong complex with Ag^{+} resulting in the higher silver ion selectivity and closed to the theoretical Nernstian slope compared to apolar DOS (ε = 4). Due to the better selectivity coefficients found in the *o*-NPOE membrane, we decide to use the membrane plasticized with *o*-NPOE for further studies.

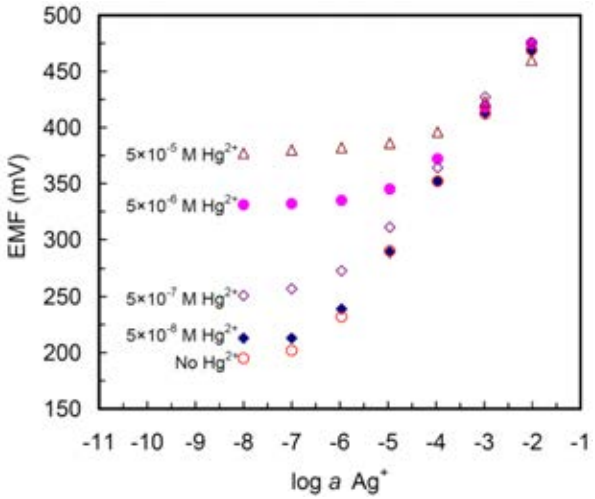

Figure 4.5 Potential response of Ag-ISE using *o*-NPOE as plasticizer in the presence of different concentrations of Hg^{2+} at pH 2.0.

4.2.3 Response characteristic

The optimized membrane compositions for ionophores **L2** were used to study the response characteristics of the sensors. As shown in Figure 4.6 (a) and (b) for the response of ISEs prepared from macro- and microelectrodes, respectively, the EMF increased upon increasing the Ag^{+} concentration with very stable potentials. The macroelectrode showed very fast response time (less than 5 seconds) to reach a stable EMF value. After the EMF signals reach the plateau at a given concentration level, the traces show very slight signal fluctuation. The microelectrode however shows slower response time (10 seconds) and more fluctuated signals as depicted in Figure 4.6 (b). A faraday cage is essentially needed in the case of the microelectrode to decrease noise. However it is not required in the case of macroelectrodes. The insets

show the corresponding calibration curves that provided Nernstian slopes of 59.7 ± 0.8 and 59.8 ± 1.0 mV decade^{-1} and lower detection limits of 4.4 × 10^{-7} and 5.0 × 10^{-7} M for macro- and microelectrodes, respectively. Both sensors could be used in a wide concentration range of Ag^+ (10^{-6} – 10^{-2} M). The response characteristics of both sensors showed that the membrane electrodes fabricated from macro- and microelectrodes were very good Ag^+ sensors.

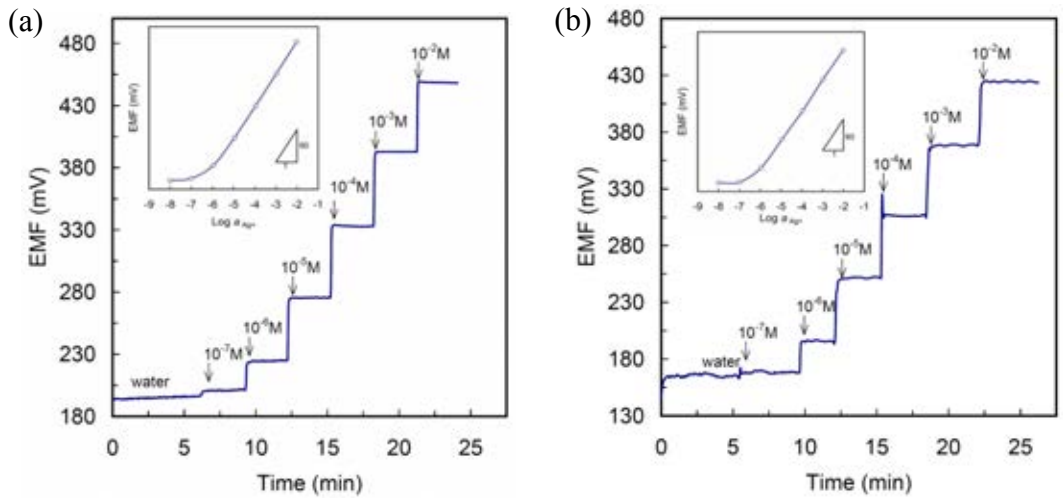

Figure 4.6 Time trace line observation of Ag-ISE after adding Ag^+ to the solution (a) macroelectrode and (b) microelectrode.

4.2.4 Effect of pH on the potential response

Acidity and alkalinity of aqueous solution always play an important role in the metal ion measurement. This may stem from the formation of hydroxo complexes of metal or protonation-deprotonation of the ionophore. The effect of solution pH towards the membrane potential was then evaluated by adding HNO_3 to Ag^+ solution at pH 8 until the significant EMF change was observed. The pH was measured concurrently with the EMF change. Three concentrations of Ag^+, 10^{-4}, 10^{-3} and 10^{-2} M are chosen to study this effect because these concentrations are in a linear working range. The results are shown in Figure 4.7 (a). It can be seen that the ISE can be used in a wide range of solution pH from pH 8 to 2.5 with no significant change in the EMF value. The electrode was affected when pH < 2.5 probably due to the interference from H^+ and pH > 8 due to the precipitation of silver hydroxide. However,

the effective pH range found in this study was wide enough to use in the sample without critical pH adjustment needed.

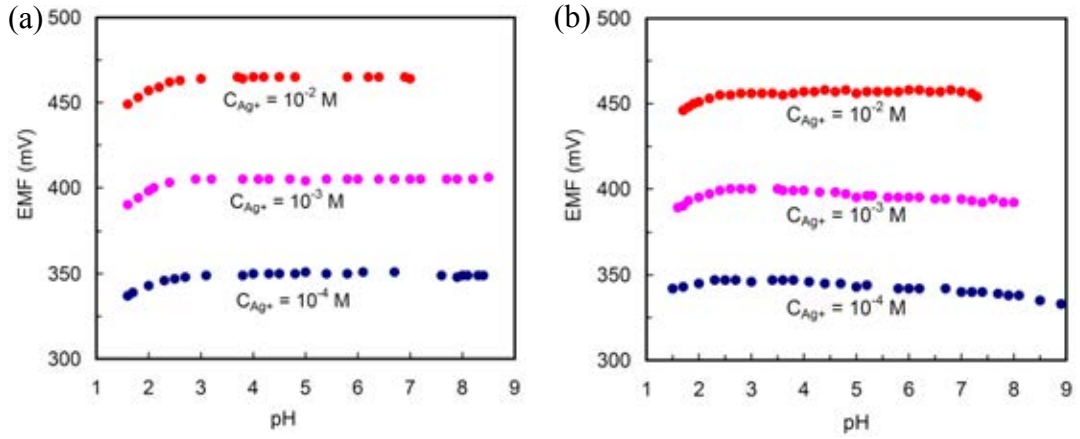

Figure 4.7 Potential response of *o*-NPOE plasticized Ag-ISE (a) macroelectrode and (b) microelectrode at variation of solution pH observed in three different Ag^+ concentrations.

The same procedure was also carried out for the microelectrode measurement. The results are shown in Figure 4.7 (b), it was found that the behavior of the microelectrode was similar to the macroelectrode with the same pH range for all concentration levels. This supported the fact that reducing the electrode size will not affect the electrode responses.

4.2.5 Reversibility and lifetime of the fabricated electrodes

The reversibility of the electrode was evaluated by alternatively measured EMF's of two different concentrations 10^{-4} and 10^{-3} M Ag^+. This property also represents to the precision of the detection. From Figure 4.8, the EMF signals were found to be restored at the same concentration of Ag^+ in every cycle. The electrode can, therefore, be used to measure the Ag^+ concentration with excellent reversibility.

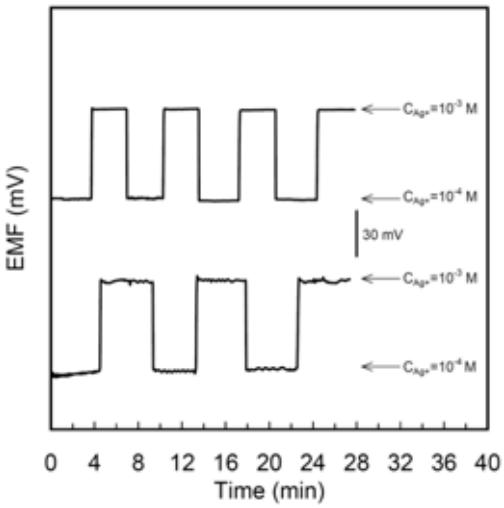

Figure 4.8 Reversibility of Ag-ISE at the concentration between 10^{-4} and 10^{-3} M. Top: macro-Ag-ISE. Down: micro-Ag-ISE.

Long-term stability of the proposed electrodes was evaluated in order to find the lifetime of the electrode membrane. The lifetime of a membrane was evaluated by frequent calibration over 1 month. The EMF responses showed no significant drift for 18 days with the concentration range 10^{-5} to 10^{-2} M as shown in Figure 4.9. The fluctuation of EMF values was found in the concentration range of 10^{-8} to 10^{-6} M due to their low concentrations (not in the working linear range). However, after 18 days the potential changed significantly from the freshly conditioned membrane arise from the leaching of components of the membrane to the aqueous phase. The electrode membrane also turned black, and silver metal-liked color appeared on the membrane surface.

The lifetime of microelectrode is shorter. It can be used for only 1 day after condition. This disadvantage stems from the fact that sensing ingredients in the membrane are very low, and leaching of the sensing ingredients makes the membrane response changed negatively. Nevertheless a microelectrode needs very small amount of membrane ingredients. It can thus be produced at a very low cost and can be disposed after use.

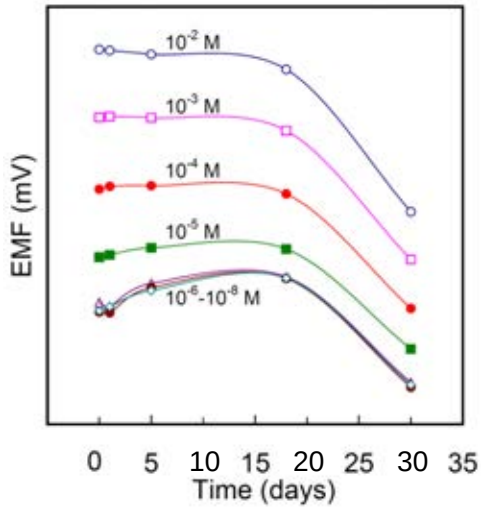

Figure 4.9 Long-term response of the macro-Ag-ISE measured by using the same electrode.

4.3 Analytical Applications of Ag-ISE from L2

4.3.1 Determination of mixed Cl^- and Br^-

The fabricated electrodes were applied in potentiometric titrations of the mixture of chloride and bromide ions because Ksp of AgBr is 1000 times lower than that of AgCl. Therefore, it is theoretically possible to potentiometrically titrate the mixture of chloride and bromide in one experiment. Titration curves of 25 µL of 1.0 M KBr and 1.0 M KCl with 0.01 M $AgNO_3$ are illustrated in Figure 4.10. Two end points are clearly established for both types of electrodes. The first end point is corresponding to the quantity of Br^- and the second end point is pertinent to the amount of Cl^-.

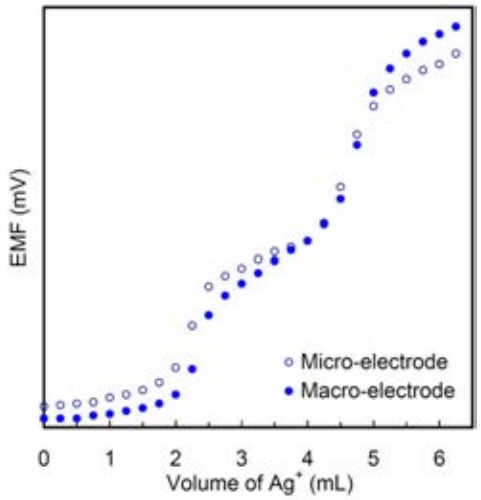

Figure 4.10 Potentiometric titration curves of the mixture of 1.0 M (25 µL) of KBr and KCl with 0.01 M $AgNO_3$ using macro- and microelectrodes.

4.3.2 Determination of concentration of AgNPs

Nowadays, nanoparticles are a subject of high interest because the nanometer-sized materials provide special characteristics that are not seen in the macro-sized materials of the same element. AgNPs are one of the most interested nanoparticles developed for industrial and medical uses [1–4]. Actually, AgNPs can be synthesized by several procedures with different size and particle size distribution [83–84].

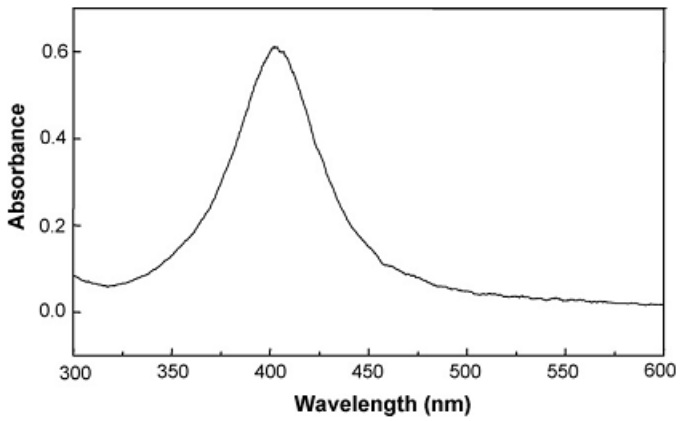

Figure 4.11 The plasmon absorption band of diluted 100 – 1000 from high concentration of the synthesized AgNPs (10,000 ppm) (λ_{max} = 403 nm).

AgNPs were synthesized via the chemical reduction process of $AgNO_3$ using $NaBH_4$ as adapted from previous reports [67–69]. The plasmon extinction of the synthesized silver nanoparticles measured by a portable UV-vis spectrophotometer (Ocean Optics USB 4000UV-Vis spectrophotometer) shown in Figure 4.11 has a maxima at 403 nm with a narrow full width at half height (FWHH ~50 nm). This indicates that the synthesized nanoparticles have a narrow size distribution. The size and shape of the synthesized silver nanoparticles have been further observed by transmission electron microscope (JEOL JEM-2010). The TEM images indicate that AgNPs are spherical and have an average particle size of 14 nm as shown in Figure 4.12.

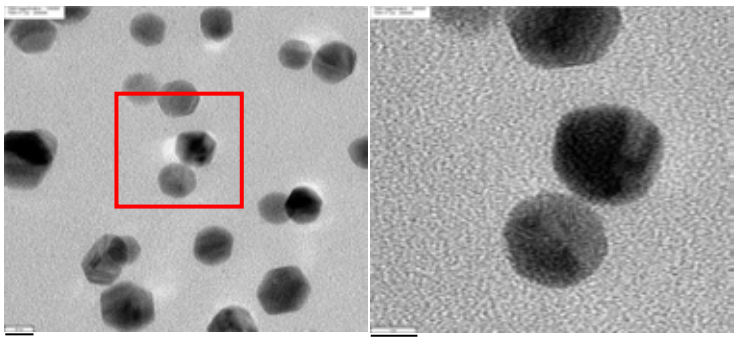

Figure 4.12 TEM images of the synthesized gNPs (a) TEM magnification 150 000 (b) TEM magnification 400 000.

Our Ag-ISEs were also explored their applications in speciation analysis of the AgNPs. The rational was from the preparative procedure of AgNPs which were reduced from salts of Ag(I). Usually, silver ions were left after reduction of a Ag(I) salt to AgNPs. The presence of residual Ag^+ would degrade the reactivity and property of AgNPs. Hence, determination of residual Ag^+ and total Ag^+ concentration is needed in order to control the nanoparticle quality. From the principle of basic atomic spectroscopy, commercial spectroscopic instruments Ag^+ and AgNPs. This problem can be solved by an ISE because the ISE senses only Ag^+ presented in the solution.

Here, we demonstrate a simple procedure to determine Ag^+ in AgNPs solution using our fabricated Ag-ISEs. Both macro- and microelectrodes can be used directly to the AgNPs solution to determine residual Ag^+. Effects of the sample matrix to the electrode response are shown in Figure 4.13. Calibration curves in the presence and absence of the gNPs show insignificant differences. Therefore, the AgNPs solution matrix does not interfere the electrode membrane.

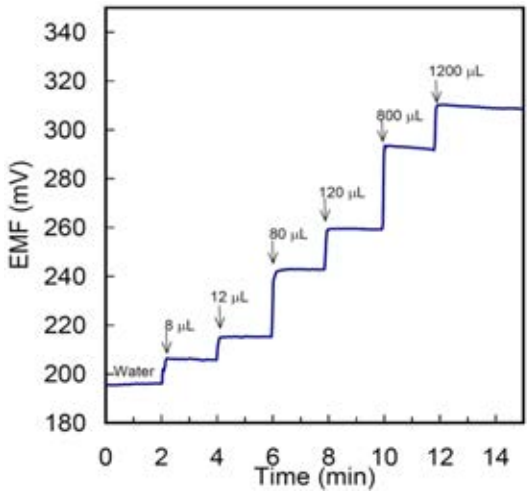

Figure 4.13 Ag-ISE response after adding appropriate volumes of concentrated AgNPs into 10.00 mL of water. The response is corresponding to the residual Ag^+ presented in the AgNPs solution.

Upon adding AgNPs solution to the sample vial, residual Ag^+ in the solution was observed from the potential jump as shown in Figure 4.13. In order to check the amount of free silver and the matrix interference in the AgNPs solution, different amounts of AgNPs were added to the solution. The pattern of potential jumps was similar to a calibration curve generated with the Ag^+ standard solution. This result showed that the response of the membrane towards the residual Ag^+ presented in the AgNPs solution could be measured without bias from the sample matrix.

AgNPs (1.00 mL) was diluted to 10.00 mL for determination of residual Ag^+ presented in the AgNPs solution. The comparison time trace lines between the system in the presence and absence of AgNPs are shown in Figure 4.14 (a) and (b) for macro- and microelectrode, respectively. The residual Ag^+ concentration that presented in the

original AgNPs solution was calculated by direct calibration curve and found to be 3.77 ± 0.2 and 3.61 ± 0.2 ppm for macro- and microelectrode, respectively. Therefore, the residual Ag^+ measured from both electrodes is not statistically different.

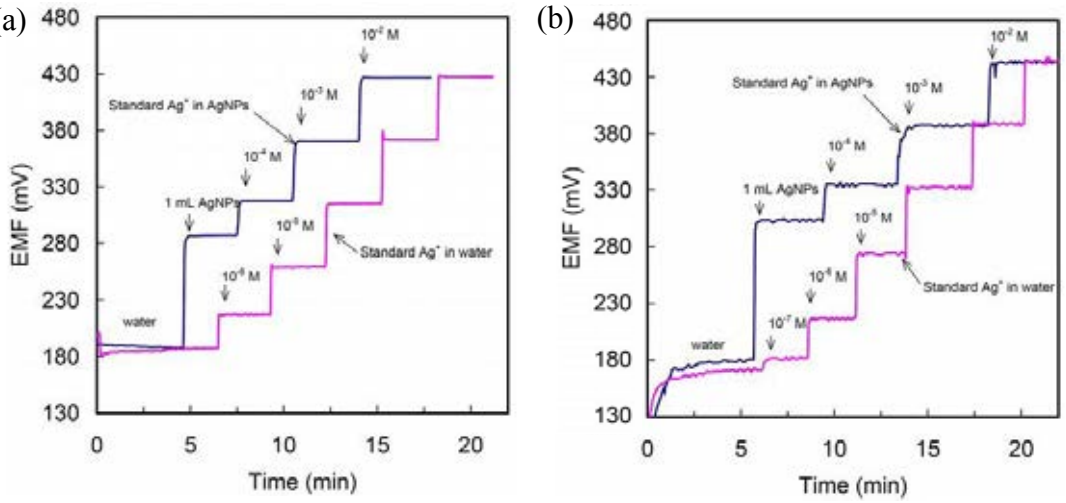

Figure 4.14 Comparison of time trace lines in the absence and presence of 1.00 mL of concentrated AgNPs solution diluted to 10.00 mL in water for (a) macro- and (b) microelectrode.

The total concentrations of the silver content in the AgNPs solution were determined by oxidizing with H_2O_2 to yield Ag^+. The complete conversion of AgNPs was confirmed by UV-visible spectrophotometry as shown in Figure 4.15. The characteristic sharp absorption peak at 403 nm disappears when 5 µL of 4% (v/v) H_2O_2 was added. The potential jumps while the H_2O_2 was added suggests the increment of Ag^+ in the solution as showed in Figure 4.16 (a). The microelectrode could be used to measure total Ag^+ content in the AgNPs solution in the same manner as the macroelectrode as illustrated in Figure 4.16 (b). After the residual Ag^+ in the mixture solution was measured, 100 µL of 4% (v/v) H_2O_2 were added. It was found that H_2O_2 was able to harm the sensing membrane. The potentials of the standard Ag^+ added to the solution (after added H_2O_2) were lower than the calibration curve (before total Ag^+ measurement) indicating the loss of the sensor materials. Therefore, the amount of H_2O_2 was reduced to the smallest volume (5 µL) that was enough to provide complete oxidation (confirmed by UV-visible spectrophotometer). The

membrane responses of both macro- and microelectrodes after contacting H_2O_2 did not changed significantly.

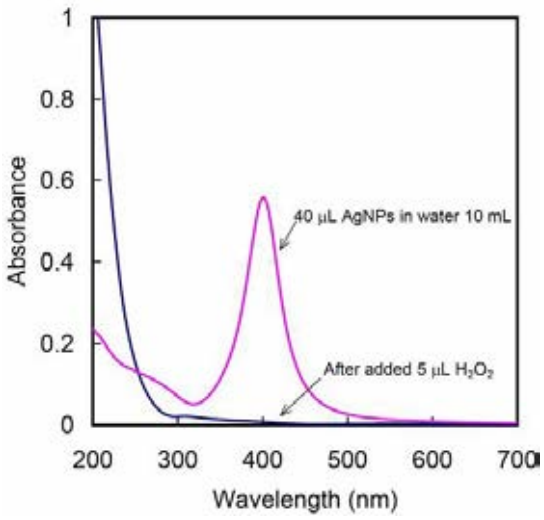

Figure 4.15 UV-visible spectrum of AgNPs solution before and after adding 5 µL of H_2O_2.

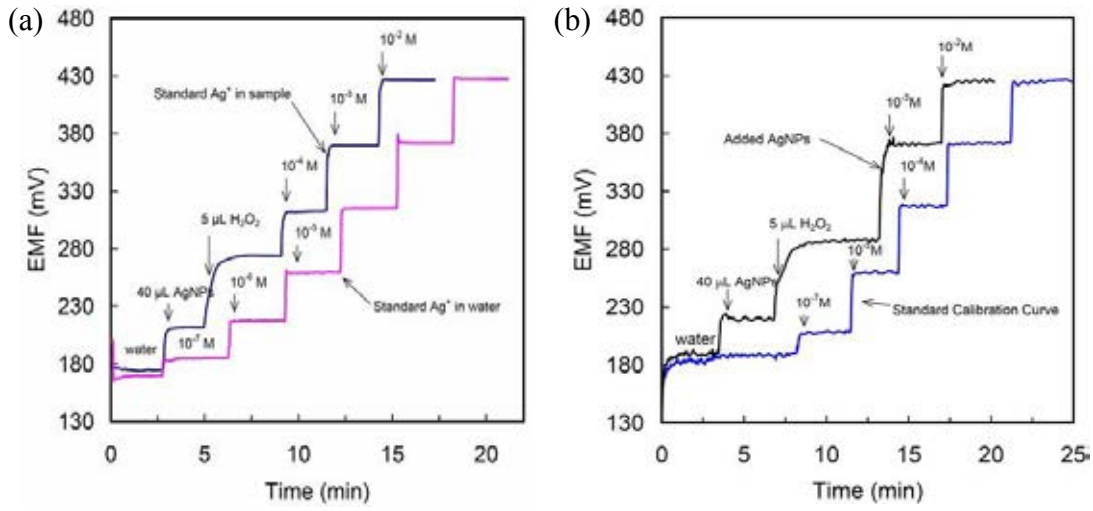

Figure 4.16 Time trace line of the Ag-ISE, comparison between calibration curve time trace line and the system containing AgNPs. In the lower line, 40 µL of concentrated AgNPs was added to 10.00 mL of water following by adding 5 µL of H_2O_2 for (a) macro- and (b) microelectrode.

The EMF values can be used to calculate the total concentration of Ag^+ by direct calibration curve. The concentration of total Ag content in the AgNPs (dilution by adding 40 µL of AgNPs to 10.00 mL solution) determined using macro- and microelectrode by direct calibration was 3.57 ± 0.17 and 3.43 ± 0.15 ppm, respectively. In addition, the concentration of total silver content in the same AgNPs solution determined by FAAS method was 3.62 ± 0.05 ppm. By using a pair t-test, the concentration of Ag^+ from ISE method was insignificantly different from the F S result at 95% confidence level. Therefore the performance of our fabricated ISE is comparable with such an expensive instrument. Moreover, the FAAS method cannot differentiate silver species in the AgNPs sample. In experiments, the concentration of AgNPs used for determination of total Ag content (Figure 4.16) was less than that used for determination of Ag^+ (Figure 4.14) because the EMF values of Ag^+ must be regulated to the working concentration range.

After determination of total concentration of AgNPs had done, the calibration curve was always rechecked again in order to confirm that the measuring value was not bias. The calibration curve after adding H_2O_2 showed insignificant difference with the original membrane observed. However, this problem did not observe in the macroelectrode because of more sensor ingredients.

4.4 Glucose Biosensor

Recently, metal nanoparticles such as gold and silver nanoparticles have been used as nanomaterial labels or "markers" in electrochemical biosensors and immunosensors [85–87]. Our group has fabricated a Ag-ISE using benzothiazole calix[4]arene as ionophore from **L2**. This Ag-ISE can be used in speciation analysis of silver nanoparticles. The key idea of this part is to use AgNPs as cation marker in glucose biosensors as shown in Figure 4.17. The enzyme-substrate reaction between glucose oxidase and glucose is well-known to yield H_2O_2. The oxidizing power of H_2O_2 is sufficient to convert Ag^0 of AgNPs to free Ag^+. The activity of Ag^+ is immediately measured by a Ag-ISE.

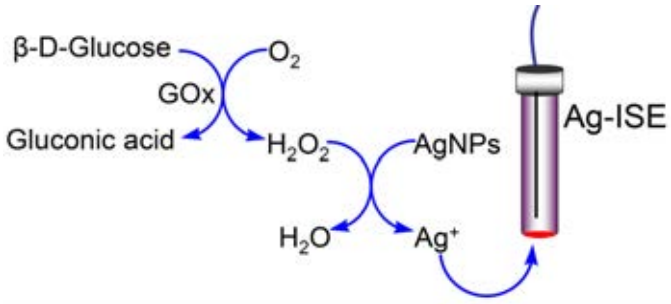

Figure 4.17 Schematic use AgNPs as a new potentiometric redox marker in a glucose biosensor.

4.4.1 Relationship between the concentration of H_2O_2 and the releasing of Ag^+ from AgNPs

The relationship between the concentration of H_2O_2 and the concentration of the free Ag^+ generated from AgNPs is investigated by using the different concentration of the mixture of H_2O_2 and AgNPs solution. The concentrations of Ag^+ in each H_2O_2 concentration are determined by direct potentiometry using our fabricated Ag-ISE. According to the results in speciation analysis of AgNPs, AgNPs always contain residual free Ag^+ in the solution. Therefore, the free Ag^+ from AgNPs is first measured and then it is subtracted from the concentration of the mixture. The response EMF is then converted to activity of Ag^+. It is found that the logarithmic of the concentration of H_2O_2 and activity of Ag^+ possesses a linear relationship as illustrated in Figure 4.18. This experiment signifies that the change of H_2O_2 concentration corresponds very well to the generation of Ag^+ from oxidized AgNPs. Therefore, free Ag^+ released from AgNPs can be used to determine glucose concentration.

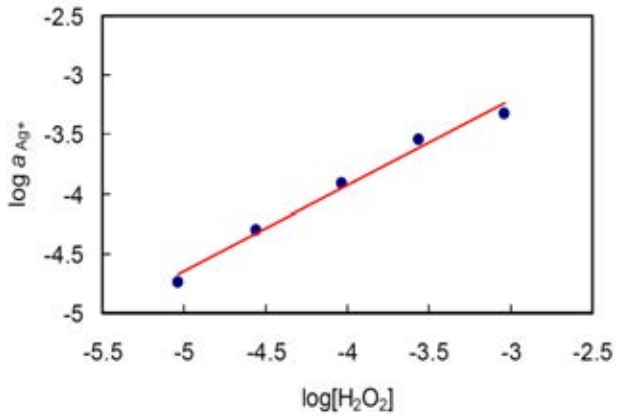

Figure 4.18 The relationship between the concentration of H_2O_2 and the activity of free Ag^+ releasing from AgNPs.

4.4.2 Measurement of Ag^+ releasing from oxidized AgNPs in reactions of glucose and GOx

Figure 4.19 (a) illustrates the resulting EMF versus time of the general experimental procedure. The Ag-ISE is first immersed in the buffer solution of glucose. After the addition of AgNPs, the EMF increases due to the presence of residual Ag^+ in AgNPs. GOx is added after the potential stabilizes. The addition of GOx dilutes the sample solution, which causes the sudden drop in EMF. As time proceeds, the GOx converts glucose to gluconic acid and H_2O_2. The generated H_2O_2 oxidizes AgNPs to free Ag^+ resulting in the gradual increase of the EMF. The increasing EMF is continuously monitored and recorded with respect to an interval sampling time. The derivative of EMF with respect to time is considered as the reaction rate of the enzyme-substrate reaction as presented in Figure 4.19 (b). This value corresponds very well to the glucose concentration, and the maximum rate is used here as a monitoring signal. This approach is quite remarkable because the absolute EMF is not required; only the differences in EMF are needed. Therefore, the accuracy of the reference electrode is rather unimportant.

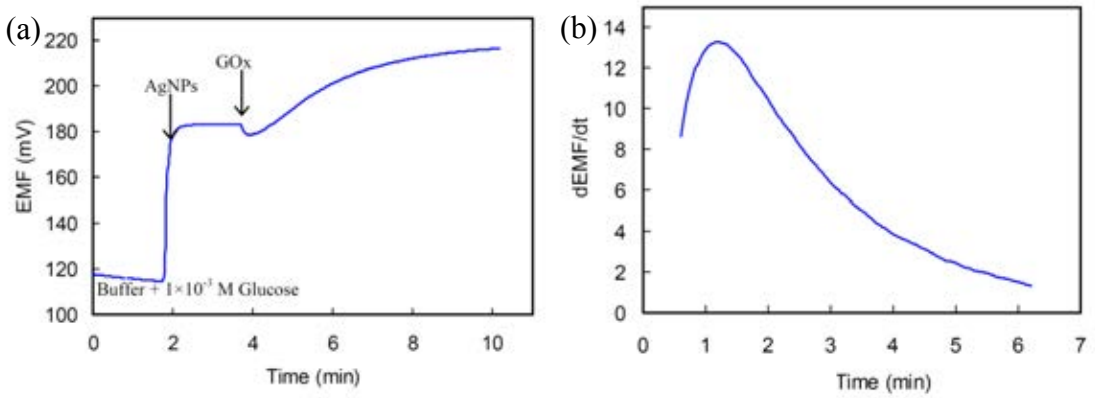

Figure 4.19 (a) Continuous time trace line of the EMF change with time (b) Change of the reaction rate with time after adding GOx.

4.4.3 Effect of the solution pH

Our Ag-ISE fabricated from **L2** works well at wide pH range (pH 2 – 8) without significant EMF change. This characteristic provides many advantages because it does not require a crucial pH adjustment. However, enzyme activity is always affected by several parameters. Solution pH is one of the important factors to the enzyme activity. Therefore, pH of the working assay must be adjusted to a suitable value. To avoid precipitation of Ag^{+}, 10 mM magnesium acetate is chosen as a working buffer. The solution pH is varied in the range of 4.5 – 7 by adjusting with acetic acid as shown in Figure 4.20. It is found that at the pH range 6 – 7, there is a slight change in the reaction rate. Therefore, pH 6 is chosen as a working pH.

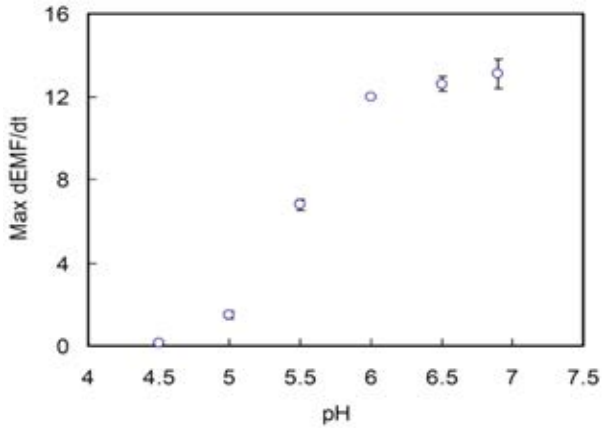

Figure 4.20 Effect of the solution pH to the maximum reaction rate.

4.4.4 Effect of GOx concentration

The effect of enzyme concentration is studied by fixing glucose concentration at 1.0 mM. The concentration of GOx is varied from 0.38 to 15.4 U mL^{-1}. The results in Figure 4.21 show that where the concentration of the enzyme is less than 7.6 U mL^{-1}, the reaction rate is depended on the enzyme concentration. This phenomenon always occurs when the concentration of the enzyme is lower than the substrate. In addition, when the concentration of enzyme is increased from 7.6 to 11.5 U mL^{-1} the reaction rate shows insignificant difference. This indicated that the reaction rate depends on the substrate concentration. However, when the concentration of GOx is higher than 7.6 U mL^{-1}, the precision of the reaction rate is aggravated considering from the variable reaction rates. In addition, the more concentration of GOx we use, the more it costs. Therefore, 7.6 U mL^{-1} is chosen as the working enzyme concentration for the given concentration range (mM range).

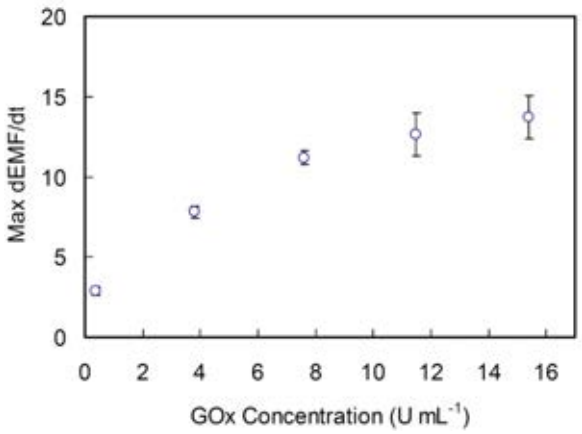

Figure 4.21 Effect of the GOx concentration to the maximum reaction rate of 1 mM glucose at pH 6 in 10 mM magnesium acetate buffer.

4.4.5 Effect of the quantity of AgNPs

Volumes of AgNPs used in the assay can affect the reaction rate. If the increasing amount of AgNPs causes of the increasing of the reaction rate, it implies that AgNPs involves in a rate-determining step. The relation between the amount of AgNPs and the reaction rate is illustrated in Figure 4.22. The results show that the

reaction between AgNPs and H_2O_2 is faster than the reaction between the enzyme and the substrate. Therefore, AgNPs do not involve in the rate-determining step. However, when the amount of AgNPs is increased, the reaction rates seem to decrease slightly. Higher volume of AgNPs added results in higher concentration of free Ag^+ that can inhibit enzyme activity. However, residual Ag^+ in 10 – 20 μL of AgNPs shows no significant inhibition to the enzyme. Therefore 20 μL of 1000 ppm AgNPs were used in further experiments.

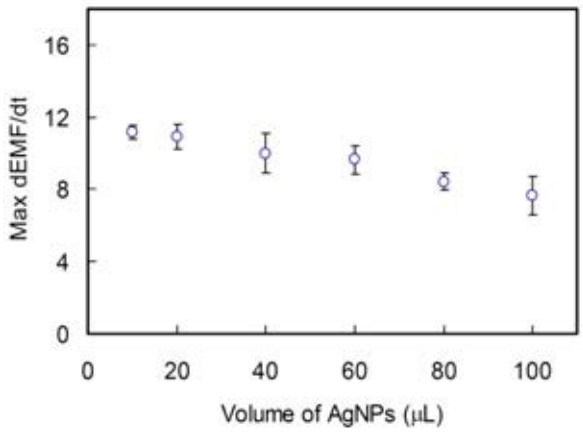

Figure 4.22 Effect of the volume of AgNPs solution used in the assay.

4.4.6 Glucose calibration curve

All optimized parameters mentioned previously are applied in order to make a glucose calibration curve. Glucose concentrations are varied from 3×10^{-5} to 3×10^{-2} M and the reaction rate is monitored at different concentration change. Figure 4.23 (a) shows that the rate of the EMF change (reaction rate) depends on the glucose concentration. The glucose calibration curve is illustrated in Figure 4.23 (b). When the concentration of glucose changes the reaction rate also changes significantly; a linear correlation between the reaction rate and logarithmic concentration of glucose is obtained (maximum [dEMF/dt] = 8.62 × log [glucose] + 38.19). The working linear range is found to be 1×10^{-4} to 3×10^{-3} M and can cover the glucose concentration in many detecting environments especially in diabetic serum. In addition, the lower detection limit of this sensor, obtained from the lowest glucose concentration that can give the EMF change after reacting with GOx, is 1.0×10^{-5} M.

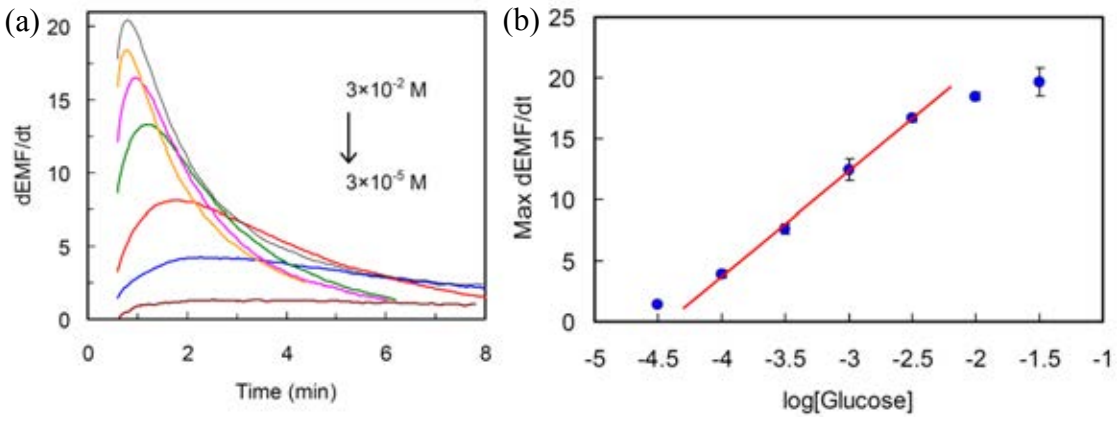

Figure 4.23 (a) The derivative of the EMF change with time at different glucose concentration. (b) Calibration curve of the glucose, plotting the maximum reaction rate against logarithmic of glucose concentration.

4.4.7 Study of interferences

The selectivity of a glucose biosensor depends on two major factors: the enzyme–substrate reaction and selective measurements. The enzyme-substrate reaction is very specific due to the nature of enzyme functionality. Glucose oxidase can only react with β-D-glucose without interfering from other types of sugars. Possible interferences in glucose determination such as urea (a protein metabolite), glycine, fructose and sucrose are tested in our measuring system since these interferences can be found in real samples such as blood serum, urine and beverages. The results are shown in Figure 4.24. The EMF does not significantly change upon addition of interferences. Therefore, the tested chemicals cannot meddle the measuring system. Furthermore after glucose is added, the EMF increases with the same behavior when compared to the system with no interferences.

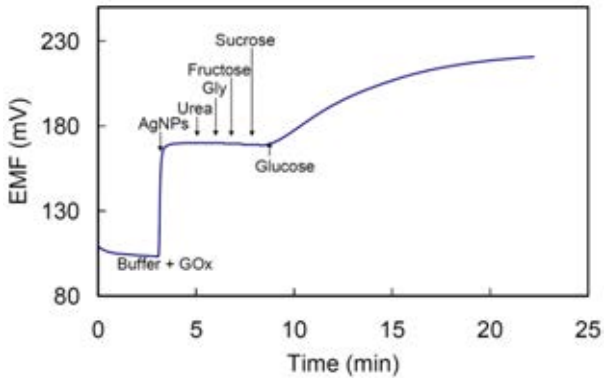

Figure 4.24 The time trace line of the EMF change with time after adding interferences.

However, our new method may have some drawback in the presence of possible interferences such as a reducing agent, for example ascorbic acid that can convert Ag^{+} to Ag^{0}. Moreover, chelating agents that possibly present in the real sample can also reduce the activity of free Ag^{+}.

4.4.8 Repeatability, sensor-to-sensor reproducibility and analysis of real samples

Our approach deals with the enzyme-substrate reaction of GOx and glucose which the rate of reaction depends on oxygen. Therefore the fluctuation of oxygen in the sample will definitely affect the reproducibility of the method. The repeatability of our proposed method can be evaluated by measuring the reaction rate of 1 mM glucose repeatedly with the same electrode. Reaction rates of each measuring experiments have showed that the Ag-ISE can be used several times with the relative standard deviation (RSD) less than 7%. Moreover, we also evaluate sensor-to-sensor reproducibility by measuring three replicates of 1 mM glucose by using five different electrodes. The results in Figure 4.25 show that the maximum of reaction rates obtained from different electrodes are not significantly different. Therefore the proposed method in detecting glucose is reliable.

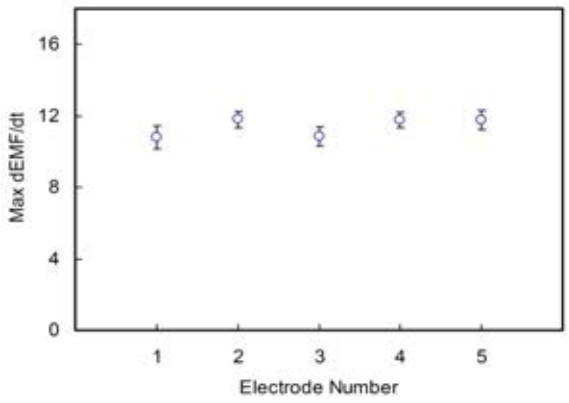

Figure 4.25 The sensor-to-sensor reproducibility of 5 Ag-ISEs (1 mM of glucose).

Glucose concentration in beverages was then measured by the proposed method, and results are shown in Table 4.4. The recovery of the spike samples is higher than 96% with good precision (RSD < 10%). Our concept thus gives good analytical characteristics of glucose detection and can be used for development of future glucose biosensors.

Table 4.4 Analysis of glucose concentration in beverages.

Sample no.	**Glucose added (μmol)**	**Glucose found (μmol[a])**	**Recovery (%)**	**RSD (%)**
1	0	1.05 ± 0.09[b]	-	-
	3	4.01 ± 0.19	98	6
2	0	1.56 ± 0.17	-	-
	3	4.46 ± 0.26	97	9
3	0	2.99 ± 0.14	-	-
	10	12.5 ± 0.80	96	8

[a] Volume used in 10.00 mL solution.
[b] Standard deviations in triplicate experiments.

4.5 DNA Biosensor

The best selective ionophore **L2** was used to fabricate Ag-ISE which has been successfully employed in speciation analysis of the AgNPs solution and in glucose biosensor by using AgNPs as cation maker. In this part, our fabricated Ag-ISµE was developed for monitoring DNA hybridization as illustrated in Figure 4.26. The target DNA is hybridized with neutral pyrrolidinyl peptide nucleic acid carrying a 2-aminocyclopentanecarboxylic acid (Lip-acpcPNA) covalently immobilized on gold substrate resulting in negatively charged surface as a result of phosphate backbone of target DNA. When a solution of positively charged CTAB-coated AgNPs is added onto the gold substrate, electrostatic interactions of hybridized Lip-acpcPNA/DNA and AgNPs take place. The deposited AgNPs are then oxidized by H_2O_2 to release Ag^+, which can be detected with our fabricated Ag-ISµE.

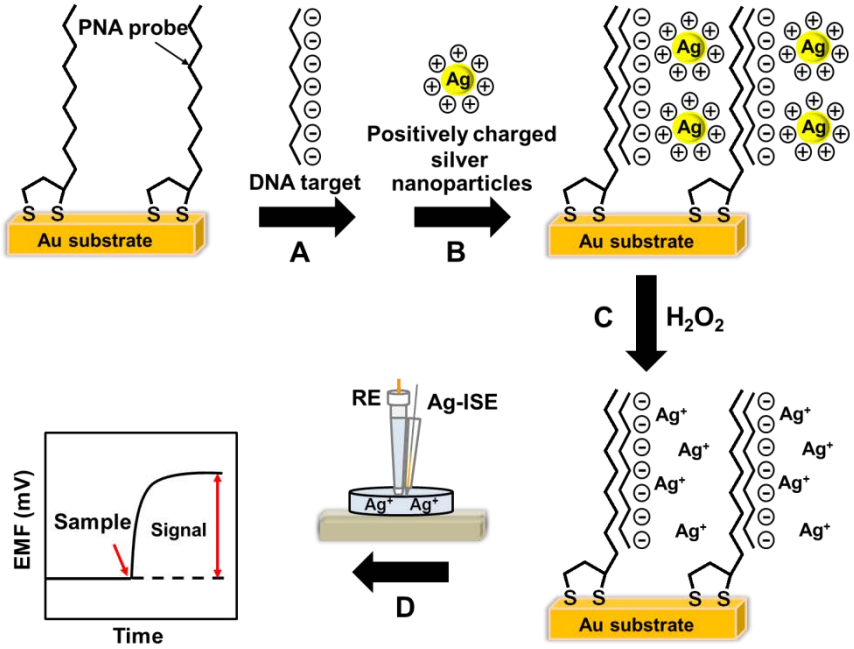

Figure 4.26 Schematic representation of AgNPs-based label-free potentiometric DNA detection.

4.5.1 Preparation and Characterization of CTAB-coated AgNPs

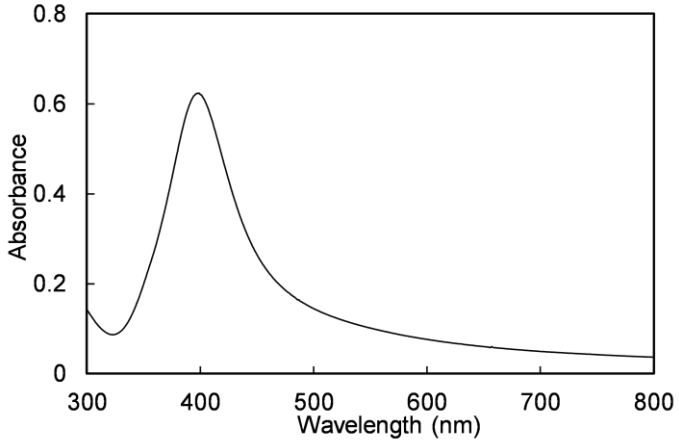

Figure 4.27 The plasmon absorption band of positively charged AgNPs (λ_{max} = 397 nm).

The positively charged CTAB-coated AgNPs were synthesized in a water-ethanol system by one step reaction by reducing $AgNO_3$ with $NaBH_4$ in the presence of CTAB. Figure 4.27 shows the UV-vis spectrum with a strong surface plasmon band at 397 nm. TEM is used to characterize shape and size of synthesized CTAB-coated AgNPs. TEM image in Figure 4.28 clearly indicates that CTAB-coated AgNPs are spherical and have an average particle size of 20 nm. The particles were found to be colloidally stable at least 2 months.

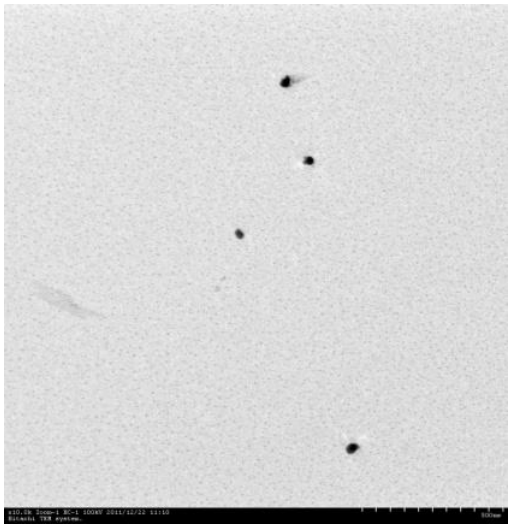

Figure 4.28 TEM image of the synthesized AgNPs. 500 nm scale bar.

4.5.2 Fabrication of Ag-ISμE from L2

The calibration curve of Ag-ISμE was performed in 1000 μL Milli-Q water and used 10 mM $NaNO_3$ (pH 6.0) as background by using Na-ISμE as pseudo reference electrode as shown in Figure 4.29. Na^+-microelectrode was chosen as a reference electrode and Na^+ was selected as the background electrolyte since this Ag-ISμE showed good selectivity towards Ag^+ compared to Na^+ with logarithmic selectivity coefficient, $\log {}^{pot}_{g\,Na} = -6.70$. The Ag-ISμE shows a low detection limit of 9.12×10^{-7} M (~ 1 μM) in 1000 μL solution with near theoretical Nernstian slope of 58.7 mV decade^{-1} (inset, Figure 4.29).

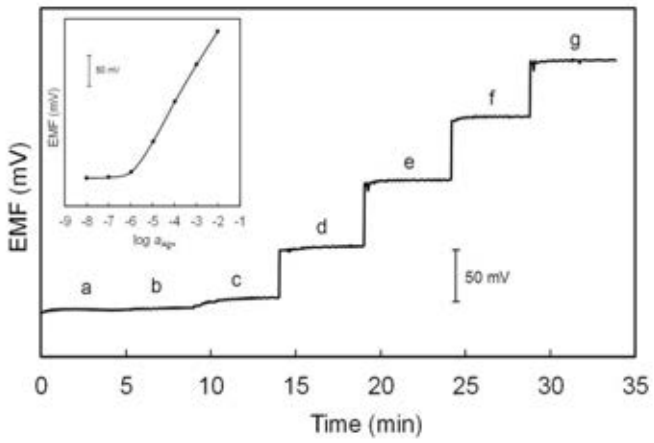

Figure 4.29 Time trace line response of the Ag-ISμE to increasing level of Ag^+: (a) 10^{-8}; (b) 10^{-7}; (c) 10^{-6}; (d) 10^{-5}; (e) 10^{-4}; (f) 10^{-3}; (g) 10^{-2} M in 1000 μL of solution with 10 mM $NaNO_3$ as background with a Na-ISμE as pseudo reference electrode. Inset displays the corresponding calibration plot.

4.5.3 Immobilization of Lip-acpcPNA on gold surface and detection of DNA hybridization

A thiol or a disulfide group can be immobilized by chemisorption onto gold surface to form self-assembled monolayer (SAM). Covalent immobilization of lipoic acid on gold surface is more stable with two S-Au bonds than that of the simple thiol [88]. Disulfide group of Lip-acpcPNA probe was attached on gold substrate by

immersing with various concentrations (1, 5 and 10 μM) to investigate a proper concentration of probe covered on gold substrates to be used for getting difference signals before and after hybridization. The potentials of gold substrate, only immobilized Lip-acpcPNA probe and Lip-acpcPNA hybridized with the target DNA on gold substrate when introducing positively charged CTAB-coated AgNPs were compared (Figure 4.30). The hybridization signals with complementary DNA were obtained when 10 μM of Lip-acpcPNA was treated onto gold surface. It indicated that disulfide of Lip-acpcPNA (10 μM) can be self-assembled formation onto gold substrate with lower potential (compared to bare gold substrate) which decreased non-specific adsorption between AgNPs and the bare gold substrate. Compared to only Lip-acpcPNA as probe (neutral charge), higher potential of Lip-acpcPNA hybridized with the target DNA resulted from electrostatic interactions between negatively charged of DNA backbone and positively charged of CTAB-coated AgNPs. From the results, it indicated that 20 nm of CTAB-coated AgNPs can access to space between Lip-acpcPNA/DNA duplexes. For lower concentrations, 1 and 5 μM of Lip-acpcPNA display no different in EMF values of Lip-acpcPNA probe and hybridization of target DNA because the amount of Lip-acpcPNA immobilized on gold substrate was not enough to hybridize effectively with the target DNA. Therefore, 10 μM of Lip-acpcPNA was selected for further experiments.

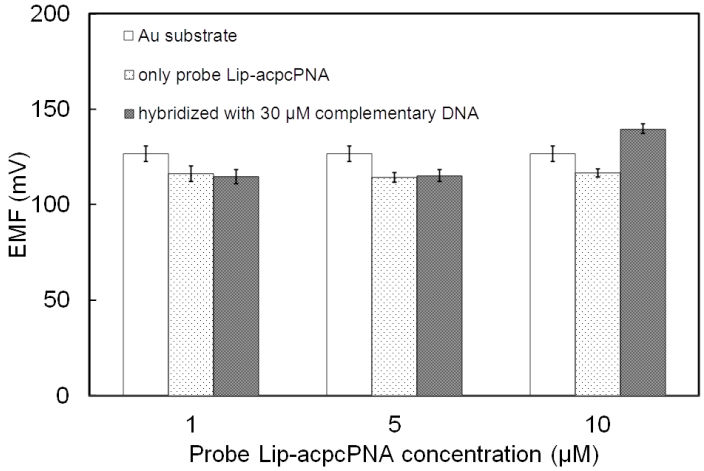

Figure 4.30 Effect of concentration of probe Lip-acpcPNA on the response.

Lip-acpcPNA (10 μM) immobilized on gold substrate was hybridized with fully complementary DNA, single base sequence mismatched DNA and non-complementary DNA under the same hybridization condition (10 mM $NaNO_3$, pH 6.0). The results exhibit in Figure 4.31 that the hybridization with fully complementary DNA produces the highest signal with 144 ± 3 mV. Hybridization with non-complementary DNA gives very low signal because of no hybridization between non-complementary DNA and Lip-acpcPNA immobilized on the gold substrate which is similar to that of single base mismatched DNA. From time trace lines in Figure 4.31, this Lip-acpcPNA probe can discriminate fully complementary DNA, non-complementary DNA and single base mismatched DNA in 10 mM $NaNO_3$.

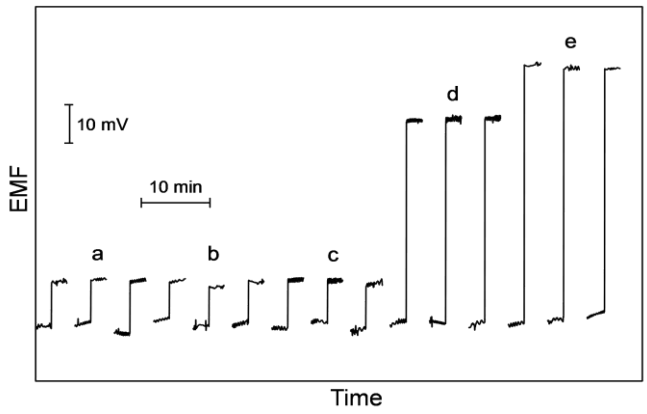

Figure 4.31 Potentiometric hybridization response: (a) control solution (10 mM $NaNO_3$, zero target), (b) 40 μM noncomplementary DNA, (c) 40 μM single base mismatched DNA, (d) 20 μM target DNA, and (e) 40 μM target DNA (as complementary targets) after DNA hybridization. Potentiometric measurements were performed in 1000 μL samples with a Na-ISμE as pseudo reference electrode and used 10 mM $NaNO_3$ as background.

10 μM of Lip-acpcPNA immobilized on gold substrate was hybridized with complementary DNA at different concentrations (2, 5, 10, 15, 20, 40 and 80 μM). Figure 4.32 shows that EMF values of hybridization depend on the increase in concentration of target DNA. The concentration of target DNA is higher resulting in higher negative charge from phosphate backbone of DNA to give larger signal of Ag^+. The lower detection limit is 2 μM of target DNA in 1000 μL sample with linear

ranging from 2 to 20 μM target DNA that correlated with concentration of Ag^+ in micro-molar range ($[Ag^+] = 0.2135 \times [DNA] + 0.7738$) as shown in Figure 4.33.

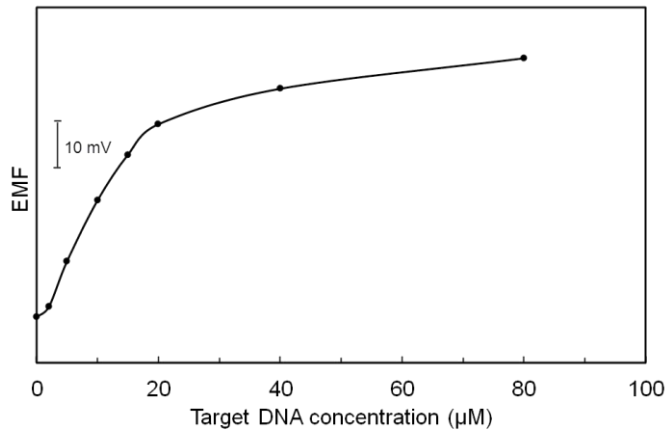

Figure 4.32 Effect of concentration of target DNA on the response.

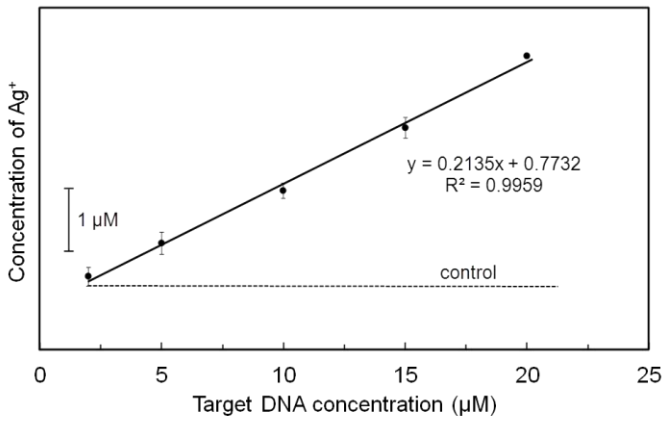

Figure 4.33 Calibration plot for the potentiometric monitoring of AgNPs-based label-free DNA hybridization in 1000 μL eppendorf tube (error bars: SD, N = 3). The dashed line corresponds to control signal (no target DNA).

The results indicate that the proposed system can detect DNA hybridization by following signals of Ag^+ which obtained from dissolution of positively charged CTAB-coated AgNPs interacting with negatively charged DNA. In addition, this system is very simple with less steps for making hybridization between Lip-acpcPNA

probe and DNA target when compared to other systems using simple potentiometry based on ISEs [40–42]. The other systems for detecting DNA hybridization are more complicated and time-consuming with modification and labeling of DNA. However, our Ag-ISμE shows high detection limits in micro-molar range leading to a large amount of DNA employed as compared to other ISEs having detection limits in nano-molar or sub-nanomalar range [40–42].

CHAPTER IV

CONCLUSIONS

Six calix[4]arene derivatives have been designed and synthesized by attaching one or two opposite phenolic groups with a benzothiazole, a dipicolylamine and a hydrazone derivatives yielding calix[4]arene derivatives, **L1 – L6**. The potentiometric studies of electrodes from compounds **L1 – L6** showed that they could be used as ionophores in Ag-ISEs. The ion selectivity patterns of electrodes based on two-substituted phenolic groups gave a higher selectivity coefficient towards Ag^{+} over Hg^{2+} than that of one-substituted phenolic group. However, **L2** containing two nitrogen and two sulfur donor atoms obviously showed the most difference between the selectivity coefficient of Ag^{+} and interfering Hg^{2+} and had high discrimination of other cations. The complex formation constant of **L2** towards Ag^{+} was high corresponding to its best selectivity towards Ag^{+}.

The optimized membrane composition of ionophore **L2** (10 mmol kg^{-1}) for both macro- and microelectrodes was 50 mol% KT*p*ClPB (relative to ionophore) in the *o*-NPOE plasticized PVC membrane (1:2; PVC:*o*-NPOE by weight) to obtain the best characteristic Ag-ISE. Nernstian's slope could be observed with the detection limit in micro-molar range. The working linear ranges were found to be 4 orders of magnitude. The response time was very fast and the measured potentials were very stable. We have demonstrated that the microelectrode could be used in a similar manner as regular-size electrode. The application in the determination of the mixture of chloride and bromide ion was successful by the presence of two distinguishable end points. We have also shown that our fabricated electrodes could remarkably be employed in speciation analysis of AgNPs solution in which both residual Ag^{+} and the total Ag content could be determined.

We have demonstrated the use of AgNPs as metal marker in our Ag-ISE glucose biosensor. The fabricated Ag-ISE from **L2** remarkably combines two specificities in glucose detection: the enzyme-substrate reaction of glucose oxidase

and glucose and the selective detection of Ag^{+}. The optimum solution pH was 6.0 in 10 mM magnesium acetate buffer. The suitable enzyme concentration used was 7.6 U mL^{-1} and the appropriate volume of AgNPs redox marker was 20 µL. The lower detection limit was 1.0×10^{-5} M. The proposed method could be used for determination of glucose concentration range of 0.1 – 3 mM with good selectivity, accuracy, repeatability and reproducibility. We optimistically think that this method can be further applied to detect other oxidase enzyme systems.

In addition, we have demonstrated that Ag-ISµE based on polymeric membrane (**L2**) could be used to detect DNA hybridization from signal of Ag^{+}, which derived from the electrostatic interactions between the positively charged CTAB-coated AgNPs and the negatively charged target DNA hybridized to the neutral Lip-acpcPNA as probe immobilized on the gold substrate. The concentration of Ag^{+} correlated with the concentration of target DNA within the range of 2 µM to 20 µM, with a detection limit of 2 µM target DNA in 1000 µL samples. It is expected that the simple potentiometric method for the label-free detection of DNA may be applied in genetic diagnosis.

Suggestion for future works:

In this research, the Ag^{+}-microelectrode used in DNA biosensor gave lower detection limit in micro-molar range leading to the use of a large amount of DNA. Thus, the inner filling solution of the Ag-ISµE fabricated from **L2** should be optimized to obtain a lower detection limit down to sub-nanomolar concentration range in microliter samples (100 – 200 µL) which can be applied in immunosensor or other assays of DNA in real samples.

REFERENCES

[1] Furno, F., and others, Silver nanoparticles and polymericmedical devices: a new approach to prevention of infection?. *J. Antimicrob. Chemother.* 54 (2004): 1019–1024.

[2] Durán, N., Marcato, P. D., De Souza, G. I. H., Alves, O. L., and Esposito, E., Antibacterial effect of silver nanoparticles produced by fungal process on textile fabrics and their effluent treatment. *J. Biomed. Nanotech.* 3 (2007): 203–208.

[3] Sondi, I., and Salopek-Sondi, B., Silver nanoparticles as antimicrobial agent: a case study on *E. coli* as a model for Gram-negative bacteria. *J. Colloid Interface Sci.* 275 (2004): 177–182.

[4] Kim, J. S., and others, Antimicrobial effects of silver nanoparticles. *Nanomedicine* 3 (2007): 95–101.

[5] Wang, J., *Analytical Electrochemistry*. 3rd edn. New York: Wiley, 2006.

[6] Rubinova, N., Chumbimuni-Torres, K., and Bakker, E., Solid-contact potentiometric polymer membrane microelectrodes for the detection of silver ions at the femtomole level. *Sens. Actuators B* 121 (2007): 135–141.

[7] Xu, D., and Katsu, T., *O,O,O*-Trialkyl phosphorothioates as simple and effective ionophores for silver ion-selective membrane electrodes. *Anal. Chim. Acta* 443 (2001): 235–240.

[8] Yan, Z., Lu, Y., and Li, X., Silver ion-selective electrodes based on bis(dialkyldithiocarbamates) as neutral ionophores. *Sens. Actuators B* 122 (2007): 174–181.

[9] Abbaspour, A., Izadyar, A., and Sharghi, H., Carbon composition PVC based membrane in a highly selective and sensitive coated wire electrode for silver ion. *Anal. Chim. Acta* 525 (2004): 91–96.

[10] Mittal, S. K., Kumar, P., Kumar S K, A., and Lindoy, L. F., A comparative study of liked 2,2'-dipyridylamine ligand system as an ion selective electrode for Ag (I) ions. *In. J. Electrochem. Sci.* 5 (2010): 1984–1995.

[11] Chung, S., Kim, W., Park, S. B., Kim, D. Y., and Lee, S. S., Silver(I)-selective membrane electrodes based on sulfur-containing podands. *Talanta* 44 (1997): 1291–1298.

[12] Mashhadizadeh, M. E., Shockravi, A., Khoubi, Z., and Heidarian, D., Efficient synthesis of a new podand and application as a suitable carrier for silver ion-selective electrode. *Electroanalysis* 21 (2009): 1041–1047.

[13] Mashhadizadeh, M. E., Mostafavi, A., Allah-Abadi, H., and Sheikhshooai, I., New Schiff base modified carbon paste and coated wire PVC membrane electrode for silver ion. *Sens. Actuators B* 113 (2006): 930–936.

[14] Hassouna, M. E. M., Elsuccary, S. A. A., and Graham, J. P., *N,N′*-Bis(3-methyl-1-phenyl-4-benzylidine-5-pyrazolone)propylenediamine Schiff base as a neutral carrier for silver (I) ion-selective electrodes. *Sens. Actuators B* 146 (2010): 79–90.

[15] Shamsipur, M., and other, Novel Ag^{+} ion-selective electrodes based on two new mixed azathioether crowns containing a 1,10-phenanthroline sub-unit. *Anal. Chim. Acta* 462 (2002): 225–234.

[16] Zhang, J., Ding, J., Yin, T., Hu, X., Yu, S., and Qin, W., Synthesis and characterization of monoazathiacrown ethers as ionophores for polymeric membrane silver-selective electrodes. *Talanta* 81 (2010): 1056–1062.

[17] Singh, A. K., and Saxena, P., Silver(I)-selective electrode based on [$Bz_2Oxo_4(18)dieneS_4$] tetrathia macrocyclic carrier. *Anal Bioanal Chem* 385 (2006): 90–95.

[18] Su, C. -C., Chang, M. -C., and Liu, L. K., New Ag^{+} and Pb^{2+}-selective electrodes with lariat crown ethers as ionophores. *Anal. Chim. Acta* 432 (2001): 261–267.

[19] Gupta, V. K., Pal, M. K., and Singh, A. K., Comparative study of Ag(I) selective poly(vinyl chloride) membrane sensors based on newly developed Schiff-base lariat ethers derived from 4,13-diaza-18-crown-6. *Anal. Chim. Acta* 631 (2009): 161–169.

[20] Mashhadizadeh, M. H., and Shamsipur, M., Silver(I)-selective membrane electrode based on hexathia-18-crown-6. *Anal. Chim. Acta* 381 (1999): 111–116.

[21] Siswanta, D., and others, Structural ion selectivity of thia crown ether compounds with a bulky block subunit and their application as an ion-sensing component for an ion-selective electrode. *Anal. Chem.* 68 (1996): 4166–4172.

[22] Bobacka, J., Lahtinen, T., Koskinen, H., Rissanen, K., Lewenstam, A., and Ivaska, A., Silver ion-selective electrodes on π-coordinating ionophores without heteroatoms. *Electroanalysis* 14 (2002): 1353–1357.

[23] Kimura, K., Yajima, S., Tatsumi, K., Yokoyama M., and Oue, M., Silver ion-selective electrodes using π-coordinate calix[4]arene derivatives as soft neutral carriers. *Anal. Chem.* 72 (2000): 5290–5294.

[24] Chen, L., He, X., Zhao, B., and Liu, Y., Calixarene derivative as the neutral carrier in silver ion-selective electrode and liquid membrane transport. *Anal. Chim. Acta* 417 (2000): 51–56.

[25] Mahajan, R. K., Kaur, I., and Kumar, M., Silver ion-selective electrode employing Schiff base *p-tert*-butyl calix[4]arene derivatives as neutral carriers. *Sens. Actuators B* 91 (2003): 26–31.

[26] Chen, L., Zeng, X., Ju, H., He, X., and Zhang, Z., Calixarene derivatives as the sensory molecules for silver ion-selective electrode. *Microchem. J.* 65 (2000): 129–135.

[27] Lu, J. -Q., Pang, D. -W., Zeng, X. -S., and He, X. -W., A new solid state silver ion-selective electrode based on a novel tweezer-type calixarene derivative. *J. Electroanal. Chem.* 568 (2004): 37–43.

[28] Demirel, A., Doğan, A., Akkuş, G., Yilmaz, M., and Kiliç, E., Silver(I)-selective PVC membrane potentiometric sensor based on a recently synthesized calix[4]arene. *Electroanalysis* 18 (2006): 1019–1027.

[29] Zeng, X., and others, The syntheses and Ag^{+}-selective electrode properites of benzothiazolylthiaalkoxy functionalized calix[4]arenes: an investigation of the structure-selectivity relationship in the ionophore-based ISEs. *Tetrahedron* 58 (2002): 2647–2658.

[30] Morakot, N., Ngeontae, W., Aeungmaitrepirom, W., and Tuntulani, T., Synthesis of novel calix[4]arenes having benzothiazolylacetamidoalkoxy pendants and their potential application as Ag^{+}-selective electrodes. *Bull. Korean Chem. Soc.* 29 (2008): 221–224.

[31] Szigeti, Z., and others, Novel potentiometric and optical silver ion-selective sensors with subnanomolar detection limits. *Anal. Chim. Acta* 572 (2006): 1–10.

[32] Zeng, X., Weng, L., Chen, L., Leng, X., Zhang, Z., and He, X., Improved silver ion-selective electrodes using novel 1,3-bis(2-benzothiazolyl)thioalkoxy-*p-tert*-butylcalix[4]arenes. *Tetrahedron Lett.* 41 (2000): 4917–4921.

[33] Chen, L., Ju, H., Zeng, X., He, X., and Zhang, Z., Silver ion-selective electrodes based on novel containing benzothiazolyl calix[4]arene. *Anal. Chim. Acta* 437 (2001): 191–197.

[34] Cattrall, R. W., *Chemical sensors*. New York: Oxford Science Publications, 1997.

[35] Górski, Ł., Klimaszewska, D., Pietrzak, M., and Malinowska, E., Enzymatic detection of glucose using fluoride-selective electrodes with polymeric membranes. *Anal. Bioanal. Chem.* 289 (2007): 533–539.

[36] Abd-Rabboh, H. S. M., and Meyerhoff, M. E., Determination of glucose using a coupled-enzymatic reaction with new fluoride selective optical sensing polymeric film coated in microtiter plate wells. *Talanta* 72 (2007): 1129–1133.

[37] Kalayci, Ş., Somer, G., and Ekmekci, G., Preparation and application of a new glucose sensor based on iodide ion selective electrode. *Talanta* 65 (2005): 87–91.

[38] Chumbimuni-Torres, K. Y., and Wang, J., Nanoparticle-induced potentiometric biosensing of NADH at copper ion-selective electrodes. *Analyst* 134 (2009): 1614–1617.

[39] Chumbimuni-Torres, K. Y., and others, Potentiometric biosensing of proteins with ultrasensitive ion-selective microelectrodes and nanoparticle labels. *J. Am. Chem. Soc.* 128 (2006): 13679–13677.

[40] Numnuam, A., and others, Potentiometric detection of DNA hybridization. *J. Am. Chem. Soc.* 130 (2008): 410–411.

[41] Wu, J., Chumbimuni-Torres, K. Y., Galik, M., Thammakhet, C., Haake D. A., and Wang, J., Potentiometric detection of DNA hybridization using enzyme-induced metallization and a silver ion selective electrode. *Anal. Chem.* 81 (2009): 10007–10012.

[42] Chumbimuni-Torres, K. Y., and others, Amplified potentiometric transduction of DNA hybridization using ion-loaded liposomes. *Analyst* 135 (2010): 1618–1623.

[43] Eugster, R., and others, Plasticizer for liquid polymeric membranes of ion selective chemical sensors. *Anal. Chim. Acta* 284 (1994): 1–13.

[44] Fiedler, U., Influence of the dielectrid constant of the medium on the selectivities of neutral carrier ligands in electrodes membranes. *Anal. Chim. Acta* 89 (1977): 111–118.

[45] Bakker, E., Buehlmann, P., and Pretsch, E., Carrier-based ion-selective electrodes and bulk optodes. 1. General characteristics. *Chem. Rev.* 97 (1997): 3083–3132.

[46] Morf, W. E., *The principles of ion-selective electrodes and of membrane transport*. New York: Elsevier, 1981.

[47] Henderson, P. Z., Zur Thermodynamic der Flüssigkeitsketten. *Phys. Chem.* 59 (1907): 118–127.

[48] Morf, W. E., Calculation of liquid-junction potentials and membrane potentials on the basis of the Planck theory. *Anal. Chem.* 49 (1977): 810–813.

[49] Guggenheim, E. A., On the conception of electrical potential difference between two Phases. II. *J. Phys. Chem.* 34 (1930): 1540–1543.

[50] Guilbault, G. G., and others, Recommemdations for nomenclature of ion-selective electrodes (IUPAC recommemdation 1975). *Pure Appl. Chem.* 48 (1976): 127–132.

[51] Umezawa, Y., *Handbook of ion-selective electrodes: Selectivity coefficients*. Boca Raton Ann Arbor Boston: CRC Press, 1990.

[52] Umezawa, Y., Umezawa, K., and Sato, H., Selectivity coefficients for ion-selective electrodes: Recommended methods for reporting $^{pot}_{A,}$ values. *Pure Appl. Chem.* 67 (1995): 507–518.

[53] Eisenman, G., Rudin, D. O., and Casby, J. U., Glass electrode for measuring sodium ion. *Science* 126 (1957): 831–834.

[54] Nikolskii, B. P., Teoria steklyannogo elektroda. *Zh. Fiz. Khim.* 10 (1937): 495–503.

[55] Bakker, E., Meruva, R. K., Pretsch, E., and Meyerhoff, M. E., Selectivity of polymer membrane-based ion-selective electrodes: self-consistent model describing the potentiometric response in mixed ion solutions of different charge. *Anal. Chem.* 66 (1994): 3021–3030.

[56] Telting-Diaz, M., and Qiu, Y., Chapter 18a Poteniometry. *Comprehensive Analytical Chemistry* 47 (2006): 625–659.

[57] Buck, R. P., and Linder, E., Recommemdations for nomenclature of ion-selective electrodes (IUPAC recommemdation 1994). *Pure Appl. Chem.* 66 (1994): 2527–2536.

[58] Gutsche, C. D., Iqbal, M., and Stewart, D., Calixarenes. 19. Syntheses procedures for *p-tert*-butylcalix[4]arene. *J. Org. Chem.* 51 (1986): 742–745.

[59] Gutsche, C. D., and Lin, L-G., Calixarenes 12: The synthesis of functionalized calixarenes. *Tetrahedron* 42 (1986): 1633–1640.

[60] Ngeontae, W., Janrungroatsakul, W., Morakot, N., Aeungmaitrepirom, W., and Tuntulani, T., New silver selective electrode fabricated from benzothiazole calix[4]arene: Speciation analysis of silver nanoparticles. *Sens. Actuators B* 134 (2008): 377–385.

[61] Joseph, R., Ramanujam, B., Acharya, A., and Rao, C. P., Lower rim 1,3-di{bis(2-picolyl)}amide derivative of calix[4]arene (L) as ratiometric primary sensor toward Ag^+ and the complex of Ag^+ as secondary sensor toward Cys: experimental, computational, and microscopy studies and INHIBIT logic gate properties of L. *J. Org. Chem.* 74 (2009): 8181–8190.

[62] van Eis, M. J., Seiler, P., Muslinkina L. A., Badertscher, M., Pretsch, E., and Diederich, F., Supramolecular fullerene chemistry: A comprehensive study of cyclophane-type mono- and bis-crown ether conjugates of C70. *Helv. Chim. Acta* 85 (2002): 2009–2055.

[63] Meier, P.C., Two-parameter debye-hückel approximation for the evaluation of mean activity coefficients of 109 electrolytes. *Anal. Chim. Acta* 136 (1982): 363–368.

[64] Bakker, E., Willer, M., Lerchi, M., Seiler, K., and Pretsch, E., Determination of complex formation constants of neutral cation-selective ionophores in solvent polymeric membranes. *Anal. Chem.* 66 (1994): 516–521.

[65] Mi, Y., and Bakker, E., Determination of complex formation constants of lipopholic neutral ionophores in solvent polymeric membranes with segmented sandwich membranes. *Anal. Chem.* 71 (1999): 5279–5287.

[66] Qin, Y., Mi, Y., and Bakker, E., Determination of complex formation constants of 18 neutral alkali and alkaline earth metal ionophores in poly(vinyl chloride) sensing membranes plasticized with bis(2-ethylhexyl)sebacate and *o*-nitrophenyloctylether. *Anal. Chim. Acta* 421 (2000): 207–220.

[67] Hyning, D. L. V., and Zukoski, C. F., Formation mechanisms and aggregation behavior of borohydride reduced silver particles. *Langmuir* 14 (1998): 7034–7046.

[68] Shirtcliffe, N., Nickel, U., and Schneider, S., Reproducible preparation of silver sols with small particle size using borohydride reduction: for use as nuclei for preparation of larger particles. *J. Colloid Interf. Sci.* 211 (1999): 122–129.

[69] Zhang, Z. Q., Patel, R. C., Kothari, R., Johnson, C. P., and Friberg, S. E., Stable silver clusters and nanoparticles prepared in polyacrylate and inverse micellar solutions. *J. Phys. Chem. B* 104 (2000): 1176–1182.

[70] Hassan, S. S. M., El-Baz, A. F., and Abd-Rabboh, H. S. M., A novel potentiometric biosensor for selective L-cysteine determination using L-cysteine-desulfhydrase producing *Trichosporon jirovecii* yeast cells coupled with sulfide electrode. *Anal. Chim. Acta* 602 (2007): 108–113.

[71] Hassan, S. S. M., and Rechnitz, G. A., Determination of glutathione and glutathione reductasewitha silver sulfide membrane electrode. *Anal. Chem.* 54 (1982): 1972–1976.

[72] Hassan, S. S. M., Marzouk, S. A. M., Abdel Fattah, M. M., and Shouckry, G. M. S. M., Potentiometric determination of arylsulfatase activity using a novel nitrocatechol sulfate PVC membrane sensor. *Anal. Chem.* 67 (1995): 1887–1891.

[73] Hassan, S. S. M., El-Bahnasawy, R. M., and Risk, N. M., Potentiometric determination of salicylhydroxamic acid (urinary struvite stone inhibitor) based on the inhibition of urease activity. *Anal. Chim. Acta* 351 (1997): 91–96.

[74] Vilaivan, T., and Srisuwannaket, C., Hybridization of pyrrolidinyl peptide nucleic acids and DNA: Selectivity, base-pairing specificity, and direction of binding. *Org. Lett.* 8 (2006): 1897–1900.

[75] Vilaivan, C., and others, Pyrrolidinyl peptide nucleic acid with α/β-peptide backbone: A conformationally constrained PNA with unusual hybridization properties. *Artificial DNA: PNA & XNA* 2 (2011): 50–59.

[76] Patil, V., Malvankar, R. B., and Sastry, M., Role of particle size in individual and competitive diffusion of carboxylic acid derivatized colloidal gold particles in thermally evaporated fatty amine films. *Langmuir* 15 (1999): 8197–8206.

[77] Wei, G., Wang, L., Zhou, H., Liu, Z., Song, Y., and Li, Z., Electrostatic assembly of CTAB-capped silver nanoparticles along predefined λ-DNA template, *Appl. Surface science* 252 (2005): 1189–1196.

[78] Pearson, P. R., Hard and soft acids and bases. *J. Am. Chem. Soc.* 85 (1963): 3533–3543.

[79] Munakata, M., Wu, L. P., and Kuroda-Sowa, T., Toward the construction of functional solid-state supramolecular metal complexes containing copper(I) and silver(I). *Adv. Inorg. Chem.* 46 (1998): 173–303.

[80] Moody, G. J., Oke, R. B., and Thomas, J. D. R., A calcium-sensitive electrode based on a liquid ion exchanger in a poly(vinyl chloride) matrix. *Analyst* 95 (1970): 910–918.

[81] Bakker, E., and Pretsch, E., The new wave of ion-selective. *Anal. Chem.* 74 (2002): 420A–426A.

[82] Morf, W. E., Kahr, G., and Simon, W., Theoretical treatment of the selectivity and detection limit of silver compound membrane electrodes. *Anal. Chem.* 46 (1974): 1538–1543.

[83] Murphy, C. J., Nanocubes and nanoboxes. *Science* 298 (2002): 2139–2141.

[84] Sun, Y., and Xia, Y., Shape-controlled synthesis of gold and silver nanoparticles. *Science* 298 (2002): 2176–2179.

[85] Liu, G. D., and Lin, Y. H., Nanomaterial labels in electrochemical immunosensors and immunoassays. *Talanta* 74 (2007): 308–317.

[86] Koncki, R., Recent developments in potentiometric biosensors for biomedical analysis. *Anal. Chim. Acta* 599 (2007): 7–15.

[87] Wang, J., Nanoparticle-based electrochemical bioassays of proteins. *Electroanalysis* 19 (2007): 769–776.

[88] Willey, T. M., and others, Surface structure and chemical switching of thioctic acid adsorbed on Au(111) as observed using near-edge X-ray absorption fine structure. *Langmuir* 20 (2004): 4939–4944.

VITA

Miss Wanwisa Janrungroatsakul was born on May 13, 1976 in Sukhothai, Thailand. She received her Bachelor's degree in Chemistry from Naresuan University in 1999, and Master's degree in Chemistry from Chulalongkorn University in 2003. She has been a graduate student in the Department of Chemistry, Faculty of Science, Chulalongkorn University, then become a member of Supramolecular Chemistry Research Unit (SCRU) and worked under the supervision of Professor Dr. Thawatchai Tuntulani since 2007.